Numerical Simulation of the Propagation of Fine-Grained Sediment Pulses in Alluvial Rivers

Celso Francisco Castro Bolinaga

Dissertation submitted to the faculty of the Virginia Polytechnic Institute and State University in partial fulfillment of the requirements for the degree of

Doctor of Philosophy
In
Civil Engineering

Panayiotis Diplas, Chair
Robert J. Bodnar, Co-Chair
Clinton L. Dancey
Adil N. Godrej
Nina Stark

August 3rd, 2016
Blacksburg, VA

Keywords: alluvial rivers, hydrodynamic, morphodynamic, numerical modeling, sediment pulse, extreme events

Numerical Simulation of the Propagation of Fine-Grained Sediment Pulses in Alluvial Rivers

Celso Francisco Castro Bolinaga

ABSTRACT

Sediment pulses are defined as large amounts of loose sediment that are suddenly deposited in river corridors due to the action of external factors or processes of natural or anthropogenic origin. Such factors and processes include landslides, debris flows from tributaries, volcanic eruptions, dam removal projects, and mining-related activities. Their occurrence is associated with a surplus in sediment load to downstream reaches, and therefore, with severe channel aggradation and degradation, significant floodplain deposition, increase in flood frequency, damage of infrastructure, and impairment of aquatic habitats. The main objective of this research is to develop a better understanding of the fundamental mechanisms that govern the propagation of these sediment-flow hazards in alluvial sand-bed rivers. Specifically, the study presented herein is divided into three separate parts to achieve this overarching goal. First, a component intended to improve the numerical modeling of morphodynamic processes in alluvial sand-bed rivers by proposing a novel solution methodology that applies either the decoupled or the coupled modeling approach based on local flow and sediment transport conditions. Secondly, a detailed numerical analysis to characterize the behavior of fine-grained sediment pulses (i.e. composed of granular material in the sand size range) in alluvial sand-bed rives by identifying the properties of these types of pulses, as well as the characteristics of riverine environments, that are most relevant to their downstream migration. And lastly, a case study application to assess the effect of the magnitude, duration, and frequency of severe hydrologic events on the overall propagation behavior of fine-grained sediment pulses in alluvial sand-bed rivers. Ultimately, this research aims to contribute towards reducing the uncertainty associated with the impact of these phenomena, and hence, improving the resilience of rivers corridors.

To Ashly, Sebastián, Celso, Diana, Andrés, José, Ingrid, and Ayleen

ACKNOWLEDGEMENTS

First of all, I want to express my sincere appreciation to my advisor, Dr. Panos Diplas. Since my arrival to Virginia Tech, he has been a source of inspiration, always encouraging me to pursue my own ideas and direction. His guidance throughout my graduate studies definitely encouraged me to pursue a career in academia. I would also like to thank Dr. Robert Bodnar. I am especially grateful for his constant support and advice, always contributing to improving the quality and presentation of this research.

My gratitude goes as well to my committee members: Dr. Adil Godrej, Dr. Nina Stark, and Dr. Clint Dancey. Thanks for challenging me throughout the course of this investigation and for broadening my perspectives on its practical applications. Additionally, I would like to especially thank Dr. Kyle Strom, Mohamad Rouhnia, and Duc Tran, who "adopted" me as part of their research group immediately after their arrival to Virginia Tech.

During my time in Blacksburg, I had the invaluable opportunity to meet and share many experiences with amazing friends: Luis Fargier, Betsy Vera, Nestor Suarez, Ana Milena Serrano, Pol Bouratsis, Nelie Loufakis, Ana Lisa Valenciano, Antonio Barbalace, Melis Sutman, Alex Reeb, Amber Reeb, John Petrie, Maria Elena Nieves, Pedro Bengochea, and Bernardo Castellanos. Thanks for your true friendship.

The financial support I received from Virginia Uranium, Inc. is gratefully acknowledged, along with the guidance provided by Walter Coles, Sr., Joseph Aylor, Alan Kuhn, and the rest of the members of the VT-VUI research group. I would also like to acknowledge the financial support received from the Department of Civil and Environmental Engineering at Virginia Tech through the G.V. Loganathan Memorial Graduate Fellowship, and additional support from the Edna Baily Sussman Fund.

Finally, accomplishing this life goal would have been impossible without the continuous support and encouragement of my family: Celso, Diana, Andres, Jose, Ingrid, and Ayleen. All of you are impregnated in every word that is written in this dissertation. Ashly and Sebastian, everything starts and finishes with you.

A todos… Gracias!

TABLE OF CONTENTS

LIST OF FIGURES

LIST OF TABLES

CHAPTER 1. INTRODUCTION

1.1. Problem Description

Fluvial processes and features in alluvial sand-bed rivers are governed by the dynamic, strong interactions among water flow, the transport of sediment, and the evolution of the mobile riverbed. In addition to controlling the morphology of rivers, the spatial and temporal scales associated with these coupled phenomena govern the propagation and reconfiguration of large amounts of loose sediment that are suddenly deposited within riverine environments, hereafter referred to as sediment pulses. Recent events, such as the landslide that occurred near Oso, Washington, USA in March of 2014 in which an estimated 8 million cubic meters of sediment were released into the North Fork Stillaguamish River (Iverson et al., 2015), and the breach of a tailings-impoundment dam at the Mount Polly Mine in British Columbia, Canada in August of 2014 that deposited nearly 25 million cubic meters of material into the West Basin of Quesnel Lake (Petticrew et al., 2015), highlight the effect of the aforementioned spatial and temporal scales on the short- and long-term effects on river corridors due to the migration of sediment pulses. These effects include severe channel aggradation and degradation, significant floodplain deposition, increase in flood frequency, damage of infrastructure, and impairment of aquatic habitats and drinking water supplies (e.g. Storey et al., 2009; Hatten et al., 2015).

Sediment-flow hazards such as the ones exemplified in the preceding paragraph are expected to become more common as the magnitude and frequency of hydrologic events have been significantly enhanced due to the influence of various human activities (e.g. Kirschbaum et al., 2012; Wooten et al., 2016). Such climatic changes will have a direct impact on the magnitude, duration, and frequency of flows in riverine environments (Viers, 2011), and therefore, on the spatial and temporal scales that govern the reconfiguration of the deposited material. The scope of this impact includes altering the rates of sediment transport, the concentration of suspended solids in the water column, and the distribution of aggradation/degradation patterns, as well as regulating the overall time period over which geomorphic and environmental effects persist. For instance, in October of 2015 a severe hydrologic event with a return period that ranged between

500-yr and 1000-yr occasioned extensive flooding from the central to the coastal areas of the state of South Carolina, USA (CISA, 2015). The storm generated peak discharge records at 17 US Geological Survey (USGS) streamflow gaging stations (Feaster et al., 2015), and triggered the failure of the retaining structure and subsequent release of the impounded sediment in 36 dam locations throughout the state (NPDP, 2016).

Existing numerical models for examining the propagation of sediment pulses have focused on studying their propagation in gravel-bed streams. These types of streams are characterized by (1) high values of the Froude (*Fr*) number (defined as $Fr = u / [gh]^{0.5}$ where u is the flow velocity, h is the water depth, and g is the acceleration of gravity) (e.g. Grant, 1997), which as suggested by Lisle et al. (2001), promote a dominant dispersive propagation behavior, (2) a limited mobility of the riverbed due to the presence of armor layers that restrict entrainment of material and facilitate the transport of finer sediment placed over a considerably coarser bed (e.g. Cui et al., 2003), (3) low concentrations of suspended solids in the water column, and (4) sediment moving downstream predominantly as bedload (e.g. Church, 2010). Accordingly, numerical models have adopted a formulation and solution technique based on the decoupled modeling approach. This approach neglects the impact of morphodynamic processes on the flow field based on the assumption that the time scale for sediment transport and riverbed evolution (i.e. the morphodynamic time scale) is much longer than that corresponding to water flow changes (i.e. the hydrodynamic time scale).

In the event of fine-grained sediment pulses (i.e. composed of granular material in the sand size range), however, morphodynamic processes that occur during the initial short-term propagation phase are characterized by suspended-load driven regimes that have the capacity to transport large amounts of fine sediment and cause a rapid movement of the deposited material (e.g. Wilcox et al., 2014). These processes do have an impact on the surrounding flow field, and therefore, hinder the use of the decoupled modeling approach for simulating the particularities of this initial period, as has been demonstrated by recent field applications (e.g. Cui and Wilcox, 2008; Cui et al., 2014). Furthermore, distinctive features of alluvial sand-bed rivers, such as the relatively low values of *Fr* (e.g. Wright and Parker, 2004), together with the dynamic and continuous interactions among water flow, the transport of sediment, and the morphological evolution of the riverbed, are

expected to influence the propagation behavior of sediment pulses, favoring a higher degree of translation as the pulse migrates downstream.

1.2. Research Objectives

The main objective of this research is to develop a better understanding of the fundamental mechanisms that govern the propagation of fine-grained sediment pulses in alluvial sand-bed rivers (hereafter simply referred to as alluvial rivers). In particular, this research aims to advance existing numerical techniques and develop innovative procedures that allow for the development of more accurate methods to examine and predict the fate of sediment pulses. Ultimately, it is envisioned that the work presented herein will contribute towards reducing the uncertainty associated with the impact of these sediment-flow hazards, and therefore, towards improving the resilience of rivers corridors to their occurrence.

The specific research objectives of this dissertation are:

1. To improve the numerical modeling of morphodynamic processes in alluvial rivers by proposing a novel solution methodology that applies either the decoupled or the coupled approach throughout the computational domain based on local flow and sediment transport conditions.
2. To characterize the behavior of fine-grained sediment pulses in alluvial rivers by identifying the properties of these types of pulses, as well as the characteristics of riverine environments, that are most relevant to their downstream migration.
3. To assess the effect of the magnitude, duration, and frequency of extreme hydrologic events, and of the ensuing severe hydraulic conditions in riverine environments, on the propagation of fine-grained sediment pulses in alluvial rivers.

It is important to note that, in the context of this study, the definition of fine-grained material encompasses non-cohesive sediment particles in the sand size range, which median grain size d_{50} approximately varies between 0.125 mm and 2 mm.

1.3. Organization of Dissertation

This dissertation consists of three self-contained chapters that have been or will be submitted for publication in scholarly journals. Chapter 2 is currently under review in *Advances in Water Resources*, and Chapters 3 and 4 will be submitted to *Environmental Fluid Mechanics* and *Journal of Hydraulic Research*, respectively. Together, these chapters provide an enhanced understanding of the mechanisms that govern the propagation and reconfiguration of the fine-grained sediment pulses in alluvial rivers, as well as of the implications that such mechanisms have towards the development and application of numerical models intended to examine and predict their fate.

Chapter 2 - Castro-Bolinaga, C.F., Diplas, P., Bodnar, R.J., (*under review*). An Adaptive Morphodynamic Model for Water Flow, Sediment Transport, and Riverbed Evolution in Alluvial Rivers. *Advances in Water Resources*.

Chapter 3 - Castro-Bolinaga, C.F., Diplas, P., Bodnar, R.J., (*to be submitted*). Numerical Analysis of the Propagation of Fine-grained Sediment Pulses in Alluvial Rivers. *Environmental Fluid Mechanics*.

Chapter 4 - Castro-Bolinaga, C.F., Zavaleta, E., Diplas, P., Bodnar, R.J., (*to be submitted*). Examining the Fate of Sediment Pulses Under Severe Hydrologic and Hydraulic Conditions. *Journal of Hydraulic Research*.

References

Carolinas Integrated Science and Assessment (CISA), 2015. *The South Carolina Flood of 2015*. Available on-line at: http://www.cisa.sc.edu (Aug. 1, 2016).

Church, M., 2010. Gravel-Bed Rivers, in: Burt, T.P., Allison, R.J. (Eds.), *Sediment Cascades: An Integrated Approach*, Wiley.

Cui, Y., Wilcox, A., 2008. Development and Application of Numerical Models of Sediment Transport Associated with Dam Removal, in: Garcia, M.H. (Ed.), *Sedimentation Engineering: Theory, Measurements, Modeling, and Practice, ASCE Manual 110*, American Society of Civil Engineers, Reston, VA, USA.

Cui, Y., Parker, G., Lisle, T.E., Gott, J., Hansler-Ball, M.E., Pizzuto, J.E., Allmendinger, N.E., Reed, J.M., 2003. Sediment pulses in mountain rivers: 1. Experiments. *Water Resour. Res.* 39(9), 1239.

Cui, Y., Wooster, J.K., Braudrick, C.A., Orr, B. K., 2014. Lessons Learned from Sediment Transport Model Predictions and Long-Term Postremoval Monitoring: Marmot Dam Removal Project on the Sandy River in Oregon. *J. Hydraul. Eng.* 04014044.

Feaster, T.D., Shelton, J.M., Robbins, J.C., 2015. *Preliminary Peak Stage and Streamflow Data at Selected USGS Streamgaging Stations for the South Carolina Flood of October 2015*. US Geological Survey Open-File Report 2015-1201, Reston, Virginia, USA.

Grant, G.E., 1997. Critical flow constrains flow hydraulics in mobile-bed streams: A new hypothesis. *Water Resour. Res.* 33(2), 349-358.

Hatten, J.R., Batt, T.R., Skalicky, J.J., Engle, R., Barton, G.J., Fosness, R.L., Warren, J., 2015. Effects of Dam Removal on Tule Fall Chinook Salmon Spawning Habitat in the White Salmon River, Washington. *River. Res. Applic.* 2015.

Iverson, R.M., George, D.L., Allstadt, K., Reid, M.E., Collins, B.D., Vallance, J.W., Schilling, S.P., Godt, J.W., Cannon, C.M., Magirl, C.S., Baum, R.L., Coe, J.A., Schulz, W.H., Bower, J.B., 2015. Landslide mobility and hazards: Implications of the 2014 Oso disaster. *Earth Planet. Sci. Lett.* 412, 197-208.

Kirschbaum, D., Adler, R., Adler, D., Peters-Lidard, C., Huffman, G., 2012. Global Distribution of Extreme Precipitations and High-Impact Landslides in 2010 Relative to Previous Years. *J. Hydrometeorol.* 13, 1536-1551.

Lisle, T.E., Cui, Y., Parker, G., Pizzuto, J.E., Dodd, A.M., 2001. The Dominance of Dispersion in the Evolution of Bed Material Waves in Gravel-Bed Rivers. *Earth Surf. Process. Landforms* 26, 1409-1420.

National Performance of Dams Program (NPDP), 2016. October 2015 South Carolina Dam Failures. Available on-line at: http://npdp.stanford.edu/ 2015_SC_Flood_Failures (Aug. 1, 2016).

Petticrew, E.L., Albers, S.J., Baldwin, S.A., Carmack, E.C., Dery, S.J., Gantner, N., Graves, K.E., Laval, B., Morrison, J., Owens, P.N., Selbie, D.T., Vagle, S., 2014. The impact of a catastrophic mine tailings impoundment spill into one of North America's largest fjord lakes: Quesnel Lake, British Columbia, Canada. *Geophys. Res. Lett.* 42.

Storey, A.W., Marshall, A.R. and Yarrao, M., 2009. Effects of Mine-Derived River Bed Aggradation on Fish Habitat of the Fly River, Papua New Guinea, in: Bolton, B. (Ed.), *The Fly River, Papua New Guinea: Environmental Studies in an Impacted Tropical River System*, Developments in Earth and Environmental Sciences, Volume 9, Elsevier.

Viers, J.H., 2011. Hydropower Relicensing and Climate Change. *J. Am. Water Resour. Assoc.* 47(4), 655-661.

Wilcox, A.C., O'Connor, J.E., Major, J.J., 2014. Rapid reservoir erosion, hyperconcentrated flow, and downstream deposition triggered by breaching of 38 m tall Condit Dam, White Salmon River, Washington. J. *Geophys. Res. Earth Surf.* 119.

Wooten, R.M., Witt, A.C., Miniat, C.F., Hales, T.C., Aldred, J.L., 2016. Frequency and Magnitude of Selected Historical Landslide Events in the Southern Appalachian Highlands of North Carolina and Virginia: Relationship to Rainfall, Geological and Ecohydrological Controls, and Effects, in: Greenberg, C.H., Collins, B.S. (Eds.), *Natural Disturbances and Historic Range of Variation, Type, Frequency, Severity, and Post-disturbances Structure in Central Hardwood Forests USA*, Springer.

Wright, S., Parker, G., 2004. Flow Resistance and Suspended Load in Sand-Bed Rivers: Simplified Stratification Model. *J. Hydraul. Eng.* 130(8), 796-805.

CHAPTER 2. AN ADAPTIVE MORPHODYNAMIC MODEL FOR WATER FLOW, SEDIMENT TRANSPORT, AND RIVERBED EVOLUTION IN ALLUVIAL RIVERS[1]

Abstract

A one-dimensional (1-D) adaptive morphodynamic model for water flow, sediment transport, and riverbed evolution in alluvial rivers is presented in this paper. The development of the model is based on the unsteady St. Venant shallow water equations for the water-sediment mixture, and considers the movement of sediment as bedload and suspended load. The system of governing equations is solved using a novel solution methodology that applies either the decoupled (quasi-steady) approach or the coupled (dynamic) approach based on local flow and sediment transport conditions. Such methodology consists of a physics-based criterion to define the range of applicability of the aforementioned modeling approaches together with an adaptive numerical scheme to formulate and solve the system of governing equations. The intent of the proposed framework is to adopt the more suitable modeling approach within different regions of the computational domain without compromising the overall accuracy and efficiency of the numerical model.

[1] This chapter is currently under review: Castro-Bolinaga, C.F., Diplas, P., and Bodnar, RJ. (*under review*), An Adaptive Morphodynamic Model for Water Flow, Sediment Transport, and Riverbed Evolution in Alluvial Rivers, *Advances in Water Resources*.

2.1. Introduction

Fluvial features and processes in alluvial rivers (e.g. bedforms, sediment transport modes, and aggradation/degradation patterns) are governed by the dynamic interactions among water flow, the transport of sediment, and the morphological evolution of the mobile riverbed. The rate and scale at which such interactions occur control the morphology of rivers, defining their slope, width, and planform, as well as the roughness and grain-size distribution of their channels (Church and Ferguson, 2015). Therefore, understanding the complex and interrelated mechanisms that dictate morphological changes in alluvial rivers is a rather challenging task that requires the combination of numerical (e.g. Majd and Sanders, 2014; Khosronejad et al., 2015), experimental (e.g. Powell et al., 2006; Cohen et al., 2010), and field (e.g. East et al., 2015; Gran and Montgomery, 2005) studies.

One-dimensional (1-D) numerical models, in particular, have been extensively used to simulate the aforementioned phenomena (e.g. Karim and Kennedy, 1982; Vieira and Wu, 2002; Chang, 2006; Brunner, 2016). They have been developed to cover a wide range of conditions, including different water flow states (e.g. steady, quasi-steady, or unsteady), sediment transport modes (e.g. bedload, suspended load, or total load), and sediment transport states (e.g. equilibrium or non-equilibrium). Nonetheless, two fundamental modeling aspects that still remain subject of significant variability are the formulation of the system of governing equations and the associated solution methodology. Over the last four decades, considerable attention has been devoted towards the simplification of these aspects in order to generate consistent and practical numerical tools for simulating morphodynamic processes in alluvial rivers (e.g. De Vries, 1975; Lyn, 1987; Morris and Williams, 1996; Cui and Parker, 1997; Kassem and Chaudhry, 1998; Cao et al., 2002; Garegnani et al., 2011, 2013).

Two types of model formulations are typically found in the literature, referred to as decoupled and coupled models. Decoupled models (e.g. Cui and Parker, 2005) are based on the premise that the time scale for sediment transport and riverbed evolution (or the morphodynamic time scale) is significantly longer than that corresponding to water flow

changes (or the hydrodynamic time scale). The basic governing equations adopted by these models are the St. Venant shallow water equations for clear-water flow and the Exner equation for the conservation of sediment mass, along with expressions to compute sediment transport rates. Given that they do not account for the impact of morphodynamic processes on the flow field, these models implement an asynchronous solution methodology based on the quasi-steady assumption. In this approach, water flow is approximated as steady when studying the evolution of the riverbed, or alternatively, the latter is considered fixed when the hydrodynamic variables are computed (Cao et al., 2002; Cui and Parker, 2005). It has been reported that decoupled models perform well in cases where sediment is mainly transported as bedload, concentrations of suspended solids in the water column are low, and the evolution of the riverbed occurs slowly (e.g. Cui et al., 2003a; Cui and Wilcox, 2008).

Coupled models (e.g. Wu and Wang, 2008), on the other hand, consider that the hydrodynamic and morphodynamic time scales are of approximately the same order of magnitude. Therefore, these models are formulated based on the St. Venant shallow water equations for the water-sediment mixture to consider for the impact of sediment transport and riverbed evolution on the flow field. They apply a synchronous procedure as part of the solution methodology that disregards the quasi-steady assumption and solves the system of governing equations simultaneously (Wu, 2008). Coupled models are typically employed to simulate flows accompanied by pronounced morphodynamic processes (e.g. propagation of dam-break waves over erodible beds), characterized by having high concentrations of suspended solids in the water column along with a rapidly evolving riverbed (e.g. Cao et al., 2006; Wu and Wang, 2007).

Different numerical criteria have been proposed to define the range of applicability of decoupled and coupled models. De Vries (1975) developed a morphological time scale for aggradation and degradation processes in alluvial rivers by studying the relative celerities of disturbances at the water level and the mobile bed. Results of this work suggest that the quasi-steady assumption (or equivalently, decoupled models) can be safely applied when the concentration of suspended sediment in the water column is negligible. Morris and Williams (1996) expanded the latter analysis by evaluating the relative celerities over a range of finite suspended sediment concentrations. They

concluded that decoupled models are appropriate when simulating flows characterized by having low Froude (Fr) numbers and carrying low concentrations of solids in suspension. More recently, Garegnani et al. (2011, 2013) proposed an approximate threshold for the application of decoupled models that is solely based on the magnitude of the depth-averaged volumetric concentration of total sediment load (C_t). They suggested a threshold of Ct equal to 1% and performed an eigenvalue analysis, together with numerical simulations, to confirm and validate the proposed limit. However, the authors do not elaborate on the effect that different flow regimes (e.g. in terms of Fr as indicated by Morris and Williams, 1996) and sediment transport conditions (e.g. dominant bedload or suspended load, or a combination of both) may have on such threshold.

In spite of the aforementioned constraints, 1-D decoupled models continue to be typically used for assessing the impact of large-scale engineering projects on river corridors due to their computational ease and efficiency (e.g. Cui et al., 2006a, 2006b). Recent field applications, such as the removal of Marmot Dam in the Sandy River, Oregon, USA (Major et al., 2012), provide evidence that these types of models are able to successfully forecast long-term geomorphic changes, but fail to accurately reproduce the particularities of fluvial processes at the initial short-term phase (Cui et al., 2014). During this phase, river corridors undergo rapid hydrodynamic and morphodynamic adaptations (e.g. Wilcox et al., 2014) that are more adequately captured by a coupled modeling approach. The present study aims to address such limitation by developing a 1-D numerical model capable of adjusting to the variety of temporal scales exhibited by water flow, sediment transport, and riverbed evolution in alluvial rivers. This is accomplished by means of a novel solution methodology that applies either the decoupled (quasi-steady) approach or the coupled (dynamic) approach depending on local flow and sediment transport conditions to formulate and solve the system of governing equations. Hence, the proposed framework allows us to adopt the more suitable modeling approach within different regions of the computational domain without compromising the overall accuracy and efficiency of the numerical model.

The specific objectives of this study are twofold: (1) to derive a physics-based criterion for defining a range of applicability for the decoupled and coupled modeling approaches, and (2) to implement and validate an adaptive numerical scheme based on the proposed

criterion for formulating and solving the system of governing equations. The intent is to provide a more thorough representation of how the relative magnitude between the hydrodynamic and morphodynamic time scales constrains the modeling of fluvial processes. It is envisioned that this study will contribute towards improving numerical techniques and prediction methods that are currently used for evaluating the response of river corridors to changing environmental conditions (e.g. landslides, dam decommissioning, or mining activities). The organization of this paper is as follows. Initially, details about the formulation of the problem are presented, including information about the governing equations, auxiliary expressions, and empirical relations. Then, as part of the solution methodology, the derivation of the proposed physics-based criterion and the application of the adaptive numerical scheme are provided. The numerical methods used to discretize and solve the system of governing equations are described next. Finally, an assessment of the model performance when applied to five validation cases is presented, and the implications of the results are discussed and contextualized.

2.2. Model Formulation

The formulation of morphodynamic numerical models typically includes three basic components to achieve an adequate representation of the mechanisms that govern physical processes in alluvial rivers. These components are a hydrodynamic sub-model, a sediment transport sub-model, and a morphological evolution sub-model. Additional sub-models may be included, for instance, to account for changes in the properties of the water-sediment mixture due to significantly high concentrations of suspended solids in the water column. For simplicity, the model formulation presented herein considers a channel with rectangular cross-sectional shape of constant width. Nonetheless, extending this framework to irregularly shaped cross-sections similar to those found in natural river corridors is relatively simple and straightforward.

2.2.1. Hydrodynamic Sub-Model

The hydrodynamic sub-model is intended to predict spatial and temporal variations of the flow field. In 1-D models, these variations are calculated in the streamwise direction and

the computed flow properties represent averaged values that remain constant over the cross-section. The governing equations are the 1-D unsteady St. Venant shallow water equations for the conservation of mass and momentum. In this study, they are formulated for the water-sediment mixture to account for the impact of sediment transport and riverbed evolution on the flow field. Thus, the corresponding equations for the conservation of mass (Equation 1) and momentum (Equation 2) are expressed as follows:

$$\frac{\partial(\rho h)}{\partial t} + \frac{\partial(\rho u h)}{\partial x} + \frac{\partial(\rho_b z_b)}{\partial t} = 0 \tag{1}$$

$$\frac{\partial(\rho u h)}{\partial t} + \frac{\partial(\rho u^2 h)}{\partial x} + \rho g h\left(\frac{\partial z}{\partial x} + S_f\right) + g\frac{h^2}{2}\frac{\partial \rho}{\partial x} = 0 \tag{2}$$

where t is time, x is the streamwise coordinate, h is the water depth, u is the flow velocity, z is the water surface elevation, z_b is the riverbed elevation, $\rho = \rho_w\ (1 - C_t) + \rho_s\ C_t$ is the density of the water-sediment mixture, $\rho_b = \rho_w\ \lambda_o + \rho_s\ (1 - \lambda_o)$ is the density of the riverbed surface layer, ρ_w is the density of water, ρ_s is the density of sediment particles, λ_o is the porosity of the riverbed surface layer, S_f is the friction slope, and g is the acceleration of gravity. Equations 1 and 2 are the hydrodynamic governing equations adopted by the coupled modeling approach. The analogous equations for the decoupled modeling approach neglect the last term on the left-hand side of each expression by assuming a fixed bed and clear-water flow conditions, respectively.

2.2.2. Sediment Transport Sub-Model

The objective of the sediment transport sub-model is to estimate the rate at which sediment moves. In this study, two equations are considered, namely, a bedload transport equation to account for the movement of sediment close to the riverbed by rolling, saltation, or sliding (Chang, 1988), and a suspended load transport equation to model sediment particles that are carried by the flow and maintained in suspension by the dispersive effects of eddies (Parker, 2004). The corresponding expressions are depicted below in Equations 3 and 4, respectively, as:

$$q_B = q_B^* \tag{3}$$

$$\frac{\partial(hC)}{\partial t}+\frac{\partial(uhC)}{\partial x}=E-D \tag{4}$$

where q_B is the volumetric bedload transport rate per unit channel width, q_B^* is the volumetric capacity bedload transport rate per unit channel width, C is the depth-averaged volumetric concentration of suspended sediment, $E = w_s\ C_b^*$ is the volumetric entrainment rate per unit riverbed area, $D = w_s\ C_b$ is the volumetric deposition rate per unit riverbed area, w_s is the settling velocity of sediment particles, C_b^* is the equilibrium near-bed suspended sediment concentration, $C_b = \alpha\ C$ is the actual near-bed suspended sediment concentration, and α is the non-equilibrium adaptation coefficient of suspended load defined after Cao et al. (2004). Equation 3 represents an equilibrium model of bedload transport under the assumption that this adapts sufficiently rapidly to local flow conditions. Numerical analyses performed by Cao et al. (2011) suggest that this assumption is suitable, even when modeling very active bedload transport processes under highly unsteady flows. In contrast, Equation 4 is a non-equilibrium model of suspended load transport that accounts for the streamwise variation of C and its gradual adjustment towards local flow conditions (Chang, 1988). This type of model is required to accurately simulate flows carrying large amounts of solids in suspension (Cao et al., 2007).

2.2.3. Morphological Evolution Sub-Model

The morphological evolution sub-model accounts for the temporal and spatial deformation of the riverbed caused by the exchange of sediment with the water column due to entrainment and deposition. This phenomenon is embedded in the Exner equation for the conservation of sediment mass, which is written as:

$$(1-\lambda_o)\frac{\partial z_b}{\partial t}=-\frac{\partial q_B^*}{\partial x}+D-E \tag{5}$$

2.2.4. Empirical Relations

Empirical relations are needed for computing S_f, q_B^*, C_b^*, and w_s in order to close the system of governing equations. The widely used Manning's approach is employed for computing S_f as:

$$S_f = \frac{n^2 u|u|}{R_h^{4/3}} \tag{6}$$

where n is the Manning's roughness coefficient and R_h is the hydraulic radius. The selection of the empirical capacity formula for computing q_B^* depends on the degree of similarity between the conditions used for its empirical derivation and those that characterize the problem of interest. In this study, the equation proposed by Ashida and Michiue (1972) for the transport of sediment in the medium sand to fine gravel size range (0.3 mm $\leq d_{50} \leq$ 7.0 mm, with d_{50} being the median grain size of sediment particles) is adopted. This equations is written as:

$$q_B^* = 17\left(\tau^* - \tau_{cr}^*\right)\left(\sqrt{\tau^*} - \sqrt{\tau_{cr}^*}\right) d_{50}\sqrt{R_s g d_{50}} \tag{7}$$

where $\tau^* = R_h\, S_f / R_s\, d_{50}$ is the dimensionless boundary shear stress, $R_s = (\rho_s - \rho_w) / \rho_w$ is the submerged specific gravity of sediment particles, and τ_{cr}^* is the dimensionless critical boundary shear stress. Regarding C_b^*, the relationship given by Ikeda and Izumi (1991) for sand-bed rivers actively transporting sediment as bedload and suspended load is used as:

$$C_b^* = 0.001\left(\frac{\tau^*}{w_s^*}\right)^2 \tag{8}$$

where $w_s^* = w_s / (R_s\, g\, d_{50})^{1/2}$ is the dimensionless settling velocity of sediment particles. Lastly, even though it is not strictly necessary as a closure relation, the expression proposed by Richardson and Zaki (1954) (Equation 9) is applied for estimating the settling velocity of granular material under the effect of sediment transport. This consideration generalizes and extends the validity of the present formulation for cases dominated by high concentration of suspended load. In Equation 9, w_{so} is the corresponding clear-water settling velocity of sediment particles.

$$w_s = w_{so}\left(1 - C_t\right)^4 \tag{9}$$

2.3. Solution Methodology

The interaction among the outlined sub-models is dictated by the rate and scale at which fluvial processes occur in alluvial rivers. From a numerical perspective, accurately modeling such interaction translates into the formulation of a consistent system of governing equations and the application of an appropriate numerical scheme to solve it. Herein, these modeling aspects are addressed by applying a novel solution methodology that consists of (1) a physics-based criterion to guide the selection between the decoupled (quasi-steady) approach and the coupled (dynamic) approach, and (2) an adaptive numerical scheme derived from this criterion to formulate and solve the system of governing equations.

2.3.1. Physics-Based Criterion

The physics-based criterion is intended to define a range of applicability for the aforementioned modeling approaches by means of a dimensionless parameter ξ.

2.3.1.1. Dimensionless Parameter ξ

The equations for the conservation of mass (Equation 1) and momentum (Equation 2) of the water-sediment mixture can be rearranged by using the definitions of ρ and ρ_b, together with the relations given by Equations 4 and 5, as:

$$\frac{\partial h}{\partial t}+\frac{\partial (uh)}{\partial x}=-\frac{\partial z_b}{\partial t} \tag{10}$$

$$\frac{\partial (uh)}{\partial t}+\frac{\partial \left(u^2 h\right)}{\partial x}+gh\left(\frac{\partial z}{\partial x}+S_f\right)=\left(\frac{\rho_s-\rho_w}{\rho}\right)\left(-g\frac{h^2}{2}\frac{\partial C_t}{\partial x}+u\left(C_{riverbed}-C_t\right)\frac{\partial z_b}{\partial t}\right) \tag{11}$$

where $C_{riverbed} = 1 - \lambda_o$ is the volumetric concentration of sediment in the riverbed surface layer. The terms on the right-hand side (RHS) of these equations are considered negligible in the decoupled modeling approach based on the assumption that the morphodynamic time scale is much longer than the hydrodynamic time scale. To evaluate the suitability of this assumption, a dimensional analysis of Equations 10 and 11 is performed using the framework presented by Garegnani et al. (2011, 2013). This type of analysis has been effectively applied by previous researchers for identifying the pertinent dimensionless parameters and studying the relative importance of the terms included in

the governing equations (e.g. Goodwin, 1986; Lyn, 1987; Cui and Parker, 1997; Sabersky et al., 1999). The non-dimensional variables, which are identified by the superscript $'$, are defined as:

$$t = \frac{l_o}{u_o} t' \quad ; \quad t = \frac{l_o}{\xi u_o} t_b' \tag{12}$$

$$x = l_o x' \quad ; \quad u = u_o u' \quad ; \quad h = h_o h' \quad ; \quad z = h_o z' \quad ; \quad z_b = h_o z_b' \quad ; \quad S_f = \frac{h_o}{l_o} S_f' \quad ; \quad C_t = C_o C_t' \tag{13}$$

where l_o is a reference length appropriate to the scale of the channel, u_o is a reference velocity, h_o is a reference flow depth, and C_o is a reference concentration. The purpose of the distinct time definitions shown in Equation 12, namely, a hydrodynamic time scale t' and a morphodynamic time scale t_b', is to establish the dimensionless parameter ξ, which is equal to the ratio of t_b' to t' (Garegnani et al., 2011, 2013). Small values of ξ (i.e. $\xi << 1$) indicate that the former time scale is significantly longer than the latter time scale, justifying the use of the decoupled modeling approach. Large values of ξ (i.e. $\xi \sim 1$), on the other hand, imply that the application of the coupled modeling approach is necessary. The non-dimensional equations for the conservation of mass and momentum of the water-sediment mixture are depicted in Equations 14 and 15, respectively, where $Fr = u_o / [g\ h_o]^{½}$, $\rho' = \rho / [C_o\ (\rho_s - \rho_w)]$ represents a dimensionless density of the water-sediment mixture, and $C'_{riverbed} = C_{riverbed} / C_o$ is the dimensionless concentration of sediment in the riverbed surface layer.

$$\frac{\partial h'}{\partial t'} + \frac{\partial (u'h')}{\partial x'} = -\xi \frac{\partial z_b'}{\partial t_b'} \tag{14}$$

$$Fr^2 \left[\frac{\partial (u'h')}{\partial t'} + \frac{\partial (u'^2 h')}{\partial x'} \right] + h' \left(\frac{\partial z'}{\partial x'} + S_f' \right) = \frac{1}{\rho'} \left[-\frac{h'^2}{2} \frac{\partial C_t'}{\partial x'} + Fr^2 u' \left(C'_{riverbed} - C_t' \right) \xi \frac{\partial z_b'}{\partial t_b'} \right] \tag{15}$$

Garegnani et al. (2011, 2013) concluded that ξ is equal to the ratio of C_t to $C_{riverbed}$, and propose a maximum value of ξ of 1% for the application of the decoupled modeling approach, which results in an upper threshold of approximately 0.01 (by volume) for C_t. The eigenvalue analysis performed by these authors, however, shows that the recommended fixed limit does not hold for cases of very active sediment transport. The

RHS of Equation 15 suggests that a suitable criterion to select between the decoupled and coupled modeling approaches must depend on the dynamic relationship between Fr and C_t, rather than only on a fixed value of the latter variable. A close inspection of the terms included therein reveals that for flows in the subcritical regime (i.e. $Fr < 1$) the impact of the mobile riverbed on the flow field may not be as important relative to the amount of solids being transported (e.g. large, low-slope sand-bed rivers as documented by Wright and Parker, 2004). Under these hydraulic conditions, the concentration of suspended sediment (C) is expected to dictate which of the modeling approaches is necessary, with a lower threshold of C as Fr decreases. Likewise, in the case of supercritical flows (i.e. $Fr > 1$) or rapidly varying hydrodynamic conditions, localized strong riverbed deformation processes may exert a greater influence on the selection of the modeling approach than the overall concentration of transported sediment (e.g. dryland ephemeral sand-bed streams as reported by Powell et al., 2006). Therefore, an expression of ξ that considers the effect of both Fr and C_t provides a more thorough representation of the constraints that the relative magnitude between the hydrodynamic and morphodynamic time scales imposes on the numerical modeling of fluvial processes.

A formulation of ξ based on the densimetric Froude (Fr_d) number is proposed in this study. The latter parameter has been effectively applied for examining various phenomena in which an important density difference exists [e.g. estuaries (Hansen and Rattray, 1966), gravity currents (Dufek and Bergantz, 2007), turbidity currents (Huang et al., 2008), and debris flows (Imran et al., 2001)]. Accordingly, Fr_d is used herein to account for the impact of adopting the density of the water-sediment mixture (as in the coupled modeling approach) rather than that corresponding to clear water (as in the decoupled modeling approach) (Equation 16). The larger the difference between these two variables, the more relevant the application of the former modeling approach becomes. Moreover, the denominator in Equation 16 is defined as a densimetric flow velocity (u_d) (Barr, 1963) (expressed as shown in Equation 17 by substituting the definition of ρ) that provides a measure of the intensity of morphodynamic processes, increasing in magnitude as sediment transport and riverbed evolution become more pronounced.

$$Fr_d = \frac{u}{\sqrt{g\left(\frac{\rho - \rho_w}{\rho_w}\right)h}} \tag{16}$$

$$u_d = \left[ghC_t R_s\right]^{0.5} \tag{17}$$

Based on the distinct time definitions provided in Equation 12, a characteristic velocity for morphodynamic processes can be established as ξu_o, where u_o is adequately represented by the flow velocity u. Small values of ξ (i.e. $\xi << 1$) account for mild geomorphic adaptations that occur much slower than variations in the flow field, resulting in $t_b^{'}$ being significantly longer than $t^{'}$. On the contrary, large values of ξ (i.e. $\xi \sim 1$) involve strong geomorphic changes that are comparable with variations in the flow field, causing $t^{'}$ and $t_b^{'}$ to be of approximately the same order of magnitude. Thus, by considering u_d to be a suitable representation of the aforementioned characteristic velocity (i.e. $u_d = \xi u$), a formulation of ξ is obtained as specified in Equation 18. This formulation can be further rearranged in order to express ξ in terms of Fr and C_t as suggested by the dimensional analysis (Equation 19).

$$\xi = \frac{u_d}{u} = \frac{\left[ghC_t R_s\right]^{0.5}}{u} = \frac{1}{Fr_d} \tag{18}$$

$$\xi = \frac{\left[C_t R_s\right]^{0.5}}{Fr} \tag{19}$$

The proposed formulation of ξ depicted in Equation 19 indicates that: (1) for clear-water flow conditions (i.e. $C_t = 0$), ξ is equal to zero and the RHS of Equations 10 and 11 can be neglected, obtaining the governing equations corresponding to the decoupled modeling approach; (2) as C_t increases, the magnitude of ξ increases, and the RHS of Equations 10 and 11 becomes progressively larger, making the application of the coupled modeling approach more important; (3) as implied by the dimensional analysis, ξ depends on the dynamic relationship between Fr and C_t, and accounts for different hydraulic and sediment transport conditions; and (4) a threshold value of ξ must be defined to set a limit for the implementation of either the decoupled or the coupled modeling approach.

2.3.1.2. Selection of a Threshold Value ξ_{cr}

The large database of laboratory experiments provided by Guy et al. (1966) is used to establish a threshold value of ξ (i.e. ξ_{cr}), and numerically define a range of applicability of the aforementioned modeling approaches. This database was selected because it includes a large array of hydraulic and sediment transport conditions typically found in alluvial rivers, providing therefore a thorough characterization of the overall phenomena. Guy et al. (1966) reported the results of ten different experimental settings (based on the d_{50} of the riverbed) for a variety of discharges and thalweg slopes, compiling a total of 339 runs. A summary of the subset that is employed in this study is presented in Table 2-1. This subset corresponds to 209 runs in which sediment was actively being transported, and accordingly, a value of C_t was recorded. Table 2-1 illustrates the wide range of hydrodynamic and morphodynamic conditions that are considered for defining ξ_{cr}. Such conditions include flows in the subcritical and supercritical regimes (as depicted by Fr), as well as sediment transport processes dominated by bedload (as indicated by low values of C/C_t) and suspended load (as indicated by high values of C/C_t). Moreover, it should be noted that the measurements collected by Guy et al. (1966) account for the impact of several riverbed configurations (e.g. ripples, plane bed, dunes, and antidunes) on the reported hydraulic and sediment transport variables.

The laboratory experiments performed by Guy et al. (1966) aimed to simulate equilibrium conditions in alluvial rivers. As described by the authors, runs were allowed to continue until statistically uniform flow velocities, sediment transport rates, and thalweg slopes were attained throughout the flume. Therefore, the hydraulic and sediment transport variables presented in Table 2-1 denote a long-term equilibrium state in which hydrodynamic and morphodynamic processes are occurring rather slowly. From a numerical perspective, this implies that the decoupled modeling approach can be safely applied for accurately simulating such processes. Based on this premise, the correlation between Fr and C_t is examined for the evaluated subset of 209 runs in order to define ξ_{cr}. As illustrated in Figure 2-1, these data collapse into a well-defined trend in which the magnitude of C_t increases as Fr increases for all the considered riverbed median grain sizes. A threshold value of 0.1 (i.e. $\xi_{cr} = 0.1$) is then established following the proposed formulation of ξ. Results indicate that the dynamic behavior of the overall phenomenon is

reflected by the selected ξ_{cr} and the form of Equation 19 (Figure 2-1). Nonetheless, due to the empirical nature of the recommended limit, small variations of ξ (i.e. $\Delta\xi = 0.01$) are included in Figure 2-1 to show the behavior of different threshold values.

As depicted in Figure 2-1, ξ_{cr} allows for the delineation of two distinct regions, namely, a decoupled approach region and a coupled approach region. The former is characterized by values of ξ smaller than ξ_{cr} (i.e. $\xi < \xi_{cr}$), implying that the morphodynamic time scale is much longer than the hydrodynamic time scale, and therefore, that the decoupled modeling approach is valid. On the other hand, the latter region considers values of ξ larger than ξ_{cr} (i.e. $\xi \geq \xi_{cr}$), indicating that both of the aforementioned time scales are of approximately the same order of magnitude, and hence, that the coupled modeling approach should be employed.

The limited number of data points that are larger than ξ_{cr} in Figure 2-1 correspond to runs characterized by supercritical flows (i.e. $Fr > 1$), elevated suspended sediment concentrations (i.e. $C/C_t \sim 1$), and steep thalweg slopes. As suggested by Guy et al. (1966), equilibrium may have not been reached in these cases. To further assess the influence of sediment transport conditions on ξ_{cr}, the correlation between Fr and C_t is evaluated as a function of the ratio of C to C_t. Results shown in Figure 2-2 suggest that cases dominated by bedload transport (i.e. $C/C_t \rightarrow 0$) are in good agreement with the decoupled approach region, which is consistent with experimental and numerical analyses that have been reported in the literature (e.g. Cui et al., 2003b). However, as the regime becomes suspended load driven (i.e. $C/C_t \rightarrow 1$), data points closely follow the proposed limit, leaning towards exceeding its value for very high concentrations of suspended solids in the water column (i.e. $C/C_t \sim 1$). Therefore, the coupled modeling approach needs to be considered in applications where fine sediment is largely present (e.g. Wilcox et al., 2014) to improve the fidelity of the numerical model (e.g. Cui et al., 2003b).

2.3.2. Adaptive Numerical Scheme

The purpose of the adaptive scheme is to provide the numerical model with the capability of adjusting to the variety of temporal scales exhibited by water flow, sediment transport, and riverbed evolution in alluvial rivers. To achieve this goal, the proposed physics-based

criterion is applied throughout the computational domain for formulating a consistent system of governing equations depending on local flow and sediment transport conditions. As indicated in Equation 20, the magnitude of ξ is used to define the form of the equations for the conservation of mass (Equation 21) and momentum (Equation 22) that is employed in the calculations. If $\xi < \xi_{cr}$, the RHS of these equations is neglected (i.e. $\Psi = 0$), resulting in the St. Venant shallow water equations for clear-water flow. Conversely, if $\xi \geq \xi_{cr}$ the full equations are utilized (i.e. $\Psi = 1$), which correspond to the St. Venant shallow water equations for the water-sediment mixture. The latter set of equations considers the exchange of mass and momentum between the water column and the mobile bed (first term on RHS of Equation 21 and third term on the RHS of Equation 22, respectively), as well as the effect of streamwise variable concentration (second term on the RHS of Equation 22) (Cao et al., 2004), accounting therefore for the impact of morphodynamic processes on the flow field.

$$\xi < \xi_{cr} \therefore \psi = 0 \quad ; \quad \xi \geq \xi_{cr} \therefore \psi = 1 \tag{20}$$

$$\frac{\partial h}{\partial t} + \frac{\partial (uh)}{\partial x} = \psi \left[-\frac{\partial z_b}{\partial t} \right] \tag{21}$$

$$\frac{\partial (uh)}{\partial t} + \frac{\partial \left(u^2 h\right)}{\partial x} + gh\left(\frac{\partial z}{\partial x} + S_f\right) = \psi \left[\left(\frac{\rho_s - \rho_w}{\rho} \right) \left(-g \frac{h^2}{2} \frac{\partial C_t}{\partial x} + u\left(C_{riverbed} - C_t\right) \frac{\partial z_b}{\partial t} \right) \right] \tag{22}$$

The temporal terms in Equations 21 and 22 can be safely neglected in the case that $\xi < \xi_{cr}$ for implementing the asynchronous solution procedure based on the quasi-steady assumption. However, these terms are retained for convenience in order to adopt a unique, more general synchronous solution procedure that is valid for both the decoupled and the coupled modeling approach. The main steps for the application of the adaptive numerical scheme are illustrated in the flowchart depicted in Figure 2-3. These steps include: (1) solving the St. Venant shallow water equations to obtain water depths and flow velocities; (2) evaluating the bedload transport equation and solving the suspended load transport equation to compute bedload transport rates and suspended sediment concentrations, respectively; (3) solving the Exner equation to estimate changes in the elevation of the riverbed; and (4) computing ξ to define the form of the St. Venant shallow water equations to be employed in the next time interval. These steps are

continuously repeated, incrementing the time in each step, until the time period of interest has been evaluated.

2.4. Numerical Methods

The system of governing equations to be solved numerically consists of the St. Venant shallow water equations for the conservation of mass (Equation 21) and momentum (Equation 22), the suspended load transport equation (Equation 4), and the Exner equation for the conservation of sediment mass (Equation 5). Nonetheless, to expedite the solution procedure, the latter formulation is treated separately given that it depends exclusively on locally determined variables (i.e. q_B^*, D, and E) (Cao et al., 2004). The reduced system of governing equations is then written in conservation form as:

$$\frac{\partial U}{\partial t} + \frac{\partial F}{\partial x} = S \tag{23}$$

$$U = \begin{bmatrix} h \\ uh \\ hC \end{bmatrix} \quad ; \quad F = \begin{bmatrix} uh \\ u^2 h \\ uhC \end{bmatrix} \quad ; \quad S = \begin{bmatrix} \psi\left[-\frac{\partial z_b}{\partial t}\right] \\ \psi\left[\left(\frac{\rho_s - \rho_w}{\rho}\right)\left(-g\frac{h^2}{2}\frac{\partial C_t}{\partial x} + u\left(C_{bed} - C_t\right)\frac{\partial z_b}{\partial t}\right)\right] - gh\left(\frac{\partial z}{\partial x} + S_f\right) \\ E - D \end{bmatrix} \tag{24}$$

where U is the solution vector, F is the flux vector, and S is the source term vector. The solution of Equation 23 is obtained through an explicit time-marching algorithm in which the dependent variables contained in U are computed progressively in time (Anderson, 1995). By applying the finite volume method to discretize the spatial domain, together with the second-order accurate Adams-Bashforth scheme for the time derivative (Ferziger and Peric, 2002), this equation is expressed as:

$$U_i^{n+1} = U_i^n + \Delta t\, H^n \quad if\ n = 1 \tag{25}$$

$$U_i^{n+1} = U_i^n + \frac{\Delta t}{2}\left(3H^n - H^{n-1}\right) \quad if\ n > 1 \tag{26}$$

$$H^n = -\frac{F_{i+1/2}^n - F_{i-1/2}^n}{\Delta x} + S_i^n \tag{27}$$

where i is the spatial index, n is the temporal index, Δx is the spatial cell size, and Δt is the time step. It should be noted that the first-order accurate Euler scheme is used to calculate the time derivative during the initial time step (Equation 25) due to the multipoint nature of the Adams-Bashforth approach that requires information at two distinct time levels (Equation 26). As indicated in Equations 25 through 27, the solution vector U is estimated at the center point of the cell (i), whereas the flux vector F is computed at its interface with the adjacent cell ($i \pm 1/2$). To evaluate the latter vector, the upwind conservative method proposed by Ying et al. (2004) is applied as depicted in Equations 28 and 29.

$$F_{i+1/2}^{n} = \begin{bmatrix} u_i^n h_i^n \\ \left(u_i^n\right)^2 h_i^n \\ u_i^n h_i^n C_i^n \end{bmatrix} \quad \& \quad F_{i-1/2}^{n} = \begin{bmatrix} u_{i-1}^n h_{i-1}^n \\ \left(u_{i-1}^n\right)^2 h_{i-1}^n \\ u_{i-1}^n h_{i-1}^n C_{i-1}^n \end{bmatrix} \quad if\ u_i \geq 0 \tag{28}$$

$$F_{i+1/2}^{n} = \begin{bmatrix} u_{i+1}^n h_{i+1}^n \\ \left(u_{i+1}^n\right)^2 h_{i+1}^n \\ u_{i+1}^n h_{i+1}^n C_{i+1}^n \end{bmatrix} \quad \& \quad F_{i-1/2}^{n} = \begin{bmatrix} u_i^n h_i^n \\ \left(u_i^n\right)^2 h_i^n \\ u_i^n h_i^n C_i^n \end{bmatrix} \quad if\ u_i < 0 \tag{29}$$

The discretization of the source term vector S is presented in Equation 30. Therein, the water surface elevation gradient ($\partial z/\partial x$) is obtained using the approach suggested by Ying et al. (2004). This approach has the advantage that it implements two weighting factors (i.e. w_1 and w_2 as formulated in Equations 31 and 32) based on the Courant number for preventing numerical instabilities and nonphysical solutions typically exhibited by other discretization techniques (e.g. central, upwind, or downwind) (Ying et al., 2004).

$$S_i^n = \begin{bmatrix} \psi_i^n \left[-\frac{1}{1-\lambda_o} \left(-\frac{q_{bi}^{*n} - q_{bi-1}^{*n}}{\Delta x} + D_i^n - E_i^n \right) \right] \\ \psi_i^n \left[\left(\frac{\rho_s - \rho_w}{\rho_i^n} \right) \left(-g \frac{\left(h_i^n\right)^2}{2} \frac{C_{ti}^n - C_{ti-1}^n}{\Delta x} + u_i^n \left(C_{bed} - C_{ti}^n \right) \frac{1}{1-\lambda_o} \left(-\frac{q_{bi}^{*n} - q_{bi-1}^{*n}}{\Delta x} + D_i^n - E_i^n \right) \right) \right] - g h_i^{n+1} \left(w_1 \frac{\Delta z}{\Delta x}\bigg|_{downwind}^{n+1} + w_2 \frac{\Delta z}{\Delta x}\bigg|_{upwind}^{n+1} \right) - g h_i^n S_{fi}^n \\ E_i^n - D_i^n \end{bmatrix} \tag{30}$$

$$w_1 = 1 - \frac{\Delta t}{\Delta x} \frac{u_{i+1}^n + u_i^n}{2} \quad \& \quad w_2 = \frac{\Delta t}{\Delta x} \frac{u_i^n + u_{i-1}^n}{2} \quad if\ u_i \geq 0 \tag{31}$$

$$w_1 = 1 - \frac{\Delta t}{\Delta x}\frac{u_i^n + u_{i-1}^n}{2} \quad \& \quad w_2 = \frac{\Delta t}{\Delta x}\frac{u_{i+1}^n + u_i^n}{2} \quad if\ u_i < 0 \tag{32}$$

Lastly, the Exner equation is discretized as illustrated in Equations 33 and 34 for estimating the temporal evolution of the riverbed.

$$\Delta z_{bi} = \frac{\Delta t}{1-\lambda_o}\left(-\frac{q_{bi}^{*n} - q_{bi-1}^{*n}}{\Delta x} + D_i^n - E_i^n\right) \tag{33}$$

$$z_{bi}^{n+1} = z_{bi}^n + \Delta z_{bi} \tag{34}$$

2.4.1. Stability Criteria and Boundary Conditions

The use of an explicit time-marching algorithm to solve Equation 23 requires the maximum value of Δt to satisfy the Courant-Friedrichs-Lewy (CFL) condition for guaranteeing a stable solution. However, given that deriving an exact CFL expression for coupled water flow, sediment transport, and riverbed evolution is outside of the scope of this study, the values of Δt adopted herein are the result of numerical tests carried out during the model performance assessment. Regarding the boundary conditions, they are specified in two ghost cells located at the upstream and downstream ends of the computational domain. The hydrodynamic boundary conditions are set following the approach of Sanders (2001), while those corresponding to sediment transport calculations only require defining a volumetric sediment discharge or concentration at the inlet. If neither of the latter quantities is specified, an equilibrium state between water flow and sediment transport is assumed (Goodwin, 1986).

2.5. Results and Discussion

A total of five validation cases are selected to assess the performance of the adaptive numerical model when simulating the dynamic interactions among water flow, sediment transport, and riverbed evolution in alluvial rivers. These cases, which are summarized in Table 2-2, include laboratory experiments and field studies that cover a wide range of hydrodynamic and morphodynamic conditions with the objective of testing the different closure empirical relations (e.g. entrainment/deposition formula) and implicit assumptions (e.g. equilibrium/non-equilibrium sediment transport) embedded in the

model. Depending on the case being evaluated, the results obtained by applying the adaptive numerical model are compared with those corresponding to either the decoupled modeling approach or the coupled modeling approach. As indicated in Table 2-2, the former approach has been effectively employed to reproduce the hydraulic and sediment transport conditions that characterize the first two validation cases, namely, riverbed aggradation due to sediment overloading (Bhallamudi and Chaudhry, 1991) and knickpoint migration (Goutiere et al., 2008). In contrast, the latter approach has been reported to be necessary for modeling the strong fluvial processes associated with the remaining scenarios shown in Table 2-2 (Cao et al., 2004; Wu and Wang, 2008). This comparison allows us to demonstrate the ability of the adaptive numerical model to accurately capture and adjust to the particularities of diverse riverine environments.

2.5.1. Validation Metrics

Validation metrics are intended to provide a quantitative assessment of the performance of a numerical model by measuring the difference between output variables from numerical simulations, and those obtained experimentally or from field measurements (Oberkampf and Roy, 2010). In this study, the Relative Mean Absolute Error (RMAE) is used as a validation metric for the water surface elevation profiles, as well as for other hydrodynamic and morphodynamic quantities of interest (e.g. overtopping discharge and erosion rate), whereas the Brier Skill Score (BSS) is utilized to determine the quality of the predictions for the evolution of the riverbed. Previous researchers have demonstrated the suitability of these indicators for the validation of similar modeling efforts (e.g. van Rijn et al., 2003; Sutherland et al., 2004; El kadi Abderrezzak and Paquier, 2009), providing confidence therefore in their implementation herein. RMAE is computed as:

$$RMAE = \frac{\left\langle \left| \phi_{\mathrm{mod}eled} - \phi_{measured} \right| \right\rangle}{\left\langle \left| \phi_{measured} \right| \right\rangle} \tag{35}$$

where ϕ represents the evaluated quantity, and $\langle \cdot \rangle$ indicates an averaging procedure over the computational domain. Moreover, BSS is defined as:

$$BSS = 1 - \frac{\left\langle \left(z_{b-\mathrm{mod}eled} - z_{b-measured} \right)^2 \right\rangle}{\left\langle \left(z_{b-initial} - z_{b-measured} \right)^2 \right\rangle} \tag{36}$$

where $z_{b\text{-}initial}$ is the initial riverbed elevation profile that is employed as a baseline prediction for the calculations. Based on the magnitude of RMAE and BSS, the performance of the adaptive numerical model is then formally assessed following the criterion suggested by van Rijn et al. (2003) as presented in Table 2-3.

2.5.2. Riverbed Aggradation Due To Sediment Overloading

The first validation case corresponds to the laboratory experiments performed by Soni et al. (1980), who examined riverbed aggradation in alluvial rivers caused by sediment supply rates larger than the corresponding transport capacity. The experimental setup consisted of a rectangular flume with a width of 0.2 m, a length of 30 m, and a thalweg slope of 0.00356. The material that formed the riverbed was medium sand with a d_{50} of 0.32 mm and a λ_o of 0.4. The inflowing water discharge was constant and equal to 0.004 m^3/s, which resulted in a uniform water depth of 0.05 m. To attain an equilibrium profile throughout the flume, bed material was supplied upstream at a steady rate of $3x10^{-6}$ m^3/s. Aggradation was then triggered by increasing this rate by a factor of four, while maintaining a constant water discharge at the inlet. For performing the numerical simulations, the spatial and temporal domains are discretized using a Δx of 0.625 m and a Δt of 0.25 s, respectively. Moreover, the relation of Strickler (1923) is employed for estimating the Manning's n as 0.0124.

The profiles of water surface and riverbed elevation at 30 min and 40 min after the onset of aggradation are depicted in Figure 2-4. Results indicate that the adaptive numerical model accurately reproduces the observed aggradation dynamics. Likewise, the high level of agreement with the decoupled modeling approach shown therein suggests that the proposed form and threshold of ξ adequately capture the relatively weak interactions among water flow, sediment transport, and riverbed evolution that justify the application of such an approach. This is confirmed by the maximum value of ξ (i.e. ξ_{max}) of 0.075 computed during the entire simulation period. Lastly, the quantitative assessment of the performance of the adaptive model presented in Table 2-4 confirms the quality of the predictions given in Figure 2-4.

2.5.3. Knickpoint Migration

Bellal et al. (2004) studied the upstream migration of a knickpoint, which is defined as a location along the channel where a rapid change in thalweg slope exists (Goutiere et al., 2008). Such abrupt change is typically associated with the occurrence of transcritical flow, affecting hence the magnitude of the boundary shear stress and the sediment transport capacity of the river reach (Brush and Wolman, 1960). The laboratory experiments were carried out in a 7.6 m long rectangular flume that was divided into two sections, namely, an upstream section with a length of 6.3 m and a thalweg slope of 0.0057, and a downstream section that extended over the remaining length with a thalweg slope of 0.0240 and a fixed elevation at the outlet of 0.11 m (measured above the bottom of the flume). The riverbed sediment consisted of very coarse sand characterized by a d_{50} of 1.65 mm and a λ_o of 0.42. At the inlet, water discharge was constant and equal to 0.0098 m^3/s and no sediment was supplied. These conditions triggered the degradation of the riverbed in the area surrounding the knickpoint until the upstream and downstream slopes became nearly identical (Goutiere et al., 2008). The spatial and temporal discretization parameters used in the numerical model correspond to a Δx of 0.1 m and a Δt of 0.025 s, respectively. Analogous with the previous validation case, the Manning's n is determined according to Strickler (1923) resulting in a value of 0.0165. The measured and simulated water surface and riverbed elevation profiles at 165 s and 851 s are illustrated in Figure 2-5.

The qualitative comparison indicates that the adaptive numerical model performs well when predicting the water depths and degradation rates associated with the upstream migration of the knickpoint. The model is able to capture the longitudinal transition from subcritical flow over the mild upstream slope to supercritical flow over the steep downstream slope that occurs accompanied by bedload-dominated sediment transport. Furthermore, Figure 2-5 shows that there is a satisfactory agreement with the results corresponding to the decoupled modeling approach. Similar to the scenario of riverbed aggradation, the computed value of ξ_{max} is smaller than the recommended threshold (ξ_{max} = 0.07), providing confidence therefore in the adequacy of ξ to characterize the relationship between the hydrodynamic and the morphodynamic time scales. The quantitative assessment of the performance of the adaptive model is presented

in Table 2-5. As denoted therein, the error associated with the predicted profiles of water surface and the riverbed elevation is rather small.

2.5.4. Dam-Break Wave Propagation Over an Erodible Bed

The laboratory study of Spinewine and Zech (2007) is selected to test the ability of the adaptive numerical model for simulating the strong, coupled hydrodynamic and morphodynamic processes that characterize the propagation of dam-break waves over erodible beds. The experiments were performed in a horizontal rectangular flume with a length of 6 m and a width of 0.25 m. Among the different tested configurations, the one consisting of a flat bed at both sides of the dam location is modeled herein. The riverbed was composed of very coarse sand with a d_{50} of 1.82 mm and a λ_o of 0.47. The dam was simulated using a vertical gate located at the middle of the flume that was rapidly lowered to release the impounded volume of water. The initial depth upstream of the dam was equal to 0.35 m, whereas dry conditions were considered in the downstream reach. The required discretization parameters for the numerical simulations are set as Δx of 0.005 m and Δt of 0.0005 s. In addition, a value of n equal to 0.0165 is adopted as recommended by Spinewine and Zech (2007).

The water surface and riverbed elevation profiles produced by the adaptive numerical model at 0.5 s and 1 s after the release of the dam-break wave are shown in Figure 2-6. Results suggest that the model generates relatively accurate predictions. They indicate that the evolution of the water surface slope is well captured, but depict a wave forefront that is steeper and moving downstream slightly slower than observed experimentally. The latter behavior is illustrated in more detail in Figure 2-7, which compares the measured and simulated rate of propagation of the wave forefront (i.e. U_{front}). Results show that the predicted rate is larger during the initial stage and then decreases as time progresses. Moreover, the model reveals the occurrence of a hydraulic jump at approximately the original location of the dam (Figure 2-6). This phenomenon was not observed during the experiments due to the low mobility of the riverbed sediment (Spinewine and Zech, 2007), but has been consistently reported in similar laboratory studies (e.g. Capart and Young, 1998; Fraccarollo and Capart, 2002).

Regarding the evolution of the riverbed, Figure 2-6 indicates that the model effectively reproduces the measured erosion profiles, including the position and depth of the largest scour hole in the area surrounding the original dam location. The comparison of the results with those corresponding to the coupled modeling approach suggests that the adaptive framework offers a more suitable representation of the variations in water surface and riverbed elevation (Figure 2-6), as well as of the rate of propagation of the dam-break wave forefront (Figure 2-7). While the magnitude of ξmax implies that the coupled modeling approach is indeed necessary (ξ_{max} = 0.18), the observed differences in the predicted values suggest that ξ_{cr} is only locally exceeded throughout the computational domain. This evidences, therefore, that the adaptive model adequately accounts for regions along the channel in which strong interactions among water flow, sediment transport, and riverbed evolution take place. Lastly, the quantitative assessment of the quality of the results presented in Table 2-6 indicates that the level of error generated by the adaptive model is acceptable for the evaluated variables.

2.5.5. Embankment Failure Triggered by Overtopping Flow

Chinnarasri et al. (2003) conducted a series of laboratory experiments to examine the breaching of earth embankments caused by the occurrence of overtopping flow. The tests were conducted in a horizontal rectangular flume with a length of 35 m and a width of 1 m. The geometric characteristics of the embankment consisted of a height of 0.8 m, a crest length of 0.3 m, and upstream and downstream side slopes of 1V:3H and 1V:2.5H, respectively. It should be noted that this configuration corresponds to the test referred to as Run 2 in the original publication. The embankment was composed of medium sand with a d_{50} of 0.86 mm and a λ_o of 0.35. As part of the experimental procedure, a vertical plate was positioned across its crest to allow filling the reservoir to a water depth of 0.83 m by means of a constant inflowing discharge of 0.00123 m^3/s. The plate was then immediately removed for creating water flow in the downstream direction where a tailwater level of 0.03 m had been initially established. The numerical simulations are performed using a value of Δx equal to 0.01 m for discretizing the spatial domain and a value of Δt equal to 0.001 s for advancing in time. Additionally, a Manning's n of 0.018 is adopted as recommended by Tingsanchali and Chinnarasri (2001) for the aforementioned type of sediment.

The predicted and measured riverbed elevation profiles at 30 s and 60 s after the onset of overtopping flow are presented in Figure 2-8. The profiles show that the adaptive numerical model effectively describes the rapid degradation process of the embankment. This process is triggered by the changing hydrodynamic conditions that vary from subcritical flow at the reservoir, to supercritical flow over the side slope, and then back to subcritical flow due to the existing tailwater level. As water flow accelerates on the side slope, the magnitude of the boundary shear stress increases, and therefore, sediment is entrained and transported downstream primarily as bedload. Further along the channel, flow velocity decreases because of the presence of a hydraulic jump, reducing the sediment transport capacity of the reach and causing aggradation in the surrounding area. This entrainment and deposition pattern is depicted in Figure 2-8 by the gradual evolution of the originally steep side slope towards a much milder inclination.

The variation of the overtopping discharge and the water level at the reservoir during the degradation process of the embankment is shown in Figure 2-9. Results indicate that the adaptive numerical model performs well, in particular when predicting the time and magnitude of the peak overtopping discharge, as well as the total drawdown in the reservoir over the evaluated time period. Furthermore, the high degree of similitude between the results of the adaptive model and the coupled modeling approach indicates that the former is able to capture the rapidly occurring hydrodynamic and morphodynamic processes previously described.

Similarly to the dam-break case, the obtained value of ξ_{max} of approximately 1.2 reveals that the coupled modeling approach should be implemented, while the differences illustrated in Figure 2-8 and Figure 2-9 imply that the value of ξ_{cr} is only locally exceeded within the computational domain. Indeed, as shown in Figure 2-10, ξ_{max} is computed during the early stages of the simulation, and as the degradation process develops, the largest value of ξ at a given time interval (i.e. $\xi_{max\text{-}t}$) progressively decreases towards ξ_{cr}. Hence, Figure 2-10 suggests that the coupled modeling approach is in fact necessary during the initial short-term phase, and thereafter only along a progressively smaller section of the reach. This behavior is consistent with the identified limitations of the decoupled modeling approach, which fail to capture the particularities of initial short-term fluvial processes, but is able to accurately forecast long-term geomorphic changes.

Therefore, Figure 2-10 demonstrates that through the implementation of ξ, the adaptive numerical model is capable of adjusting to the variety of rates and scales typically found in alluvial rivers, accounting for sections along the channel where the application of the coupled modeling approach is required. Finally, the quantitative assessment presented in Table 2-7 confirms the satisfactory performance of the model when predicting the degradation process of the embankment.

2.5.6. Scour And Fill In A Dryland Sand-Bed Stream

The last validation case corresponds to the field study by Powell et al. (2006), the objective of which was to examine the patterns of scour and fill exhibited by dryland sand-bed streams when subjected to hydrologic events of various intensities. The work focused on a 90 m long section of an ephemeral watercourse located in the Experimental Watershed of the US Department of Agriculture, Agricultural Research Service in southeastern Arizona (www.tucson.ars.ag.gov). The selected reach was relatively straight and uniform, with an average thalweg slope of 0.019 and a channel width of 3 m. The riverbed consisted of a mixture of predominantly coarse sand with fine gravel characterized by d_{50} of 1 mm. Scour chains were used to measure maximum erosion depths and net deposition levels in 30 cross-sections along the reach for ten separate hydrologic events. Three storms are considered herein, namely, the storm of 30-Jul-00 with a peak discharge (Q_{peak}) of 4.55 m^3/s, the storm of 19-Jul-02 with Q_{peak} of 0.44 m^3/s, and the storm of 26-Jul-02 with Q_{peak} of 1.45 m^3/s. The intent is to cover the wide range of measured conditions that varied from relatively low flow regimes (storm of 19-Jul-02) to nearly bankfull events (storm of 30-Jul-00). To perform the numerical simulations, the spatial and temporal discretization parameters are set as Δx equal to 1.25 m and Δt equal to 0.01 s, respectively. Additionally, a Manning's n of 0.035 is adopted following Powell et al. (2006), λ_o is estimated as 0.34 by employing the formulation of Wu and Wang (2006), and the input discharge hydrographs for each storm are obtained from the website of the Agricultural Research Service Experimental Watershed.

The measured and modeled mean scour depths along the study reach are presented in Table 2-8. Results indicate that the adaptive numerical model accurately predicts the average response of the ephemeral sand-bed stream during the passage of the evaluated

storms. This implies, therefore, that the model is able to capture the intense sediment entrainment and transport that take place during the rising limb of the hydrograph, which is rapidly followed by riverbed aggradation during the falling limb (Powell et al., 2006). Moreover, the satisfactory agreement with the results corresponding to the coupled modeling approach (Table 2-8) further validates the proposed form of ξ as a suitable criterion for estimating the ratio between the hydrodynamic and morphodynamic time scales. This is supported by the computed values of ξ_{max} that fluctuate between 1.6 and 2 depending on the particular hydrologic event being considered. Lastly, the adequacy of the predictions is demonstrated by the quantitative assessment of the performance of the adaptive model that is presented in Table 2-9.

2.6. Conclusions

A 1-D adaptive numerical model for water flow, sediment transport, and riverbed evolution in alluvial rivers has been presented in this paper. The model is based on a novel solution methodology that applies either the decoupled (quasi-steady) approach or the coupled (dynamic) approach based on local flow and sediment transport conditions. This is accomplished by means of a physics-based criterion to define the range of applicability of the modeling approaches together with an adaptive numerical scheme to formulate and solve the system of governing equations. A dimensional analysis of the St. Venant shallow water equations for the water sediment-mixture revealed that such criterion must depend on the dynamic relationship between Fr and C_t, rather than on a fixed value of the latter variable as has been suggested by previous researchers. Accordingly, a dimensionless parameter ξ, which is proportional to the ratio of the morphodynamic to the hydrodynamic time scale, was derived based on the densimetric Froude number. The proposed form of ξ considers the effect of different hydraulic regimes (as embedded in Fr) and sediment transport conditions (as embedded in C_t) to guide the selection between the aforementioned modeling approaches.

A threshold value of ξ equal to 0.1 (i.e. $\xi_{cr} = 0.1$) was established using the large database of laboratory experiments reported by Guy et al. (1966), delineating thus two distinct regions, namely, a decoupled approach region (i.e. $\xi < \xi_{cr}$) and a coupled approach region (i.e. $\xi \geq \xi_{cr}$). The recommended limit was set by means of the correlation between Fr and

C_t, which data points collapsed into a well-defined trend for the range of evaluated riverbed median grain sizes. The database of Guy et al. (1966) suggested that bedload dominated processes are in good agreement with the decoupled approach region, whereas suspended load driven regimes closely follow the recommended limit, in particular as the concentration of suspended solids in the water column increases. Therefore, the coupled modeling approach needs to be especially considered in applications where fine sediment is largely present to improve the fidelity of the numerical model. Nonetheless, due to the empirical nature of the proposed threshold value, factors such as required accuracy, global efficiency, simulation time, and computational cost should be evaluated as well when defining the modeling approach.

Results from the evaluated validation cases indicate that the adaptive numerical model is able to adjust to the variety of temporal scales exhibited by fluvial processes in alluvial rivers. The comparison of the results with those corresponding to the implementation of the decoupled or the coupled modeling approach verified the adequacy of the proposed form and recommended threshold of ξ to capture the range of the hydrodynamic and morphodynamic conditions that justify the use of either of these approaches. Therefore, the solution methodology described in this study addresses a key limitation of the commonly used decoupled technique, which fails to reproduce the particularities of rapidly occurring fluvial processes at the initial short-term phase, allowing us to adopt the more suitable modeling approach within different regions of the computational domain without compromising the overall accuracy and efficiency of the numerical model. Finally, it is envisioned that this work will contribute towards improving numerical techniques and prediction methods that are currently used for evaluating the response of river corridors to environmental hazards such as landslides, dam decommissioning, or mining relating activities

References

Anderson, J.D., 1995. *Computational Fluid Dynamics: The Basics with Applications*. McGraw-Hill.

Ashida, K., Michiue, M., 1972. Study on Hydraulic Resistance and Bedload Transport Rate in Alluvial Streams. *Jpn. Soc. Civil Engineers* 206, 59-69 (in Japanese).

Barr, D.I.H., 1963. Densimetric Exchange Flow in Rectangular Channels: I. - Definitions, Review and Relevance to Model Design. *La Houille Blanche* 7, 739-756.

Bellal, M., Iervolino, M., Zech, Y., 2004. Knickpoint migration process: experimental and numerical approaches, in: *Proc. 12th Conference on Sediment and Sedimentation Particles*, Prague, Czech Republic, September 20-24, 2004.

Bhallamudi, S.M., Chaudhry, M.H., 1991. Numerical Modeling of Aggradation and Degradation in Alluvial Channels. *J. Hydraul. Eng.* 117(9), 1145-1164.

Brunner, G.W., 2016. *HEC-RAS River Analysis System, Users Manual, Version 5.0*. US Army Corps of Engineers, Hydrologic Engineering Center, Davis, CA, USA.

Brush, L.M., Wolman, M.G., 1960. Knickpoint behavior in noncohesive material: A laboratory study. *Bull. Geol. Soc. Am.* 71(1), 59-73.

Cao, Z., Day, R., Egashira, S., 2002. Coupled and Decoupled Numerical Modeling of Flow and Morphological Evolution in Alluvial Rivers. *J. Hydraul. Eng.* 128(3), 306-321.

Cao, Z., Pender, G., Wallis, S., Carling, P., 2004. Computational Dam-Break Hydraulics over Erodible Sediment Bed. *J. Hydraul. Eng.* 130(7), 689-703.

Cao, Z., Pender, G., Carling P., 2006. Shallow water hydrodynamic models for hyperconcentrated sediment-laden floods over erodible bed. *Adv. Water Resour.* 29, 546-557.

Cao, Z., Li, Y., Yue, Z., 2007. Multiple time scales of alluvial rivers carrying suspended sediment and their implications for mathematical modeling. *Adv. Water Resour.* 30, 715-729.

Cao, Z., Hu, P., Pender, G., 2011. Multiple Time Scales of Fluvial Processes with Bed Load Sediment and Implications for Mathematical Modeling. *J. Hydraul. Eng.* 137(3), 267-276.

Capart, H., Young, D.L., 1998. Formation of a jump by the dam-break wave over a granular bed. *J. Fluid Mech.* 372, 165-187.

Chang, H.H., 1988. *Fluvial Processes in River Engineering*. Krieger.

Chang, H.H., 2006. *FLUVIAL-12 Mathematical Model for Erodible Channels, Users Manual*. Chang Consultants, Rancho Santa Fe, CA, USA.

Chinnarasri, C., Tingsanchali, T., Weesakul, S., Wongwises, S., 2003. Flow Patterns and Damage of Dike Overtopping. *Int. J. Sediment Res.* 18(4), 301-309.

Church, M., Ferguson, R.I., 2015. Morphodynamics: Rivers beyond steady state. *Water Resour. Res.* 51, 1883-1897.

Cohen, H., Laronne, J.B., Reid, I., 2010. Simplicity and complexity of bed load response during flash floods in a gravel bed ephemeral river: A 10 year field study. *Water Resour. Res.* 46, W11542.

Cui, Y., Parker, G., 1997. Linear Analysis of Coupled Equations for Sediment Transport, in: *Proc. XXVII IAHR Congress*, San Francisco, CA, USA, August 10-15, 1997.

Cui, Y., Parker, G., 2005. Numerical Model of Sediment Pulses and Sediment-Supply Disturbances in Mountain River. *J. Hydraul. Eng.* 131(8), 646-656.

Cui, Y., Wilcox, A., 2008. Development and Application of Numerical Models of Sediment Transport Associated with Dam Removal, in: Garcia, M.H. (Ed.), *Sedimentation Engineering: Theory, Measurements, Modeling, and Practice, ASCE Manual 110*, American Society of Civil Engineers, Reston, VA, USA, pp. 995-1020.

Cui, Y., Parker, G., Lisle, T.E., Gott, J., Hansler-Ball, M.E., Pizzuto, J.E., Allmendinger, N.E., Reed, J.M., 2003a. Sediment pulses in mountain rivers: 1. Experiments. *Water Resour. Res.* 39(9), 1239.

Cui, Y., Parker, G., Lisle, T.E., Gott, J., Hansler-Ball, M.E., Pizzuto, J.E., Allmendinger, N.E., Reed, J.M., 2003b. Sediment pulses in mountain rivers: 2. Comparison between experiments and numerical predictions. *Water Resour. Res.* 39(9), 1240.

Cui, Y., Parker, G., Braudrick, C., Dietrich, W.E., Cluer, B., 2006a. Dam Removal Express Assessment Models (DREAM), Part 1: Model development and validation. *J. Hydraul. Res.* 44(3), 291-307.

Cui, Y., Braudrick, C., Dietrich, W.E., Cluer, B., Parker, G., 2006b. Dam Removal Express Assessment Models (DREAM), Part 2: Sample runs/sensitivity tests. *J. Hydraul. Res.* 44(3), 308-323.

Cui, Y., Wooster, J.K., Braudrick, C.A., Orr, B. K., 2014. Lessons Learned from Sediment Transport Model Predictions and Long-Term Postremoval Monitoring: Marmot Dam Removal Project on the Sandy River in Oregon. *J. Hydraul. Eng.* 04014044.

De Vries, M., 1975. *A Morphodynamic Time-Scale for Rivers*. Delft Hydraulics Laboratory.

Dufek, J., Bergantz, G.W., 2007. Suspended load and bed-load transport of particle-laden gravity currents: The role of particle-bed interaction. *Theor. Comput. Fluid Dyn.* 21(2), 119-145.

East, A. E., Pess, G.R., Bountry, J.A., Magirl, C.S., Ritchie, A.C., Logan, J.B., Randle, T.J., Mastin, M.C., Minear, J.T., Duda, J.J., Liermann, M.C., McHenry, M.L., Beechie, T.J., Shafroth, P.B., 2015. Large-scale dam removal on the Elwha River, Washington, USA: River channel and floodplain geomorphic change. *Geomorphology* 228, 765-786.

El kadi Abderrezzak, K., Paquier, A., 2009. One-dimensional numerical modeling of sediment transport and bed deformation in open channels. *Water Resour. Res.* 45, W05404.

Ferziger, J. H., Peric, M., 2002. *Computational Methods for Fluid Dynamics*. Springer.

Fraccarollo, L., Capart, H., 2002. Riemann wave description of erosional dam-break flows. *J. Fluid Mech.* 461, 183-228.

Garegnani, G., Rosatti, G., Bonaventura, L., 2011. Free surface flows over mobile bed: Mathematical analysis and numerical modeling of coupled and decoupled approaches. *Commun. Appl. Indus. Math.* 3(1), 1-22.

Garegnani, G., Rosatti, G., Bonaventura, L., 2013. On the range of validity of the Exner-based models for mobile-bed river flow simulations. *J. Hydraul. Res.* 4, 380-391.

Goodwin, P. 1986. *Sediment Transport in Unsteady Flows*. Doctoral Dissertation, University of California, Berkeley, California, USA.

Goutiere, L., Soares-Frazao, S., Savary, C., Laraichi, T., Zech, Y., 2008. One-Dimensional Model for Transient Flows Involving Bed-Load Sediment Transport and Changes in Flow Regimes. *J. Hydraul. Eng.* 134(6), 726-735.

Gran, K.B., Montgomery, D.R., 2005. Spatial and temporal patterns in fluvial recovery following volcanic eruptions: Channel response to basin-wide loading at Mount Pinatubo, Philippines. *GSA Bulletin* 117(1/2), 195-211.

Guy, H.P., Simons, D.B., Richardson, E.V., 1966. *Summary of Alluvial Channel Data from Flume Experiments 1956-61*. US Geological Survey Professional Paper 462-I, Washington, DC, USA.

Hansen, D.V., Rattray, M., 1966. New Dimensions in Estuary Classification. *Limnology and Oceanography* 11(3), 319-326.

Huang, H., Imran, J., Pirmez, C., 2008. Numerical Study of Turbidity Currents with Sudden-Release and Sustained-Inflow Mechanisms. *J. Hydraul. Eng.* 134(9), 1199-1209.

Ikeda, S., Izumi, N., 1991. Stable Channel Cross-Sections of Straight Sand Rivers. *Water Resour. Res.* 27(9), 2429-2438.

Imran, J., Harff, P., Parker, G., 2001. A Numerical Model of Submarine Debris Flow with Graphical User Interface. *Computers & Geosciences* 27, 717-729.

Karim, M.F., Kennedy, J.F., 1982. *IALLUVIAL: A computer-based flow and sediment routing model for alluvial streams and its application to the Missouri river*. Iowa Institute of Hydraulic Research, University of Iowa, Iowa City, IA, USA.

Kassem, A.A., Chaudhry, M.H., 1998. Comparison of Coupled and Semicoupled Numerical Models for Alluvial Channels. *J. Hydraul. Eng.* 124(8), 794-802.

Khosronejad, A., Kozarek, J.L., Palmsten, M.L., Sotiropoulos, F., 2015. Numerical simulation of large dunes in meandering streams and rivers with in-stream rock structures. *Adv. Water Resour.* 81, 45-61.

Lyn, D.A., 1987. Unsteady Sediment-Transport Modeling. *J. Hydraul. Eng.* 113(1), 1-15.

Majd, M.S., Sanders, B.F., 2014. The LHLLC scheme for Two-Layer and Two-Phase transcritical flows over a mobile bed with avalanching, wetting and drying. *Adv. Water Resour.* 67, 16-31.

Major, J.J., O'Connor, J.E., Podolak, C.J., Keith, M.K., Grant, G.E., Spicer, K.R., Pittman, S., Bragg, H.M., Wallick, J.R., Tanner, D.Q., Rhode, A., Wilcock, P.R., 2012. *Geomorphic Response of the Sandy River, Oregon, to Removal of Marmot Dam*. US Geological Survey Professional Paper 1792, Reston, VA, USA.

Morris, P.H., Williams, D.J., 1996. Relative Celerities of Mobile Bed Flows with Finite Solids Concentrations. *J. Hydraul. Eng.* 112(4), 281-299.

Oberkampf, W.L., Roy, C.J., 2010. *Verification and Validation in Scientific Computing*. Cambridge University Press.

Parker, G., 2004. *1-D Sediment Transport Morphodynamics with Applications to Rivers and Turbidity Currents*. Available on-line at: http://hydrolab.illinois.edu/people/parkerg//morphodynamics_e-book.htm (Aug. 1, 2016).

Powell, D.M., Brazier, R., Wainwright, J., Parsons, A., Nichols, M., 2006. Spatial patterns of scour and fill in dryland sand bed streams. *Water Resour. Res.* 42, W08412.

Richardson, J.F., Zaki, W.N., 1954. Sedimentation and fluidization, Part I. *Trans. Inst. Chem. Eng.* 32(1), 35-53.

Sabersky, R.H., Acosta, A.J., Hauptmann, E.G., Gates, E.M. 1999. *Fluid Flow A First Course in Fluid Mechanics*. Prentice Hall.

Sanders, B.F., 2001. High-resolution and non-oscillatory solution of the St. Venant equations in non-rectangular and non-prismatic channels. *J. Hydraul. Res.* 39(3), 321-330.

Soni, J.P., Grade, R.J., Raju, K.G., 1980. Aggradation in streams due to overloading. *J. Hydraul. Div.* 106(1), 117–32.

Spinewine, B., Zech, Y., 2007. Small-scale laboratory dam-break waves on movable beds. *J. Hydraul. Res.* 45(1), 73-86.

Strickler, A., 1923. *Some Contributions to the Problem of the Velocity Formula and Roughness Factors for Rivers, Canals, and Close Conduits*. Federal Office for Water Management, Bern, Switzerland (in German).

Sutherland, J., Peet, A.H., Soulsby, R.L., 2004. Evaluating the performance of morphodynamic models. *Coastal Eng.* 51, 917-939.

Tingsanchali, T., Chinnarasri, C., 2001. Numerical modeling of dam failure due to flow overtopping. *Hydrol. Sciences J.* 46(1), 113-130.

van Rijn, L.C., Walstra, D.J.R., Grasmeijer, B., Sutherland, J., Pan, S., Sierra, J.P., 2003. The predictability of cross-shore bed evolution of sandy beaches at the time scale of storms and seasons using process-based Profile models. *Coastal Eng.* 47, 295-327.

Vieira, D.A., Wu, W., 2002. *One-Dimensional Channel Network Model CCHE1D, Users Manual, Version 3.0*. National Center for Computational Hydroscience and Engineering, The University of Mississippi, University, MS, USA.

Wilcox, A.C., O'Connor, J.E., Major, J.J., 2014. Rapid reservoir erosion, hyperconcentrated flow, and downstream deposition triggered by breaching of 38 m tall Condit Dam, White Salmon River, Washington. *J. Geophys. Res. Earth Surf.* 119.

Wright, S., Parker, G., 2004. Flow Resistance and Suspended Load in Sand-Bed Rivers: Simplified Stratification Model. *J. Hydraul. Eng.* 130(8), 796-805.

Wu, W., 2008. *Computational River Dynamics*. Taylor & Francis Group.

Wu, W., Wang, S.S.Y., 2006. Formulas for Sediment Porosity and Settling Velocity. J. *Hydraul. Eng.* 132(8), 858-862.

Wu, W., Wang, S.S.Y., 2007. One-Dimensional Modeling of Dam-Break Flow over Movable Beds. *J. Hydraul. Eng.* 133(1), 48-58.

Wu, W., Wang, S.S.Y., 2008. One-dimensional explicit finite-volume model for sediment transport with transient flows over movable beds. *J. Hydraul. Res.* 46(1), 87-98.

Ying, X., Khan, A.A., Wang, S.S.Y., 2004. Upwind Conservative Scheme for the Saint Venant Equations. *J. Hydraul. Eng.* 130(10), 977-987.

Table 2-1: Summary of the experimental subset from Guy et al. (1966) used to define ξ_{cr}

d_{50}	Sediment	Fr	Mean
mm	Class		C/C_t
0.19	Fine Sand	0.27 - 1.10	0.76
0.27		0.22 - 1.17	0.76
0.28		0.17 - 1.33	0.58
0.32	Medium Sand	0.30 - 1.29	0.35
0.33		0.25 - 1.55	0.41
0.45		0.14 - 1.70	0.13
0.93	Coarse Sand	0.26 - 1.63	0.24

Table 2-2: Validation cases selected to assess the performance of the adaptive numerical model

Validation Case	Suitable Modeling Approach	Reference
1. Riverbed aggradation due to sediment overloading	Decoupled	Soni et al. (1980)
2. Knickpoint migration	Decoupled	Bellal et al. (2004)
3. Dam-break wave propagation over an erodible bed	Coupled	Spinewine and Zech (2007)
4. Embankment failure triggered by overtopping flow	Coupled	Chinnarasri et al. (2003)
5. Scour and fill in a dryland sand-bed stream	Coupled	Powell et al. (2006)

Table 2-3: Criterion to formally assess the performance of the adaptive numerical model as suggested by van Rijn et al. (2003)

Assessment	z	Other Quantities	z_b
	RMAE	**RMAE**	**BSS**
Excellent	< 0.05	< 0.1	0.8 - 1.0
Good	0.05 - 0.1	0.1 - 0.3	0.6 - 0.8
Fair	0.1 - 0.2	0.3 - 0.5	0.3 - 0.6
Poor	0.2 - 0.3	0.5 - 0.7	0.0 - 0.3
Bad	> 0.3	> 0.7	< 0.0

Table 2-4: Performance of the adaptive numerical model when simulating riverbed aggradation due to sediment overloading

Variable	Adaptive Model		Decoupled Model	
	Value	**Assessment**	**Value**	**Assessment**
z	0.03	Excellent	0.03	Excellent
z_b	0.98	Excellent	0.98	Excellent

Table 2-5: Performance of the adaptive numerical model when simulating knickpoint migration

Variable	Adaptive Model		Decoupled Model	
	Value	**Assessment**	**Value**	**Assessment**
z	0.01	Excellent	0.01	Excellent
z_b	0.90	Excellent	0.90	Excellent

Table 2-6: Performance of the adaptive numerical model when simulating dam-break wave propagation over an erodible bed

Variable	Adaptive Model		Coupled Model	
	Value	**Assessment**	**Value**	**Assessment**
z	0.08	Good	0.09	Good
z_b	0.69	Good	0.67	Good
U_{front}	0.05	Excellent	0.10	Good

Table 2-7: Performance of the adaptive numerical model when simulating embankment failure triggered by overtopping flow

Variable	Adaptive Model		Coupled Model	
	Value	**Assessment**	**Value**	**Assessment**
z_b	0.95	Excellent	0.95	Excellent
Q_{crest}	0.27	Good	0.23	Good
$z_{reservoir}$	0.08	Good	0.07	Good

Table 2-8: Measured and modeled mean reach scour depth

Event	Q_{peak}	Mean Reach Scour Depth (m)		
	m^3/s	Measured	Adaptive Model	Coupled Model
30-Jul-00	4.55	0.066	0.064	0.064
19-Jul-02	0.44	0.023	0.022	0.032
26-Jul-02	1.45	0.057	0.051	0.053

Table 2-9: Performance of the adaptive numerical model when simulating mean reach scour depth in a dryland sand-bed stream

Variable	Adaptive Model		Coupled Model	
	Value	**Assessment**	**Value**	**Assessment**
Mean reach scour depth	0.06	Excellent	0.18	Good

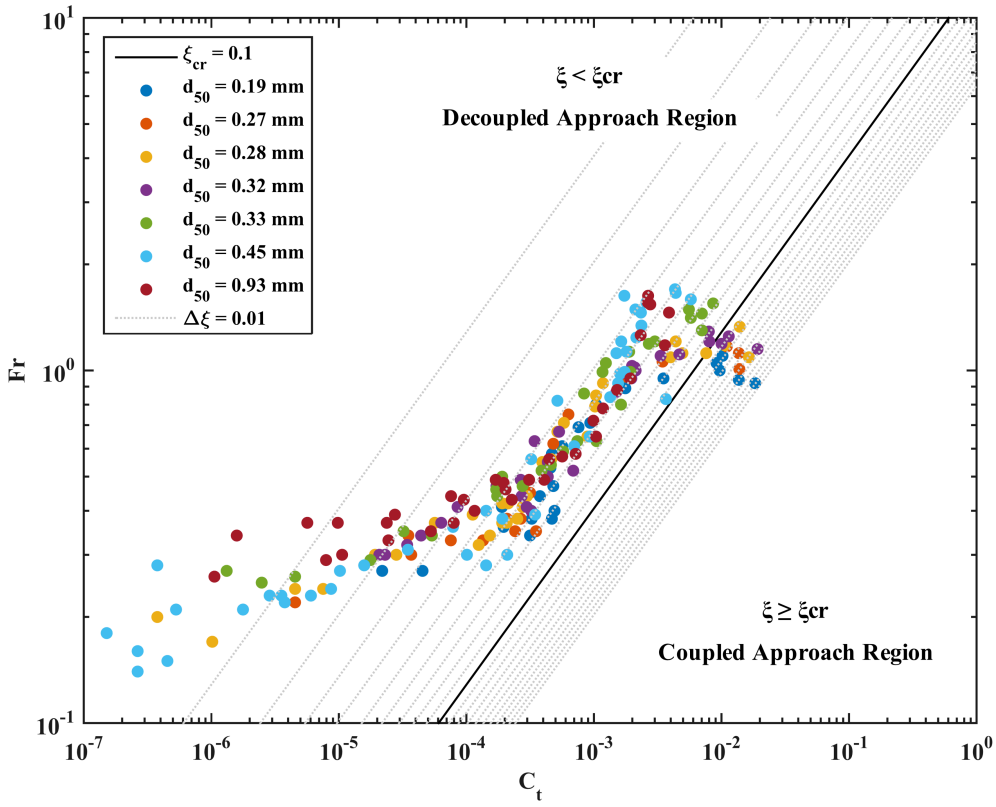

Figure 2-1: Threshold value ξ_{cr} based on the experimental subset from Guy et al. (1966)

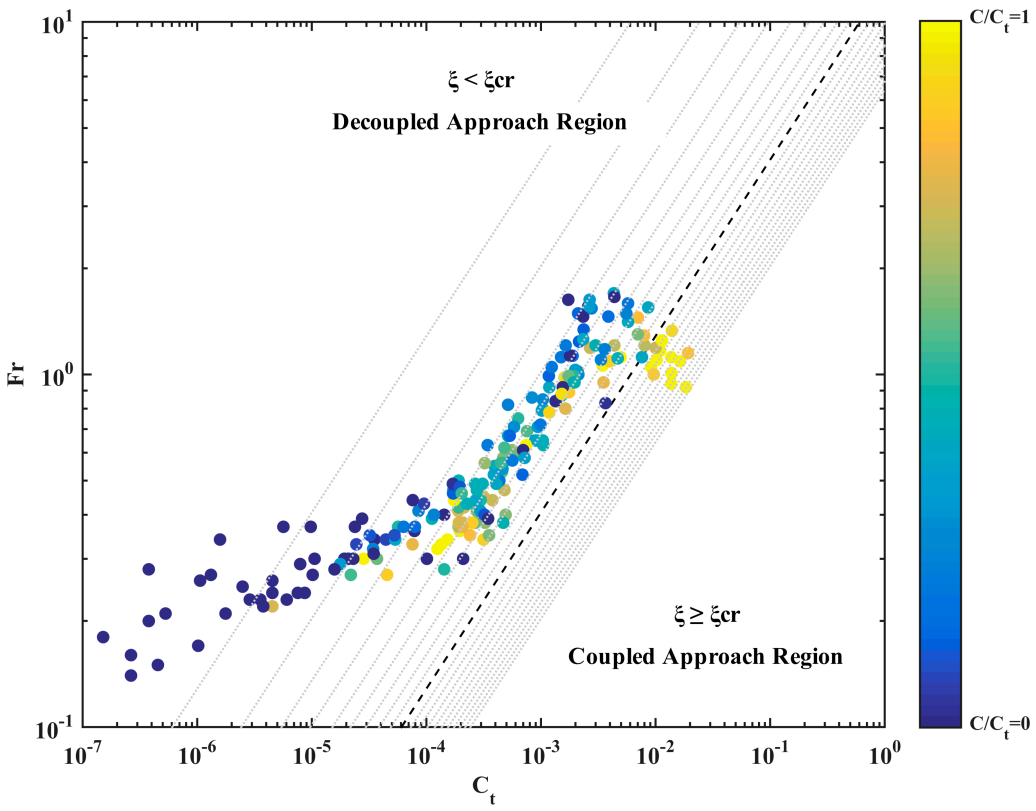

Figure 2-2: Influence of sediment transport conditions on ξ_{cr}

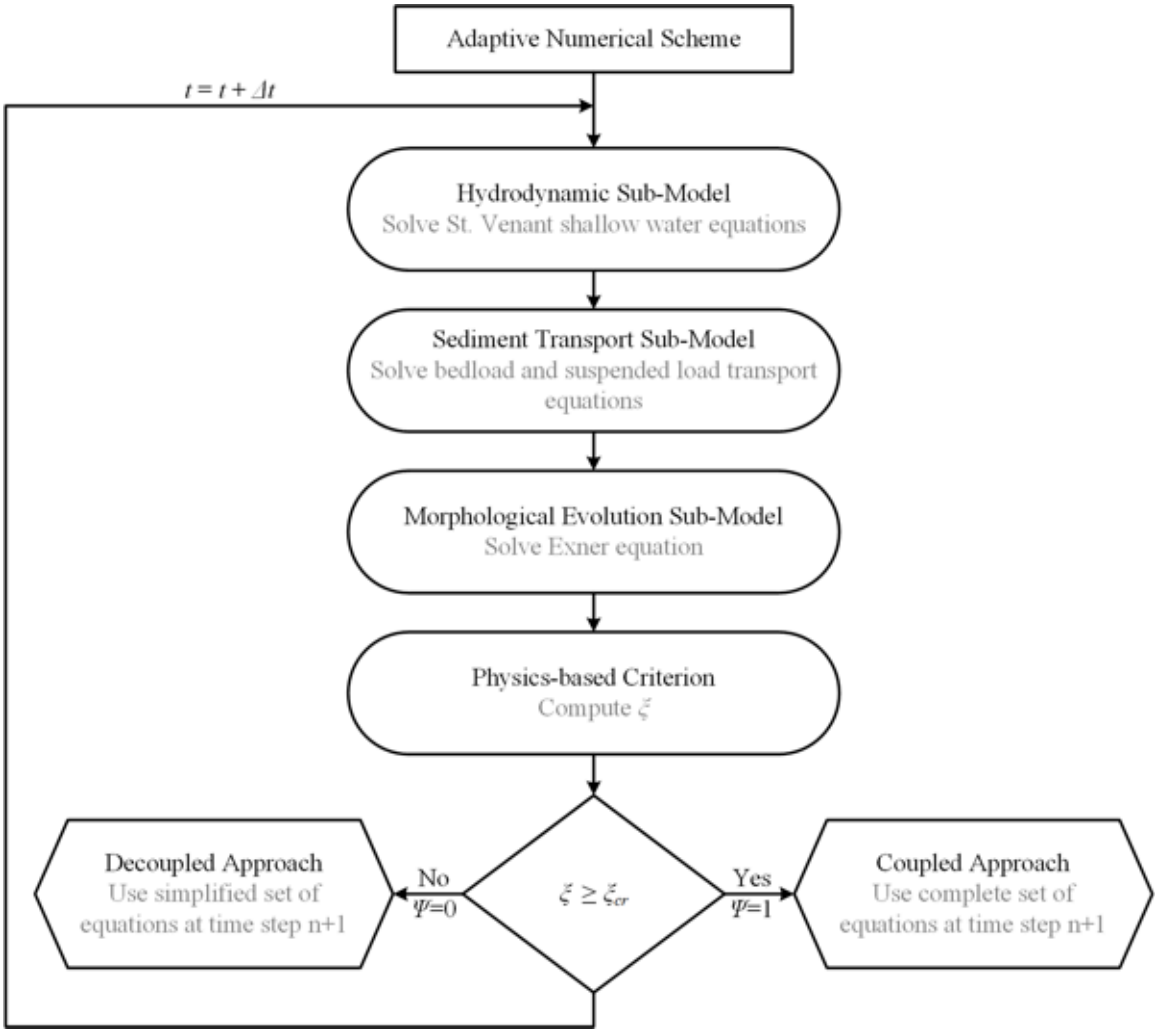

Figure 2-3: Main steps for the application of the adaptive numerical scheme

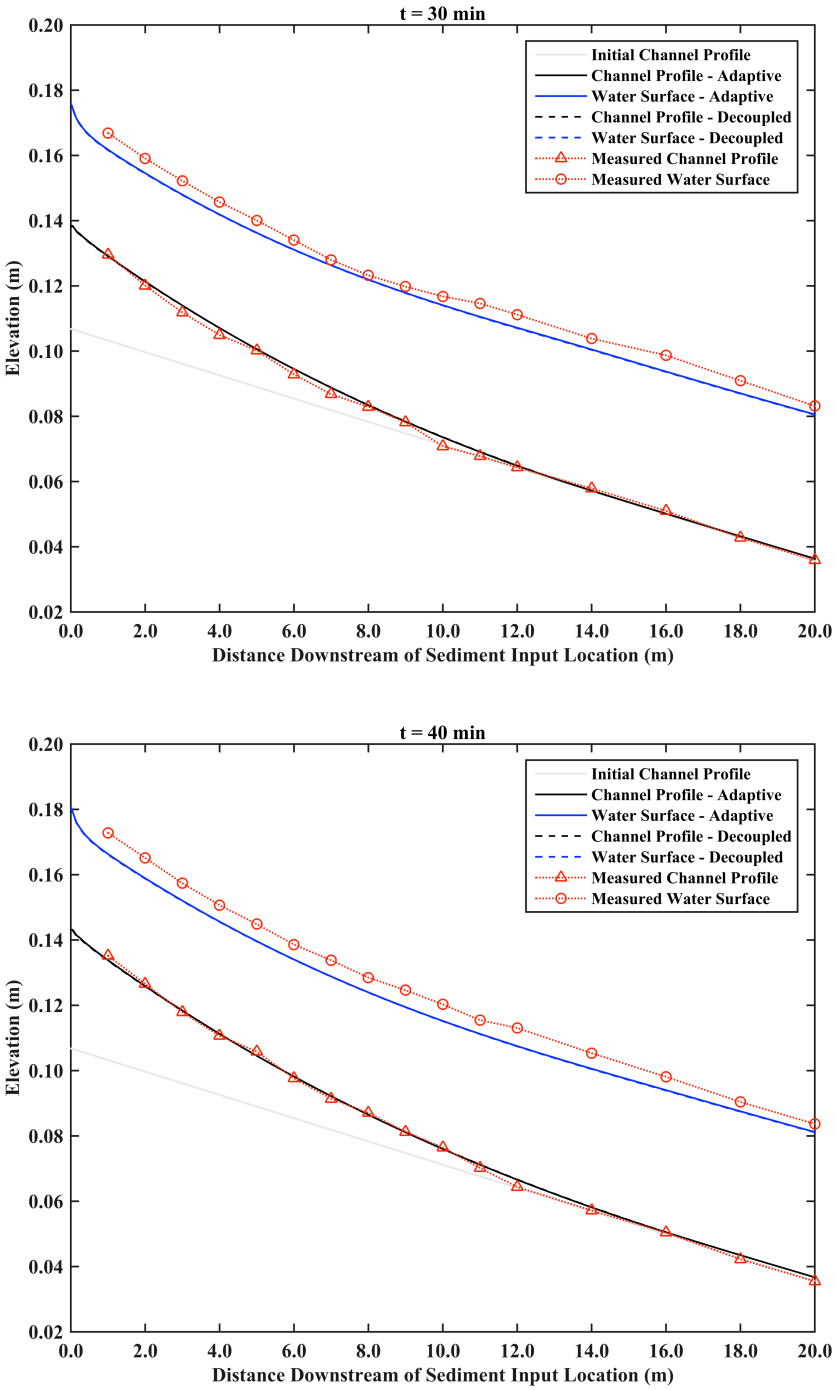

Figure 2-4: Water surface and riverbed elevation profiles at 30 min and 40 min after the onset of aggradation (results of the adaptive numerical model coincide with those of the decoupled modeling approach)

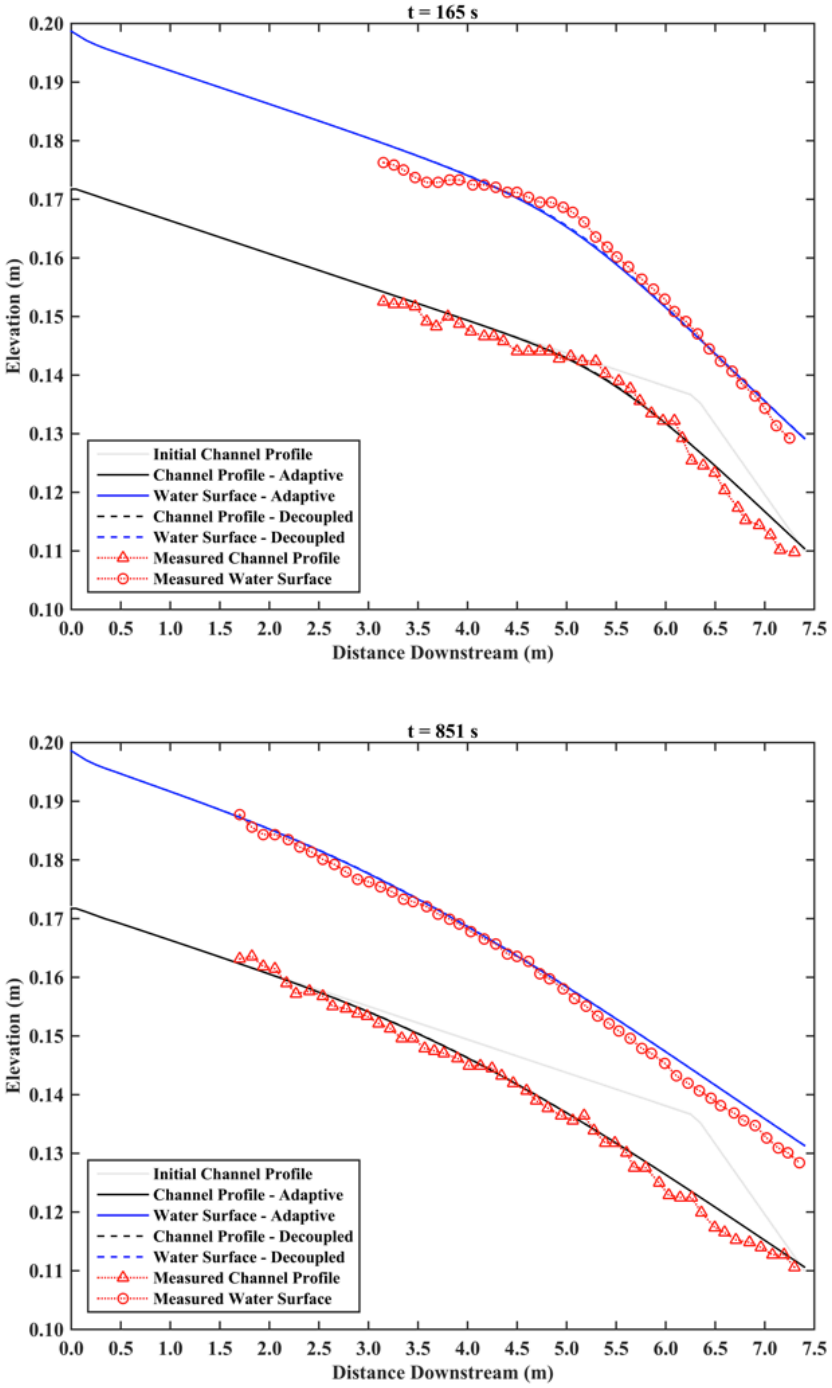

Figure 2-5: Water surface and riverbed elevation profiles at 165 s and 851 s (results of the adaptive numerical model coincide with those of the decoupled modeling approach)

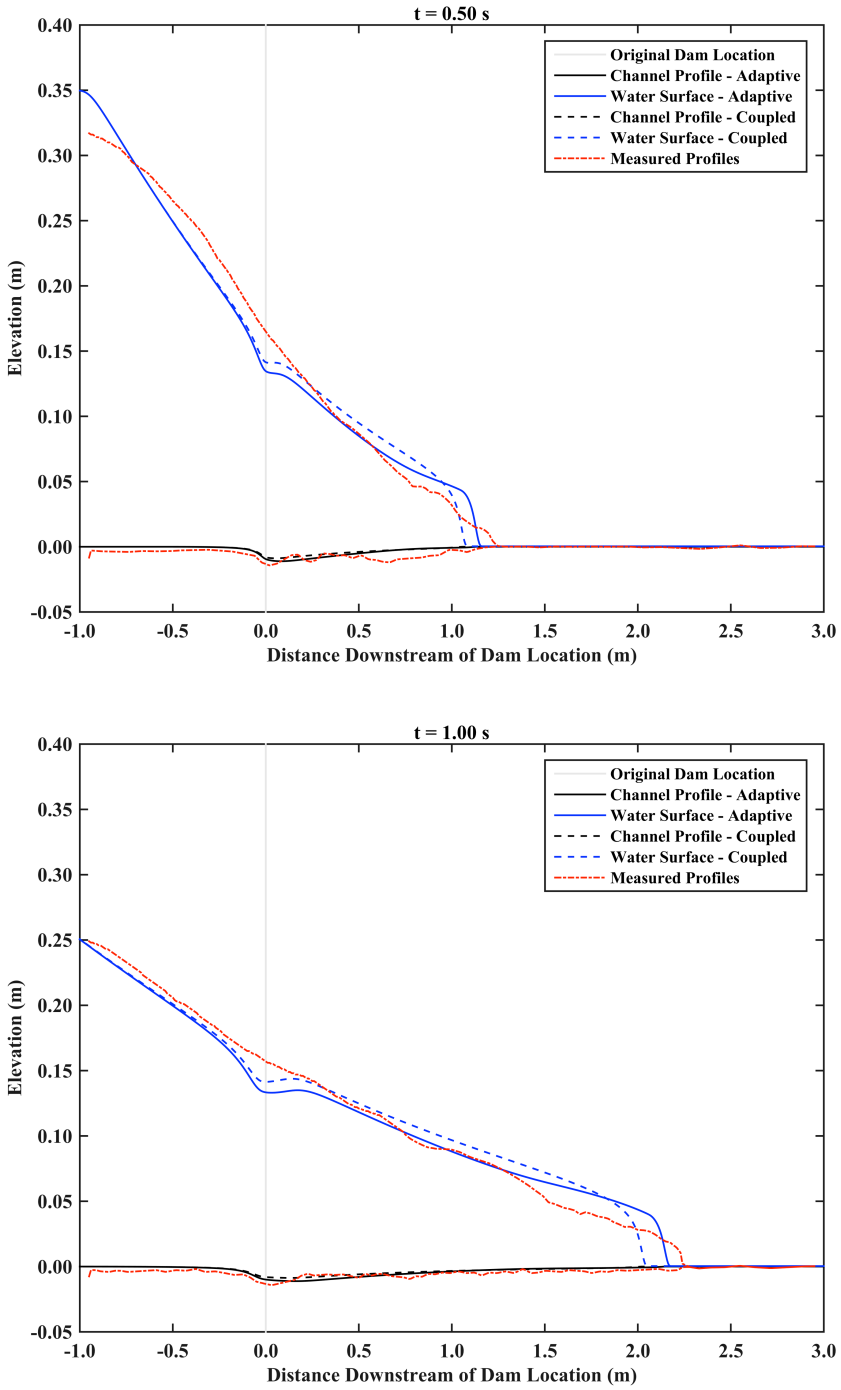

Figure 2-6: Water surface and riverbed elevation profiles at 0.5 s and 1 s after the release of the dam-break wave

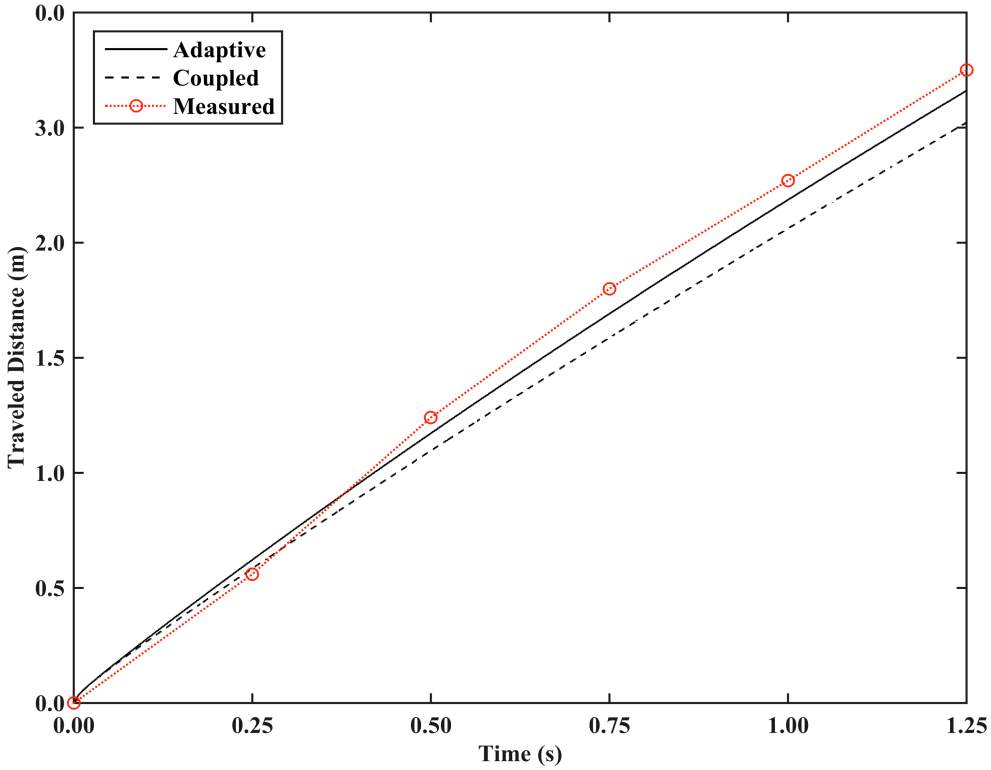

Figure 2-7: Rate of propagation of dam-break wave forefront

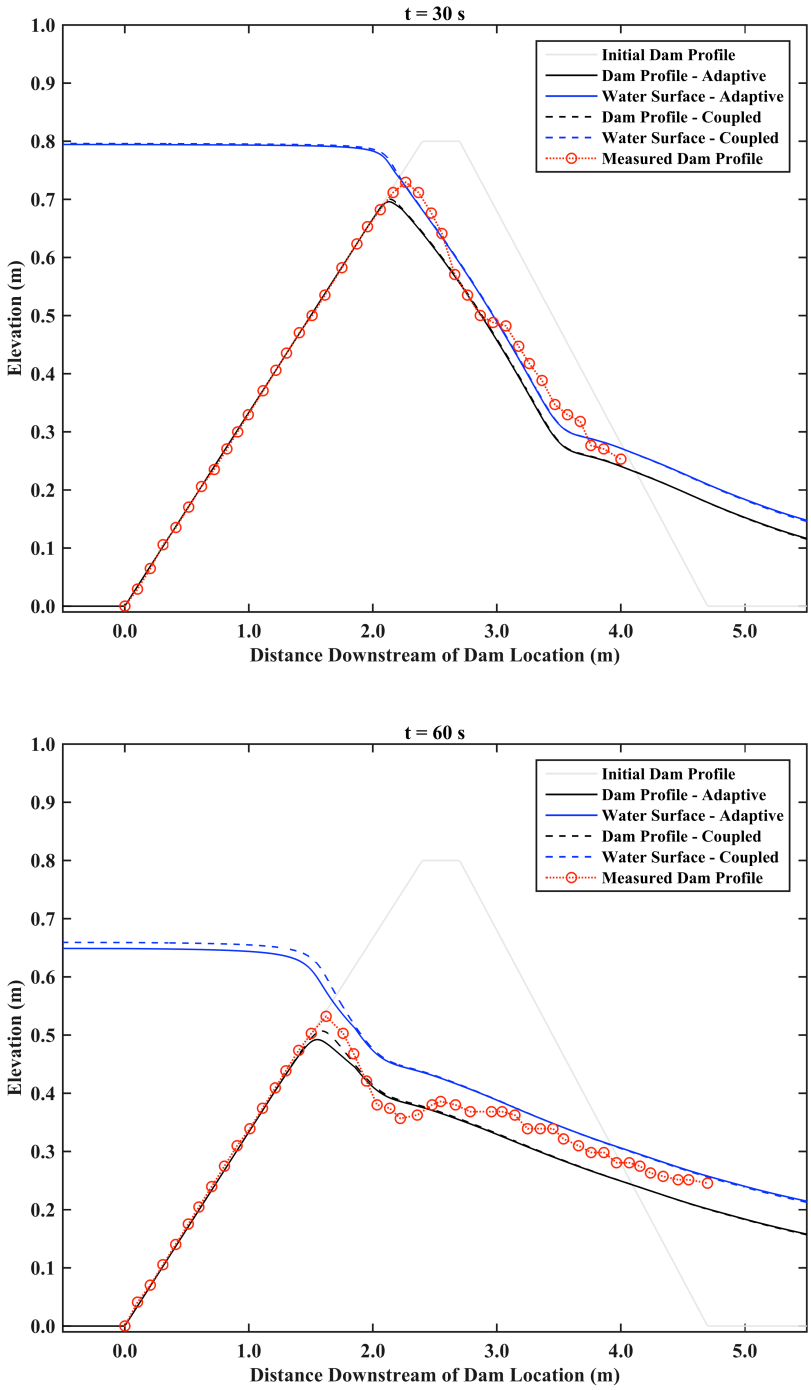

Figure 2-8: Riverbed elevation profiles at 30 s and 60 s after the onset of overtopping flow

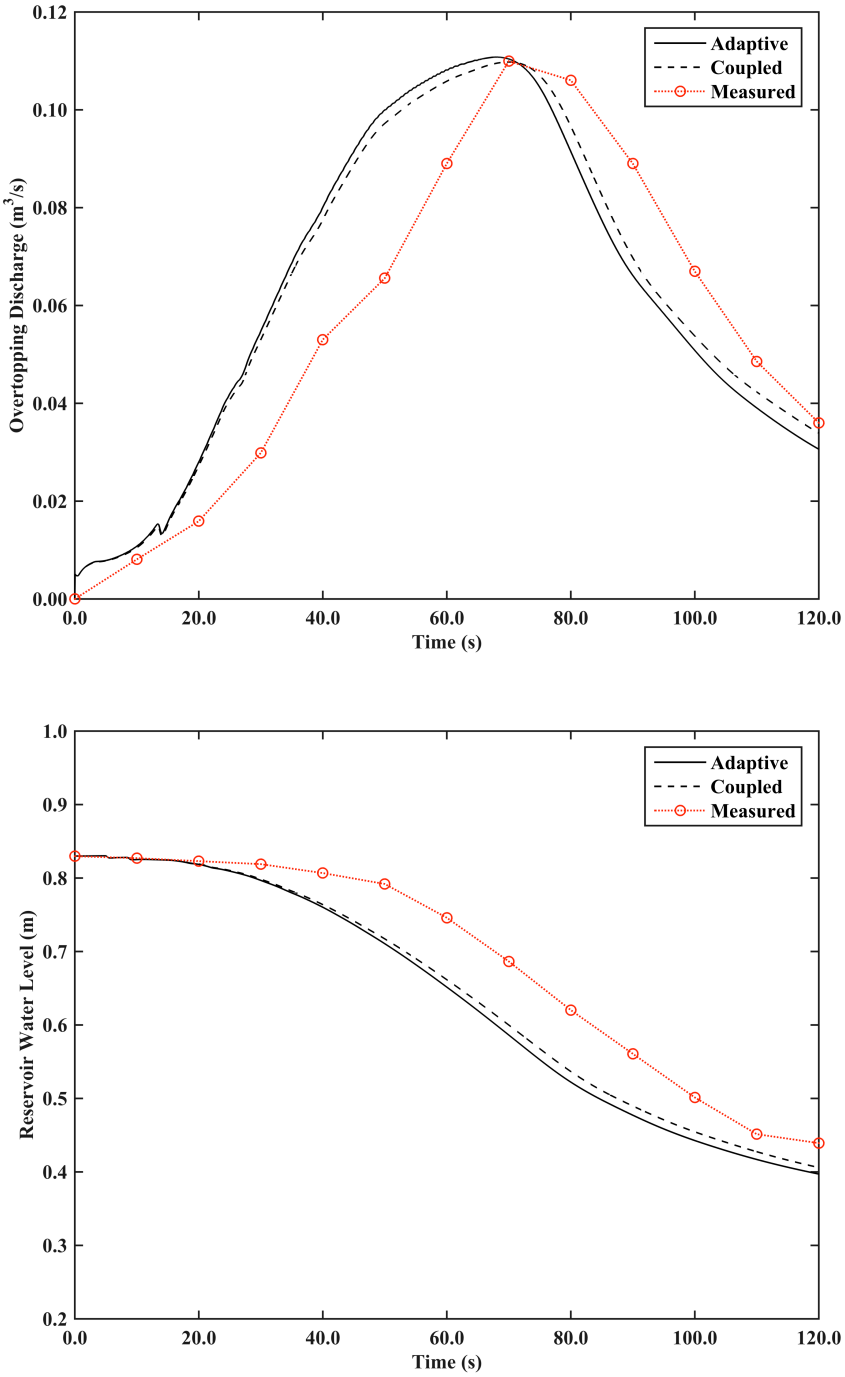

Figure 2-9: Overtopping discharge and water level at the reservoir during the degradation process of the embankment

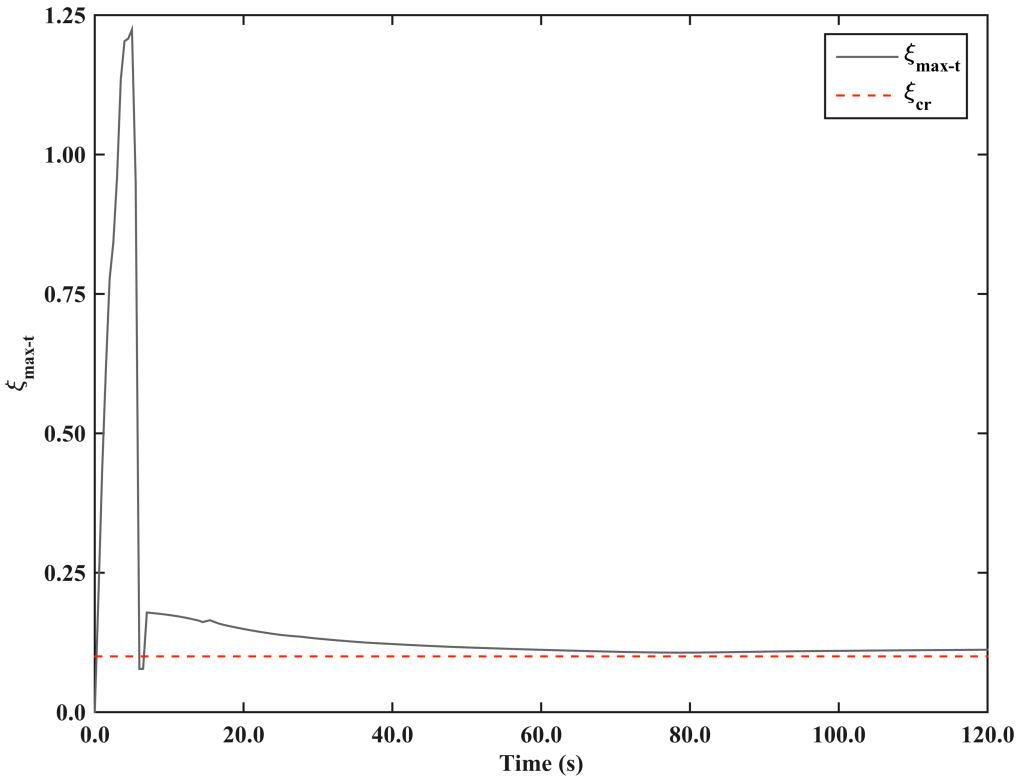

Figure 2-10: Variation of ξ_{max-t} during the evaluated time period

CHAPTER 3. NUMERICAL ANALYSIS OF THE PROPAGATION OF FINE-GRAINED SEDIMENT PULSES IN ALLUVIAL RIVERS

Abstract

A numerical analysis to characterize the propagation of fine-grained sediment pulses in alluvial rivers is presented in this paper. The objective is to identify the properties of these types of pulses and those of riverine environments that are more relevant to their downstream migration. To accomplish this, numerical tests are carried out to investigate the influence of the pulse grain size distribution and volume, as well as the influence of the ambient discharge and channel slope, on the dominant propagation mechanisms. Results indicate that the reconfiguration of the deposited material is governed by an initial dispersion-dominated phase during which there is a rapid movement of the pulse forefront, followed by a subsequent phase characterized by a pronounced translational movement of the pulse apex. The transition between these two phases is controlled by the value of the Froude number over the pulse topography, whereas their intensity and duration are dictated by the magnitude of the evaluated properties.

3.1. Introduction

Sediment pulses are defined as large amounts of loose sediment that are suddenly deposited in river corridors due to the action of external factors or processes of natural or anthropogenic origin. Such factors and processes include landslides (e.g. Iverson et al., 2015), debris flows from tributaries (e.g. Garcia-Martinez and Lopez, 2005), volcanic eruptions (e.g. Major et al., 2016), dam removal projects (e.g. Wilcox et al., 2014), and mining-related activities (e.g. Petticrew et al., 2015). Their occurrence is associated with a surplus in sediment load to downstream reaches, and therefore, with severe channel aggradation and degradation, significant floodplain deposition, increase in flood frequency, damage of infrastructure, and impairment of aquatic habitats (e.g. Storey et al., 2009; Hatten et al., 2015).

Two characteristic behaviors, namely, dispersion and translation, have been identified as the dominant propagation mechanisms of sediment pulses through the combination of laboratory experiments (e.g. Sklar et al., 2009), numerical modeling (e.g. Cui and Parker, 2005), and field studies (e.g. Thomas et al., 2015). In particular, Cui et al. (2003a) examined the influence of the pulse grain size distribution on the overall propagation behavior. Their experimental results suggest that, in gravel-bed streams, dispersion governs the evolution of coarse-grained pulses (i.e. formed by particles in the gravel size range), whereas those composed of fine-grained material (i.e. formed by particles in the sand size range) exhibit an important degree of translation during their downstream migration. More recently, flume experiments by Sklar et al. (2009) and Venditti et al. (2009) examined how sediment pulses evolve in armored (gravel) channels and verified these findings, indicating that the amount of deposited material also affects the dominant propagation mechanism, with smaller volumes enhancing the magnitude of the translational component.

Regarding numerical modeling efforts, the model of Cui and Parker (2005) has been used as the foundation for the majority of existing models intended to simulate the propagation of sediment pulses (e.g. Cui et al., 2003b; Cui et al., 2006a, 2006b; Cui and Wilcox, 2008). Cui and Parker (2005) developed a one-dimensional (1-D) decoupled model for

gravel-bed rivers, which describes the flow field by means of the St. Venant shallow water equations for clear-water flow, accounts for the conservation of sediment through the Exner equation for gravel mixtures (Parker, 1991a, 1991b), and considers the transport of granular material only as bedload according to the equation derived by Parker (1990a, 1990b). Even though it has been reported that this model performs well in the event of coarse-grained sediment pulses, numerical tests carried out by Cui et al. (2003b) and Cui et al. (2006a, 2006b) revealed that it underestimates the rate of propagation of fine-grained pulses when compared to the experimental results of Cui et al. (2003a). This limitation was still observed even when a more adequate framework based on Brownlie (1983) was adopted to compute sediment transport rates and boundary friction values. Likewise, a field monitoring campaign undertaken by Cui et al. (2014) showed that the model of Cui and Wilcox (2008) under predicted the initial evolution of a dam-break induced sediment pulse after the removal of Marmot Dam in the Sandy River, Oregon, USA (Major et al., 2012). They indicated that this initial period was characterized by high concentrations of suspended sediments and rapid morphodynamic adaptations in the river reach located downstream of the site.

As indicated in the preceding paragraphs, the bulk of the work that has been performed to date focuses primarily on studying the propagation of sediment pulses in gravel-bed streams. These types of streams are characterized by (1) high values of the Froude (*Fr*) number (which is defined as $Fr = u / [gh]^{0.5}$ where u is the flow velocity, h is the water depth, and g is the acceleration of gravity) (e.g. Grant, 1997), which as suggested by Lisle et al. (2001), promote the dispersive behavior of sediment pulses, (2) a limited mobility of the riverbed due to the presence of armor layers that restrict entrainment of material and facilitate the transport of finer sediment placed over a considerably coarser bed (e.g. Cui et al., 2003a), (3) low concentrations of suspended solids in the water column, and (4) sediment moving downstream predominantly as bedload (e.g. Church, 2010). Accordingly, the aforementioned numerical models have adopted a formulation and solution technique based on the decoupled modeling approach. This approach neglects the impact of morphodynamic processes on the flow field based on the premise that the time scale for sediment transport and riverbed evolution (i.e. the morphodynamic time

scale) is much longer than that corresponding to water flow changes (i.e. the hydrodynamic time scale).

In the case of fine-grained pulses, however, morphodynamic processes that occur during the initial short-term propagation phase (e.g. Wilcox et al., 2014) are characterized by suspended-load driven regimes that have the capacity to transport large amounts of fine sediment and cause a rapid movement of the deposited material. These processes do have an impact on the surrounding flow field, and therefore, hinder the use of the decoupled modeling approach for simulating the particularities of this initial period (e.g. Cao et al., 2002; Cui et al., 2014). Furthermore, the occurrence of sediment pulses in alluvial rivers (e.g. Zinger et al., 2011) has received rather limited attention despite the fact that the governing hydrodynamic and morphodynamic conditions are considerably different from those of gravel-bed streams. It is expected that relevant features of alluvial rivers, such as the relatively low values of *Fr* (e.g. Wright and Parker, 2004), and the dynamic and continuous interactions among water flow, the transport of sediment, and the morphological evolution of the riverbed, will indeed affect the propagation of sediment pulses.

The objective of the study presented in this paper is to characterize the behavior of fine-grained sediment pulses in alluvial rives by identifying the properties of these types of pulses and those of riverine environments that are most relevant to their downstream migration. Specifically, numerical tests are carried out to investigate the influence of the pulse grain size distribution and volume, as well as the influence of the ambient discharge and channel slope, on the dominant propagation mechanisms. The analyses are performed using the adaptive morphodynamic model of Castro-Bolinaga et al. (2016), which has the advantage that it allows us to directly assess the suitability of the decoupled modeling approach during the aforementioned initial short-term propagation phase. The intent is to provide a better understanding of the spatial and temporal scales associated with the migration of sediment pulses, in order to reduce the uncertainty related to the impact of these natural disasters and improve the capacity of river corridors to recover from their effects.

Initially, information about the numerical model of Castro-Bolinaga et al. (2016) is provided. This includes an overview of its main capabilities and adopted solution technique, along with details about the system of governing equations. Next, a description of the numerical tests is given, specifying the degree of variation considered for each of the selected variables, as well as the characteristics of the corresponding numerical simulations. Finally, the influence of these variables on behavior of fine-grained sediment pulses in alluvial rivers is assessed, and the results are discussed and contextualized.

3.2. Modeling Methodology

3.2.1. Overview of the Numerical Model

Castro-Bolinaga et al. (2016) developed a one-dimensional (1-D) adaptive morphodynamic model for water flow, sediment transport, and riverbed evolution in alluvial rivers. The model is formulated based on the St. Venant shallow water equations, the Exner equation for the conservation of sediment mass, and considers the movement of uniform granular material as both bedload and suspended load. The system of governing equations is solved using a novel solution methodology that applies either the decoupled or the coupled approach based on local flow and sediment transport conditions. Unlike the former approach, coupled modeling assumes that the hydrodynamic and morphodynamic time scales are of approximately the same order of magnitude, and therefore, accounts for the impact of sediment transport and riverbed evolution on the flow field. From a numerical perspective, this implies that the hydrodynamic governing equations are formulated for the conservation of mass and momentum of the water-sediment mixture rather than for those of clear-water flow (e.g. Wu, 2008). It has been reported that this approach is required to accurately simulate flows accompanied by pronounced morphodynamic processes (e.g. propagation of dam-break waves over erodible beds), characterized by having high concentrations of suspended solids in the water column along with a rapidly evolving riverbed (e.g. Cao et al., 2006; Wu and Wang, 2008).

The adopted solution methodology consists of a physics-based criterion to define the range of applicability of the aforementioned modeling approaches, together with an

adaptive numerical scheme to formulate and solve the system of governing equations. The criterion is based on a dimensionless parameter ξ that is proportional to the ratio of the morphodynamic to the hydrodynamic time scale, and depends on Fr and the depth-averaged volumetric concentration of total sediment load (C_t) as depicted in Equation 1. Therein, $R_s = (\rho_s - \rho_w) / \rho_w$ is the submerged specific gravity, ρ_w is the density of water, and ρ_s is the density of sediment particles. According to the magnitude of ξ and of an experimentally derived threshold ξ_{cr} equal to 0.1, two distinct modeling regions are defined, namely, a decoupled approach region characterized by $\xi < \xi_{cr}$, and a coupled approach region in which $\xi \geq \xi_{cr}$ (Castro-Bolinaga et al., 2016). The adaptive numerical scheme applies this criterion throughout the computational grid and formulates a consistent system of governing equations based on the local value of ξ. The adopted solution methodology, therefore, allows the use of the more suitable modeling approach within different sections of the domain without compromising the global accuracy and efficiency of the numerical model.

$$\xi = \frac{\left[C_t R_s\right]^{0.5}}{Fr} \tag{1}$$

In order to account for the effect of different grain sizes on the sediment pulse propagation behavior, the model of Castro-Bolinaga et al. (2016) is expanded in this study to consider non-uniform sediment transport conditions. These changes include adding the capabilities of handling fractional rates of bedload and suspended load transport, entrainment, and deposition, as well as the temporal variation of the riverbed material gradation. Details of the main revised equations are provided in the following section. The reader is referred to the original publication for a thorough description of other pertinent information, such as the empirical closure relations used or the implemented numerical methods.

3.2.2. Non-uniform Sediment Transport

The form of the St. Venant shallow water equations for the conservation of mass and momentum of the water-sediment mixture adopted by the model of Castro-Bolinaga et al. (2016) are written as:

$$\frac{\partial h}{\partial t} + \frac{\partial (uh)}{\partial x} = \psi \left[\frac{\partial z_b}{\partial t} \right] \tag{2}$$

$$\frac{\partial (uh)}{\partial t} + \frac{\partial (u^2 h)}{\partial x} + gh\left(\frac{\partial z}{\partial x} + S_f \right) = \psi \left[\left(\frac{\rho_s - \rho_w}{\rho} \right) \left(-g \frac{h^2}{2} \frac{\partial C_t}{\partial x} + u (C_{riverbed} - C_t) \frac{\partial z_b}{\partial t} \right) \right] \tag{3}$$

where t is time, x is the streamwise coordinate, z is the water surface elevation, z_b is the riverbed elevation, $\rho = \rho_w$ (1 - C_t) + ρ_s C_t is the density of the water-sediment mixture, $C_{riverbed} = 1 - \lambda_o$ is the volumetric concentration of sediment in the riverbed surface layer, λ_o is the porosity of the riverbed surface layer, and S_f is the friction slope. The variable ψ is utilized by the adaptive numerical scheme to locally formulate the system of governing equations throughout the computation domain. In the case of $\xi < \xi_{cr}$ (i.e. a point in the decoupled approach region), $\psi = 0$ and the RHS of Equations 2 and 3 are neglected, obtaining the expressions corresponding to clear-water flow conditions. On the other hand, if $\xi \geq \xi_{cr}$ (i.e. a point in the coupled approach region), $\psi = 1$ and the complete equations are used.

Separate equations for bedload and suspended load are considered for the sediment transport calculations. As in Castro-Bolinaga et al. (2016), the empirical bedload transport equation of Ashida and Michiue (1972) for the transport of sediment in the medium sand to fine gravel size range (0.3 mm < d_{50} < 7.0 mm, where d_{50} is the median grain size) is adopted in its non-uniform form as (Dey, 2014):

$$q_{B-k}^{*} = 17 \left(\tau_k^{*} - \tau_{cr}^{*} \right) \left(\sqrt{\tau_k^{*}} - \sqrt{\tau_{cr}^{*}} \right) \tag{4}$$

where q_{B-k}^{*} is the dimensionless bedload transport rate per unit channel width for sediment class k, $\tau_k^{*} = R_h S_f / R_s d_k$ is the dimensionless boundary shear stress for grain size d_k, R_h is the hydraulic radius, and τ_{cr}^{*} is the dimensionless critical boundary shear stress. Moreover, Equations 5 and 6 are used to compute the fractional and total volumetric bedload transport rates per unit channel width, respectively. In these equations, p_k represents the fraction of sediment contained in class k and N is the number of selected classes.

$$q_{B-k} = q_{B-k}^{*} p_k d_k \sqrt{R_s g d_k} \tag{5}$$

$$q_B = \sum_{k=1}^{N} q_{B-k} \tag{6}$$

Regarding suspended load transport, Equation 7 is applied to consider the streamwise variation of the fractional depth-averaged volumetric suspended sediment concentration (C_k) and its gradual adjustment towards equilibrium conditions. Such variation is dictated by the exchange rate of material between the water column and the mobile riverbed due to entrainment and deposition. The latter variables are calculated for each sediment class k as shown in Equations 8 and 9, where E_k is the fractional volumetric entrainment rate per unit riverbed area and D_k is the fractional volumetric deposition rate per unit riverbed area. Therein, $C_{b\text{-}k}^{*} = p_k\, C_b^{*}$ is the equilibrium fractional near-bed suspended sediment concentration, C_b^{*} is the equilibrium total near-bed suspended sediment concentration estimated through the relation of Ikeda and Izumi (1991) for each sediment class k, $C_{b\text{-}k} = \alpha\, C_k$ is the actual fractional near-bed suspended sediment concentration, α is the non-equilibrium adaptation coefficient of suspended load defined after Cao et al. (2004), and $w_{s\text{-}k}$ is the settling velocity of sediment particles of size d_k.

$$\frac{\partial(hC_k)}{\partial t} + \frac{\partial(uhC_k)}{\partial x} = E_k - D_k \tag{7}$$

$$E_k = w_{s-k} C_{b-k}^{*} \tag{8}$$

$$D_k = w_{s-k} C_{b-k} \tag{9}$$

The spatial and temporal deformation of the riverbed are determined by means of the Exner equation for the conservation of sediment mass as depicted in Equations 10 and 11. Lastly, the variation of the riverbed gradation in the vertical direction is accounted for by using the methodology presented in Wu and Wang (2008). Herein, in particular, the riverbed is divided into two layers, a top layer in which all particles are subject to entrainment by the flow, referred to as the active layer (Rahuel et al., 1989), and a substrate immobile layer located underneath (Wu, 2008). The variation of p_k is then determined based on mass balance as shown in Equations 12 and 13 (Wu and Wang, 2008), where δ_m is the thickness of the active layer estimated following Brunner (2016) and p_k^{*} is intended to recognize the influence of aggradation or degradation in the grain

size distribution of the active layer. It should be noted that for the derivation of Equations 12 and 13, it was assumed that the gradation of the substrate ($p_{k\text{-}sub}$) does not change with time.

$$(1-\lambda_o)\frac{\partial z_{b-k}}{\partial t} = -\frac{\partial q_{B-k}}{\partial x} + D_k - E_k \tag{10}$$

$$z_b = \sum_{k=1}^{N} z_{b-k} \tag{11}$$

$$\delta_m \frac{\partial p_k}{\partial t} = \frac{\partial z_{b-k}}{\partial t} - p_k^* \frac{\partial z_b}{\partial t} \tag{12}$$

$$p_k^* = p_k \quad if \quad \frac{\partial z_b}{\partial t} \geq 0 \quad \& \quad p_k^* = p_{k-sub} \quad if \quad \frac{\partial z_b}{\partial t} < 0 \tag{13}$$

3.3. Numerical Analysis

The numerical analysis consists of five different runs intended to investigate the influence of various characteristics pertinent to both the pulse itself and the riverine environment in which it propagates. In terms of the sediment pulse, its grain size distribution and volume were varied, whereas the ambient discharge and channel slope were selected as relevant parameters to characterize the riverine environment. The degree of variation considered for the selected variables is provided in Table 3-10. As denoted therein, the results of each run are compared against an initial base run to guarantee that they exclusively reflect the influence of the tested parameter.

3.3.1. Base Run

The purpose of the base run is to establish a reference set of results that permit an unbiased assessment of the effect of each of the selected parameters. To attain realistic hydrodynamic and morphodynamic conditions typically found in alluvial rivers, a prototype reach based on the Banister River was used for the numerical simulations. This river, located in the southern part of the state of Virginia, USA, is characterized as a sand-bed watercourse with a d_{50} that varies from 7.2 mm close to its confluence with Whitethorn Creek to a value of 0.75 mm about 17 km upstream of the Banister Lake Dam in the Town of Halifax, Virginia (Castro-Bolinaga and Diplas, 2014). Specifically, a 7.7

km long reach located between Riceville Road and Leda Road was selected as the prototype. The geomorphic features of this reach consist of an averaged bankfull channel width and depth equal to 31.1 m and 3.1 m, respectively, a mean channel slope of 0.349 m/km, and a riverbed formed by very coarse sand with a d_{50} of 1.55 mm. Castro-Bolinaga and Diplas (2014) estimated the bankfull discharge for this section as 111.9 m^3/s by means of stage-discharge predictor curves developed from riverbed sediment samples. Under these conditions, the mean flow velocity is equal to 1.16 m/s, which results in a value of *Fr* well into the subcritical flow regime of 0.21. As indicated by Wright and Parker (2004), the relatively low value of *Fr* even during high flows is an important characteristic that distinguishes large, low-slope sand-bed rivers.

In addition to the aforementioned reach characteristics, the base run considered a sediment pulse that blocked the entire channel, triggering an increase of water depth in the upstream section and a subsequent progressive degradation of its downstream slope due to overtopping flow. This scenario is representative, for instance, of the sediment pulse generated after the landslide that occurred near Oso, Washington, USA in March of 2014. During this massive event, an estimated 7.7 million cubic meters of material were deposited into the North Fork Stillaguamish River, blocking the stream channel and generating significant flooding in the surrounding area (USGS, 2014). A triangular pulse with an initial height equal to twice the average bankfull channel height (i.e. H_{pulse} = 6.2 m), a length of 1 km, and a material graduation identical to that of the riverbed was assumed, resulting in a total volume of deposited sediment of 96,410 m^3. For the numerical simulations, a rectangular channel of constant width was adopted based on the bankfull cross-sectional geometry of the prototype reach. Additionally, the inflowing water discharge was considered constant and equal to that of bankfull conditions (i.e. Q_{inlet} = 111.9 m^3/s), a Manning's *n* value of 0.030 was selected after Castro-Bolinaga and Diplas (2014), the magnitude of λ_o was estimated as 0.32 by using the formula of Wu and Wang (2006), and the spatial and temporal discretization parameters were set as Δx equal to 100 m and Δt equal to 1 s, respectively. It should be noted that for the numerical tests presented in this paper, only the variables indicated in Table 3-10 were altered; the remaining variables, initial conditions, and modeling parameters continued to be the same as those provided in this section.

3.3.2. Sediment Pulse Parameters

Runs 1 and 2 consider two additional grain size distributions of the sediment pulse in addition to that of the base run, in which the pulse was composed of the same material as the riverbed. Specifically, the propagation of a finer (d_{50} = 0.3 mm) and a coarser (d_{50} = 4.02 mm) pulse was examined (Figure 3-11) with the purpose of generating a direct comparison with the experimental results that have been obtained for similar conditions in gravel-bed channels (Cui et al., 2003a; Sklar et al., 2009; Venditti et al., 2009). The material gradation curves that are shown in Figure 3-11 correspond to riverbed sediment samples that were collected by Castro-Bolinaga and Diplas (2014) along the Banister River. Therefore, they are an accurate representation of material that could be potentially deposited in the study reach in the form of a sediment pulse due to, for instance, debris flow from tributaries.

The reduction of the sediment pulse volume was accomplished by decreasing its initial height. Hence, Run 3 was carried out with a value of H_{pulse} that was half the average bankfull channel height (i.e. H_{pulse} = 1.55 m), resulting in a total volume of deposited material of approximately 24,100 m^3. This particular run has the advantage that, in addition to assessing the influence of the pulse volume, it allows us to examine the effect that different initial hydrodynamic conditions have on the overall propagation. Since the pulse is not blocking the channel, water depth in the upstream section does not rise significantly, and the initial short-term propagation phase in not triggered by overtopping flow, but rather by a much milder increase in velocity as water flows over the disturbance.

3.3.3. Riverine Environment Parameters

The inflowing water discharge was reduced by a factor of 2 in Run 4, from its initial value of 111.9 m^3/s to a value of 55.95 m^3/s, while in Run 5 the considered channel slope was two times as large as that of the base run (i.e. S = 0.698 m/km). Both of these alterations directly impact the hydrodynamic conditions in the study reach. A decrease in inflowing discharge reduces flow velocities and sediment transport rates, while an increase in channel slope has the opposite effect, producing an increase in the magnitude of these two quantities. Therefore, these runs provide a measure of how different flow

regimes affect the propagation of sediment pulses, from low flow conditions as those encountered in Run 4, to relatively high flows as reflected in the ensuing increase of discharge that takes place in Run 5.

3.4. Results and Discussion

3.4.1. Base Run

Longitudinal profiles of the temporal variation of the sediment pulse height are shown in Figure 3-12. Results indicate that the initial deformation of the deposited material is dominated by dispersion, followed by a translational movement that begins when the pulse height is approximately the same as that of the channel bankfull level. This behavior is better illustrated if the evolution of the pulse apex is examined. As depicted in Figure 3-12, its initial trajectory is nearly vertical with negligible variation in the horizontal direction, which constitutes a key feature of dispersive pulses. As time progresses, however, the elevation of the apex starts to decrease rather slowly, accompanied by a more pronounced change in its horizontal position as it gradually migrates downstream. Such a relationship is typical of pulses experiencing a high degree of translation.

The variation of the propagation velocity of the sediment pulse forefront is closely related to the aforementioned behavior. Figure 3-13 indicates that during the initial dispersion-dominated period there is a rapid movement of the forefront, and then a progressive reduction of its velocity towards a much lower, nearly steady value. This variation is caused by a suspended-load driven regime that actively entrains material from the top part of the pulse, subsequently carrying the finer sediment further downstream while depositing the coarser particles close to the original forefront location. As the pulse height continues to decrease, the velocity in the surrounding flow field decreases as well, the sediment transport regime is no longer controlled by suspended load, and finer material that was able to travel long distances during the early propagation phase begins to deposit in the vicinity of the advancing forefront. This process is illustrated in Figure 3-14, where the variations of the mean, maximum, and minimum values of the pulse d_{50} are shown. As observed therein, there is an initial coarsening of the pulse material due to the large capacity of the flow to transport fine sediment, followed by a gradual fining of

its surface layer as the latter capacity starts to weaken. It should be noted that the locations of the maximum and minimum values of the pulse d_{50} shown in Figure 3-14 correspond to its upstream and downstream end, respectively.

To better understand the implications of the initial suspended-load driven regime during the propagation of fine-grained sediment pulses, the spatial and temporal variation of the ratio of suspended load to total load (Q_s/Q_t) is presented in Figure 3-15a, along with the location of the pulse forefront and apex. The magnitude of Q_s/Q_t shows that suspended load is indeed the dominant mode of sediment transport across the pulse topography during the initial dispersive period. Afterwards, it indicates that this mode of sediment transport is relevant only to the migration of the pulse forefront, where finer sediment is being continuously deposited and entrained by the surrounding flow, producing the gradual fining observed in Figure 3-14. Moreover, Figure 3-15a indicates that bedload transport is responsible for the translation component exhibited by the pulse, triggering the progressive downstream migration of its apex.

It was observed during the numerical simulations that the magnitude of *Fr* also affects the degree of dispersion and translation experienced by the pulse as shown in Figure 3-15b. Results suggest that the initial dispersive phase is characterized by high values of *Fr* (i.e. $Fr \sim 0.7\text{-}0.9$), whereas the onset of the translation component is caused by a sizable reduction of *Fr* (i.e. $Fr < 0.5$). This reduction is due to the continuous degradation of the pulse height that causes an ensuing reduction of the flow velocity and an increase of the water depth over its topography. The correlation depicted in Figure 3-15b agrees with the findings of Lisle et al. (2001), who indicated that high values of *Fr* (as those typically found in gravel-bed streams) enhance the dispersive behavior of sediment pulses, while translation would only be achieved if the magnitude of *Fr* is sufficiently low (as in the case of alluvial rivers even during high flow conditions).

From a numerical perspective, the coupled approach is required during the initial suspended-load dominated phase and becomes less relevant as time progresses. This is evidenced in Figure 3-16a by the computed magnitude of ξ during the entire simulation. As illustrated therein, the value of ξ is larger than ξ_{cr} in the early stages of the propagation, implying that the application of the coupled modeling approach is necessary

during this initial period. Subsequently, the value of ξ starts to decrease, resulting in sections of the computational domain where $\xi < \xi_{cr}$, and hence, where the decoupled modeling approach can be implemented. This tendency is demonstrated in Figure 3-16b, which shows the temporal variation of the largest value of ξ at a given time interval (i.e. $\xi_{max\text{-}t}$). Results denote that the coupled approach is indeed necessary during the initial short-term phase, and thereafter only along a progressively smaller section over the pulse as $\xi_{max\text{-}t}$ continuously approaches ξ_{cr}. These results are consistent with identified limitations of existing decoupled sediment pulse propagation models (e.g. Cui and Parker, 2005), which fail to capture the characteristics of the initial short-term phase associated with the occurrence of fine-grained pulses, but are able to adequately reproduce their long-term behavior.

3.4.2. Influence of Grain Size Distribution

The longitudinal profiles showing the variation of the finer and coarser sediment pulse heights (Figure 3-17a and Figure 3-17b, respectively) indicate that the overall behavior is similar to that of the base run, in which a dispersion component governs the initial reconfiguration of the deposited material, followed by a more noticeable translational movement once the pulse height is reduced to a certain threshold. The velocity propagation of the pulse forefront, however, does differ considerably depending on the evaluated grain size distribution. As depicted in Figure 3-18, the forefront of the finer pulse moves rather rapidly downstream, whereas that of the coarser pulse migrates at a much slower rate when compared to the propagation velocity of the base run. These different velocities are directly related to the initial capacity of the flow to transport fine material and its availability within the pulse gradation. During the first hour after the onset of overtopping flow, suspended load transport rates for the case of the finer pulse are as much as fourteen times larger than those corresponding to the coarser pulse, and approximately ten times larger than those of the base run. Nonetheless, once the finer sediment is carried out further downstream and the sediment transport capacity of the flow declines, the propagation velocity of the pulse forefront for the three evaluated grain size distributions converges to the same value. Therefore, the gradation of the pulse plays an important role during the initial suspended-load driven regime that governs the migration process, in which the flow has the capacity to entrain and transport large

amounts of fine material. This consideration is especially relevant if the pulse is primarily composed of very fine sediment in the silt and clay size range, because the high concentration of solids in suspension may have the potential to trigger hyperconcentrated flows during the propagation process (e.g. Wilcox et al., 2014).

The influence of Q_s/Q_t and the magnitude of *Fr* on the propagation behavior of the finer and coarser sediment pulses are shown in Figure 3-19 and Figure 3-20, respectively. Results indicate that suspended load governs the propagation of the finer pulse during a longer period of time when compared to the base run (Figure 3-19a). In the case of the coarser pulse, on the other hand, bedload transport is clearly the responsible mechanism for the deformation of the deposited material, with suspended load being important only for the migration of the pulse forefront (Figure 3-20a). Additionally, the influence of *Fr* on the overall behavior is similar to that described for the base run, in which the onset of the translation component occurs when the value of *Fr* is close to 0.4-0.5 (Figure 3-19b and Figure 3-20b). Hence, the pulse grain size distribution does not appear to have an impact on the relationship between the degree of translation and the dispersion, and the magnitude of *Fr*. Lastly, the variation of $\xi_{max\text{-}t}$ during the propagation of the finer and the coarser pulses is analogous to that of the base run (Figure 3-16b).

3.4.3. Influence of Pulse Volume

As illustrated in Figure 3-21, a reduction of the pulse height, and thus of its volume, results in a less pronounced dispersion-dominated deformation during the early propagation phase, along with the initiation of the translational component taking place much faster than in the case of the base run. Such behavior is due to the reduced capacity of the flow to entrain and transport sediment downstream, as the velocity over the pulse topography is not as large as that of the overtopping flow that continuously degrades the side slope of the pulse during the base run. This reduced transport capacity also influences the rate of propagation of the pulse forefront, initially causing a slower streamwise migration as shown in Figure 3-22. Eventually, the propagation velocity of the smaller pulse converges with that of the base run, comparable to the case of the finer and coarser sediment pulses described in the previous section. This phenomenon is

attributed to the continuous sorting of the pulse and riverbed material due to entrainment and deposition fluxes.

The overall propagation characteristics presented in Figure 3-21 and Figure 3-22 differ from those suggested by experimental results for the evolution of sediment pulses in gravel-bed channels (Sklar et al., 2009; Venditti et al., 2009), in which smaller pulses propagated downstream rapidly. The slower rate is closely related to the low magnitude of *Fr* as water flows over the smaller pulse. Figure 3-23b indicates that the value of this parameter remains quite low during the entire propagation process (i.e. $Fr \sim 0.2\text{-}0.3$). This constitutes a key difference with respect to the base run, as well as with the experimental setup of Sklar et al. (2009) and Venditti et al. (2009), in which high values of *Fr* (i.e. $Fr \sim 0.7\text{-}0.9$ and $Fr \sim 0.6\text{-}0.8$, respectively) characterize the hydrodynamics of the riverine environment, causing therefore a much more rapid movement of the sediment. Moreover, as shown in Figure 3-23a, there is a prolonged dominance of suspended load during the propagation of the smaller pulse because less intense bedload transport processes result from reduced values of the boundary shear stress. In general, the modified initial hydraulic conditions generated by the smaller pulse not blocking the entire channel, considerably alter the propagation mechanics and dominant transport modes. Moreover, the maximum value of $\xi_{max\text{-}t}$ is computed during the early stages of the simulation, followed by a continuous decrease of its magnitude towards ξ_{cr}. This implies that, similarly to previous runs, the application of the coupled modeling approach is necessary during the initial short-term phase despite the overall evolution of the smaller pulse happening at a slower rate.

3.4.4. Influence of Ambient Discharge

A reduction of the ambient discharge results in a predominantly dispersive pulse, as evidenced by the longitudinal profiles of pulse height and the temporal evolution of its apex shown in Figure 3-24. The high degree of dispersion is enhanced by a decrease of the overall capacity of the flow to move sediment as suspended load in the reach located downstream of the original pulse location. Additionally, the reduced flow velocity limits the entrainment of material, and produces a slower erosion rate of the pulse apex triggered by particles moving downstream primarily as bedload. When compared to the

base run, for instance, the maximum pulse height after 100 hours of simulation is approximately 35% larger in this case. These conditions result in material being deposited at a lower rate downstream, and hence, in a slower propagation velocity of the pulse forefront (Figure 3-25).

Figure 3-26a reveals that the propagation of the pulse core is governed by bedload transport, whereas that of its forefront by a combination of the latter mode and suspended load. Results of the influence of *Fr* on the overall behavior are consistent with those from the previous runs, indicating that the onset of the translation component takes place when the magnitude of *Fr* is close to 0.4-0.5. As depicted in Figure 3-26b, only a minor degree of translation is observed towards the end of the numerical simulation when *Fr* approaches the aforementioned threshold.

The relatively high values of *Fr* (i.e. *Fr* ~ 0.7-0.9) that are shown in Figure 3-26b during the bulk of the propagation period are due to the slowly degrading apex and the ensuing accelerating flow to surpass it. Nonetheless, it is interesting to note that these values are close to the average *Fr* that was measured during the laboratory experiments carried out to examine the propagation of pulses in gravel-bed channels (e.g. Cui et al., 2003a; Sklar et al., 2009; Venditti et al., 2009). The intent of this comparison is to highlight the major influence of *Fr* on the dominant propagation behavior, in which higher values of *Fr* promote a more pronounced degree of dispersion (e.g. Lisle et al., 2001) whereas lower values enhance the translational component as has been demonstrated in this study.

3.4.5. Influence of Channel Slope

The longitudinal profiles of pulse height presented in Figure 3-27 suggest that an increase in channel slope generates a rapidly moving sediment mass, characterized by an initial dispersion-dominated phase, as in the case of the base run, but then followed by a much more pronounced translation component as it continuously migrates downstream. This accelerated movement is due to the amplified water discharge that results from the increased channel slope, generating higher flow velocities, and therefore, augmenting the capacity to entrain large amounts of material and transport them as suspended load. Additionally, as indicated in Figure 3-28, the propagation velocity of the pulse forefront is initially faster than that corresponding to the base run, and then gradually decreases

towards a lower, nearly steady value, similar to the behavior observed in the runs described in the preceding sections.

Results presented in Figure 3-29a suggest that suspended load is the dominant mode of sediment transport during the initial propagation phase, and then becomes only relevant to the propagation of the forefront as the core region is subjected to primarily bedload transport processes. Moreover, Figure 3-29b shows that the magnitude of *Fr* is relatively high during the aforementioned initial phase, in part due to the large flow velocities and shallow water depths caused by the increase in channel slope. Consistent with the tendency observed in previous runs, the translation behavior starts to become more perceptible once *Fr* reaches a value of approximately 0.4-0.5. Lastly, the computed temporal variation of $\xi_{max\text{-}t}$ indicates that the coupled modeling approach is required during the early stages of the simulation, and then its application is limited to an increasingly smaller section of the pulse topography as its value continues to approach that of ξ_{cr}.

3.5. Conclusions

A numerical analysis to characterize the propagation of fine-grained sediment pulses in alluvial rivers has been presented in this paper. The objective was to identify the properties of these types of pulses and those of riverine environments that are more relevant to their downstream migration. To accomplish this, five numerical tests were carried out to investigate the influence of the pulse grain size distribution and volume, as well as the influence of the ambient discharge and channel slope, on the dominant propagation mechanisms. The analyses were performed with the adaptive morphodynamic model of Castro-Bolinaga et al. (2016), which was expanded in this study to consider non-uniform sediment transport conditions.

In the event of fine-grained sediment pulses in alluvial rivers, it was found that the reconfiguration of the deposited material occurs in two distinct phases. An initial dispersion-dominated phase in which there is a rapid movement of the pulse forefront, followed by a subsequent phase characterized by a pronounced translational movement of the pulse apex. The former phase is governed by suspended-load driven regimes that

actively entrain material from the top part of the pulse, carrying finer sediment further downstream while depositing coarser particles close to the original forefront location. During the latter phase, on the other hand, the velocity in the flow field surrounding the pulse topography decreases and the sediment transport regime is no longer controlled by suspended load, but rather by a combination of this mode of transport in the vicinity of the pulse forefront and bedload transport across the pulse core region.

The transition between the aforementioned phases is controlled by the magnitude of the Froude (*Fr*) number. Results suggest that the initial dispersive phase is characterized by high values of *Fr* (i.e. $Fr \sim 0.7\text{-}0.9$), whereas the translation component detected during the second phase is generated by a sizable decrease of *Fr* (i.e. $Fr < 0.5$). The numerical simulations indicated that, independently of the parameter being tested, the degree of translation is enhanced as the magnitude of *Fr* decreases, and the transition between dispersion and translation occurs around a threshold value of $Fr \sim 0.4\text{-}0.5$. Moreover, the influence of the evaluated parameters was observed to be relevant to the intensity and duration of each phase. The grain size distribution of the pulse, in particular, plays an important role during the initial suspended-load driven phase, in which the flow has the capacity to entrain and transport large amount of fine material downstream.

The hydrodynamic and morphodynamic conditions that govern the behavior of alluvial rivers, namely, relatively low values of *Fr*, a continuous interaction between water flow and the mobile riverbed, and sediment moving downstream primarily as suspended load, pose additional challenges to the propagation of sediment pulses when compared to gravel-bed streams. These include, for instance, the use of an adequate modeling approach as demonstrated by the results of this study. The intent is to develop a better understanding of the fundamental mechanisms that govern these types of flow hazards for improving our prediction tools, and consequently, our capacity to mitigate their impacts.

References

Ashida, K., Michiue, M., 1972. Study on Hydraulic Resistance and Bedload Transport Rate in Alluvial Streams. *Jpn. Soc. Civil Engineers* 206, 59-69 (in Japanese).

Brownlie, W.R., 1983. Flow Depth in Sand-Bed Channels. *J. Hydraul. Eng.* 109(7), 959-990.

Brunner, G.W., 2016. *HEC-RAS River Analysis System, Users Manual, Version 5.0*. US Army Corps of Engineers, Hydrologic Engineering Center, Davis, CA, USA.

Cao, Z., Day, R., Egashira, S., 2002. Coupled and Decoupled Numerical Modeling of Flow and Morphological Evolution in Alluvial Rivers. *J. Hydraul. Eng.* 128(3), 306-321.

Cao, Z., Pender, G., Wallis, S., Carling, P., 2004. Computational Dam-Break Hydraulics over Erodible Sediment Bed. *J. Hydraul. Eng.* 130(7), 689-703.

Cao, Z., Pender, G., Carling P., 2006. Shallow water hydrodynamic models for hyperconcentrated sediment-laden floods over erodible bed. *Adv. Water Resour.* 29, 546-557.

Castro-Bolinaga, C.F., Diplas, P., 2014. Hydraulic Modeling of Extreme Hydrologic Events: Case Study in Southern Virginia. *J. Hydraul. Eng.* 05014007.

Castro-Bolinaga, C.F., Diplas, P., Bodnar, R.J., 2016. An Adaptive Morphodynamic Model for Water Flow, Sediment Transport, and Riverbed Evolution in Alluvial Rivers, *Adv. Water Resour.* (under review).

Church, M., 2010. Gravel-Bed Rivers, in: Burt, T.P., Allison, R.J. (Eds.), *Sediment Cascades: An Integrated Approach*, Wiley.

Cui, Y., Parker, G., 2005. Numerical Model of Sediment Pulses and Sediment-Supply Disturbances in Mountain River. *J. Hydraul. Eng.* 131(8), 646-656.

Cui, Y., Wilcox, A., 2008. Development and Application of Numerical Models of Sediment Transport Associated with Dam Removal, in: Garcia, M.H. (Ed.), *Sedimentation Engineering: Theory, Measurements, Modeling, and Practice, ASCE Manual 110*, American Society of Civil Engineers, Reston, VA, USA.

Cui, Y., Parker, G., Lisle, T.E., Gott, J., Hansler-Ball, M.E., Pizzuto, J.E., Allmendinger, N.E., Reed, J.M., 2003a. Sediment pulses in mountain rivers: 1. Experiments. *Water Resour. Res.* 39(9), 1239.

Cui, Y., Parker, G., Lisle, T.E., Gott, J., Hansler-Ball, M.E., Pizzuto, J.E., Allmendinger, N.E., Reed, J.M., 2003b. Sediment pulses in mountain rivers: 2. Comparison between experiments and numerical predictions. *Water Resour. Res.* 39(9), 1240.

Cui, Y., Parker, G., Braudrick, C., Dietrich, W.E., Cluer, B., 2006a. Dam Removal Express Assessment Models (DREAM), Part 1: Model development and validation. *J. Hydraul. Res.* 44(3), 291-307.

Cui, Y., Braudrick, C., Dietrich, W.E., Cluer, B., Parker, G., 2006b. Dam Removal Express Assessment Models (DREAM), Part 2: Sample runs/sensitivity tests. *J. Hydraul. Res.* 44(3), 308-323.

Cui, Y., Wooster, J.K., Braudrick, C.A., Orr, B. K., 2014. Lessons Learned from Sediment Transport Model Predictions and Long-Term Postremoval Monitoring: Marmot Dam Removal Project on the Sandy River in Oregon. *J. Hydraul. Eng.* 04014044.

Dey, S., 2014. *Fluvial Hydrodynamics: Hydrodynamic and Sediment Transport Phenomena*. Springer.

Garcia-Martinez, R., Lopez, J.L., 2005. Debris flows of December 1999 in Venezuela, in: Jakob, M., Hungr, O. (Eds.), *Debris-flow Hazards and Related Phenomena*, Springer.

Grant, G.E., 1997. Critical flow constrains flow hydraulics in mobile-bed streams: A new hypothesis. *Water Resour. Res.* 33(2), 349-358.

Hatten, J.R., Batt, T.R., Skalicky, J.J., Engle, R., Barton, G.J., Fosness, R.L., Warren, J., 2015. Effects of Dam Removal on Tule Fall Chinook Salmon Spawning Habitat in the White Salmon River, Washington. *River. Res. Applic.* 2015.

Ikeda, S., Izumi, N., 1991. Stable Channel Cross-Sections of Straight Sand Rivers. *Water Resour. Res.* 27(9), 2429-2438.

Iverson, R.M., George, D.L., Allstadt, K., Reid, M.E., Collins, B.D., Vallance, J.W., Schilling, S.P., Godt, J.W., Cannon, C.M., Magirl, C.S., Baum, R.L., Coe, J.A., Schulz, W.H., Bower, J.B., 2015. Landslide mobility and hazards: Implications of the 2014 Oso disaster. *Earth Planet. Sci. Lett.* 412, 197-208.

Lisle, T.E., Cui, Y., Parker, G., Pizzuto, J.E., Dodd, A.M., 2001. The Dominance of Dispersion in the Evolution of Bed Material Waves in Gravel-Bed Rivers. *Earth Surf. Process. Landforms* 26, 1409-1420.

Major, J.J., O'Connor, J.E., Podolak, C.J., Keith, M.K., Grant, G.E., Spicer, K.R., Pittman, S., Bragg, H.M., Wallick, J.R., Tanner, D.Q., Rhode, A., Wilcock, P.R., 2012. *Geomorphic Response of the Sandy River, Oregon, to Removal of Marmot Dam*. US Geological Survey Professional Paper 1792, Reston, VA, USA.

Major, J.J., Bertin, D., Pierson, T.C., Amigo, A., Iroume, A., Ulloa, H., Castro, J., 2016. Extraordinary sediment delivery and rapid geomorphic response following the 2008-2009 eruption of Chaiten Volcano, Chile. *Water Resour. Res.* 52.

Parker, G., 1990a. *The ACRONYM series of PASCAL program for computing bedload transport in gravel rivers*. External Memorandum M-220, University of Minnesota, St. Anthony Falls Laboratory, Minnesota, USA.

Parker, G., 1990b. Surface-based bedload transport relation for gravel rivers. *J. Hydraul. Res.* 28(4), 17-436.

Parker, G., 1991a. Selective sorting and abrasion of river gravel. I: Theory. *J. Hydraul. Eng.* 117(2), 131-149.

Parker, G., 1991b. Selective sorting and abrasion of river gravel. II: Applications. *J. Hydraul. Eng.* 117(2), 150-171.

Petticrew, E.L., Albers, S.J., Baldwin, S.A., Carmack, E.C., Dery, S.J., Gantner, N., Graves, K.E., Laval, B., Morrison, J., Owens, P.N., Selbie, D.T., Vagle, S., 2014. The impact of a catastrophic mine tailings impoundment spill into one of North America's largest fjord lakes: Quesnel Lake, British Columbia, Canada. *Geophys. Res. Lett.* 42.

Rahuel, J., Holly, F., Chollet, J., Belleudy, P., Yang, G., 1989. Modeling of Riverbed Evolution for Bedload Sediment Mixtures. *J. Hydraul. Eng.* 115(11), 1521-1542.

Sklar, L.S., Fadde, J., Venditti, J.G., Nelson, P., Wydzga, M.A., Cui, Y., Dietrich, W.E., 2009. Translation and dispersion of sediment pulses in flume experiments simulating gravel augmentation below dams. *Water Resour. Res.* 45, W08439.

Storey, A.W., Marshall, A.R. and Yarrao, M., 2009. Effects of Mine-Derived River Bed Aggradation on Fish Habitat of the Fly River, Papua New Guinea, in: Bolton, B. (Ed.), *The Fly River, Papua New Guinea: Environmental Studies in an Impacted Tropical River System*, Developments in Earth and Environmental Sciences, Volume 9, Elsevier.

Thomas, R.J., Constantine, J.A., Gough, P., Fussell, B., 2015. Rapid Channel Widening Following Weir Removal Due to Bed-Material Wave Dispersion on the River Monnow, Wales. *River Res. Applic.* 31, 1017-1027.

US Geological Survey, 2014. *Science Features: Landslide in Washington State*. Available on-line at: http://www.usgs.gov/blogs/features/usgs_top_story/landslide-in-washington-state/ (Sep. 23, 2014).

Venditti, J.G., Dietrich, W.E., Nelson, P.A., Wydzga, M.A., Fadde, J., Sklar, L., 2010. Effect of sediment pulse grain size distribution on sediment transport rates and bed mobility in gravel bed rivers. *J. Geophys. Res.* 115, F03039.

Wilcox, A.C., O'Connor, J.E., Major, J.J., 2014. Rapid reservoir erosion, hyperconcentrated flow, and downstream deposition triggered by breaching of 38 m tall Condit Dam, White Salmon River, Washington. *J. Geophys. Res. Earth Surf.* 119.

Wright, S., Parker, G., 2004. Flow Resistance and Suspended Load in Sand-Bed Rivers: Simplified Stratification Model. *J. Hydraul. Eng.* 130(8), 796-805.

Wu, W., 2008. *Computational River Dynamics*. Taylor & Francis Group.

Wu, W., Wang, S.S.Y., 2006. Formulas for Sediment Porosity and Settling Velocity. *J. Hydraul. Eng.* 132(8), 858-862.

Wu, W., Wang, S.S.Y., 2008. One-dimensional explicit finite-volume model for sediment transport with transient flows over movable beds. *J. Hydraul. Res.* 46(1), 87-98.

Zinger, J.A., Rhoads, B.L., Best, J.L., 2011. Extreme sediment pulses generated by bed cutoffs along a large meandering river. *Nat. Geosci.* 4, 675-678.

Table 3-10: Degree of variation considered for the tested pulse and riverine environment properties

Run	Tested Parameter	Degree of Variation
Base Run	-	-
Run 1	Pulse Grain Size	Pulse d_{50} reduced by a factor of 0.2
Run 2	Distribution	Pulse d_{50} increased by a factor of 2.6
Run 3	Pulse Volume	Pulse height reduced by a factor of 4
Run 4	Ambient Discharge	River discharge reduced by a factor of 2
Run 5	Channel Slope	River channel slope increased by a factor of 2

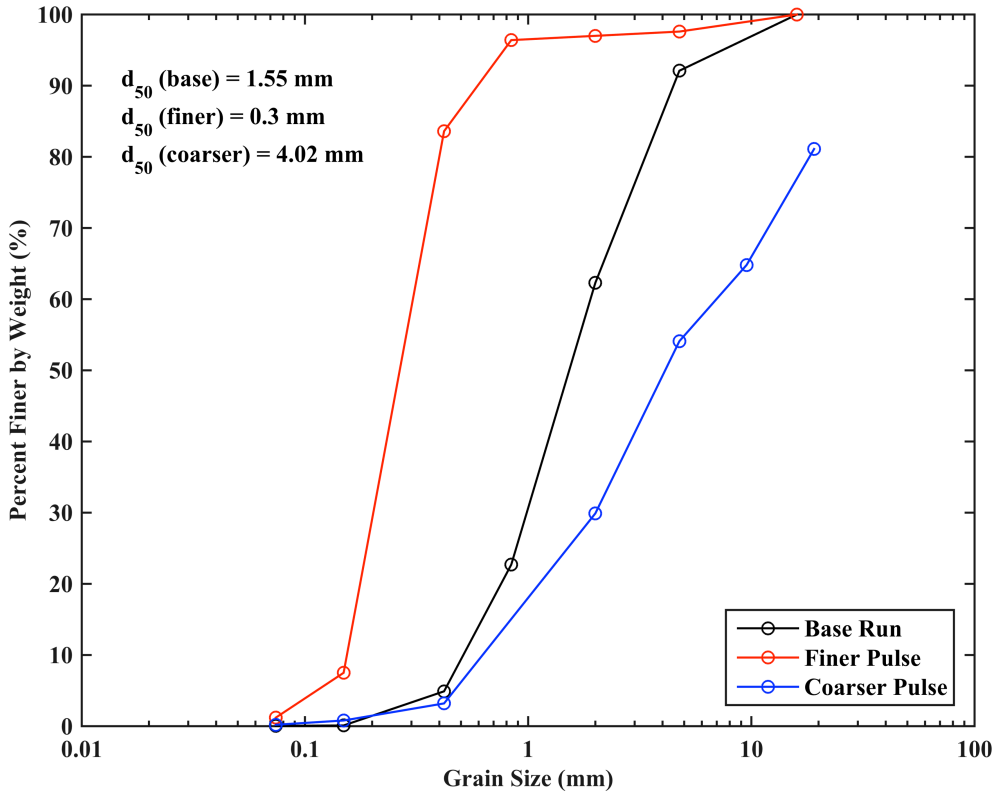

Figure 3-11: Sediment pulse grain size distributions considered for the numerical tests

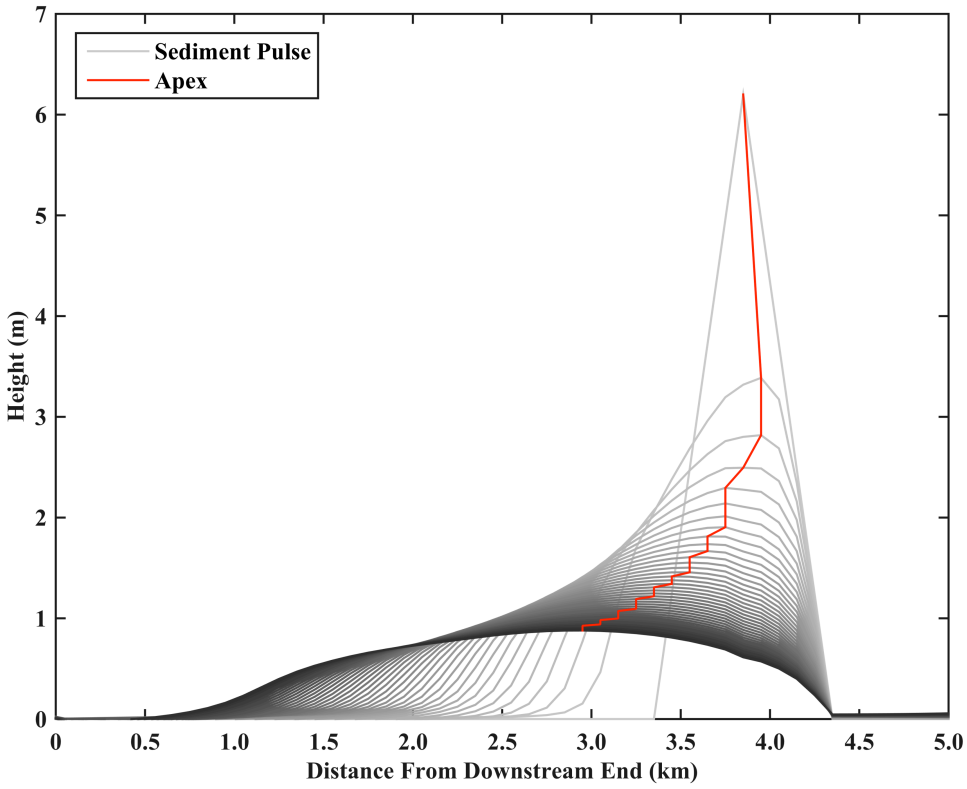

Figure 3-12: Longitudinal profiles of the temporal evolution of the sediment pulse height (profiles are shown every 5 hours)

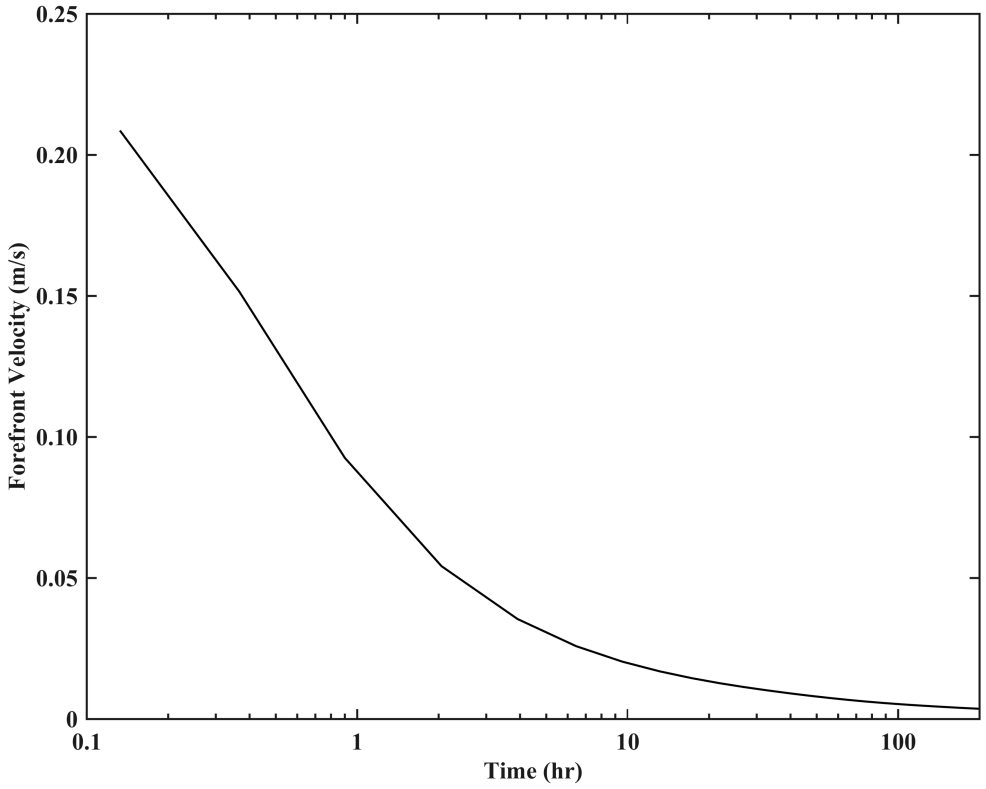

Figure 3-13: Propagation velocity of the sediment pulse forefront

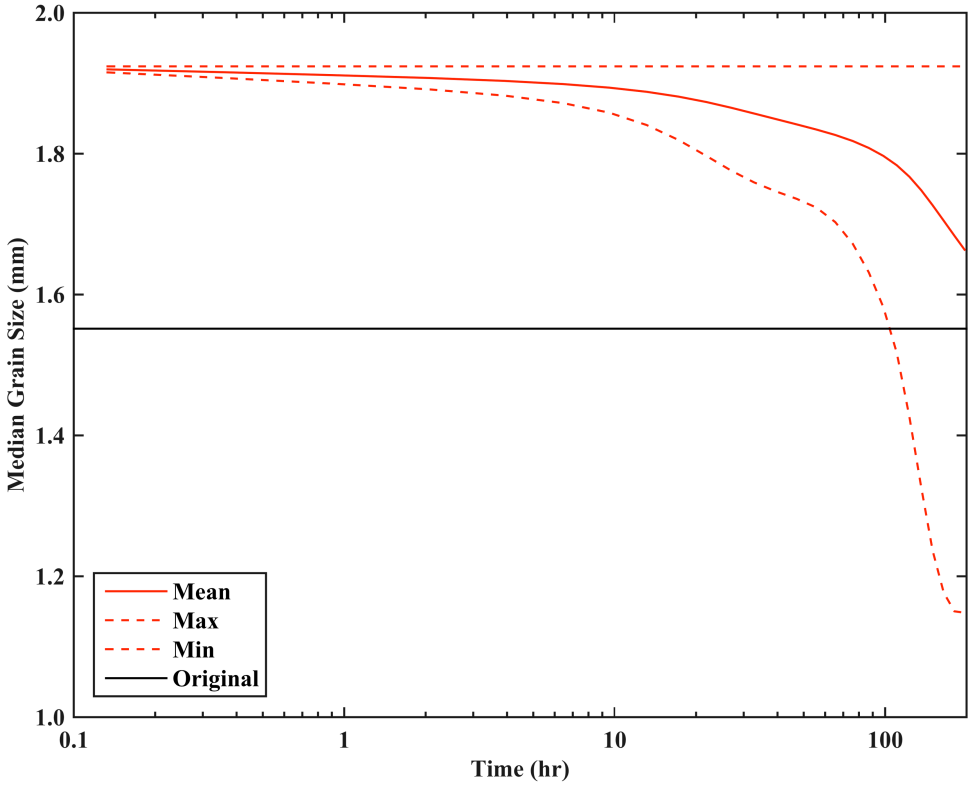

Figure 3-14: Variation of the mean, maximum, and minimum values of the pulse d_{50}

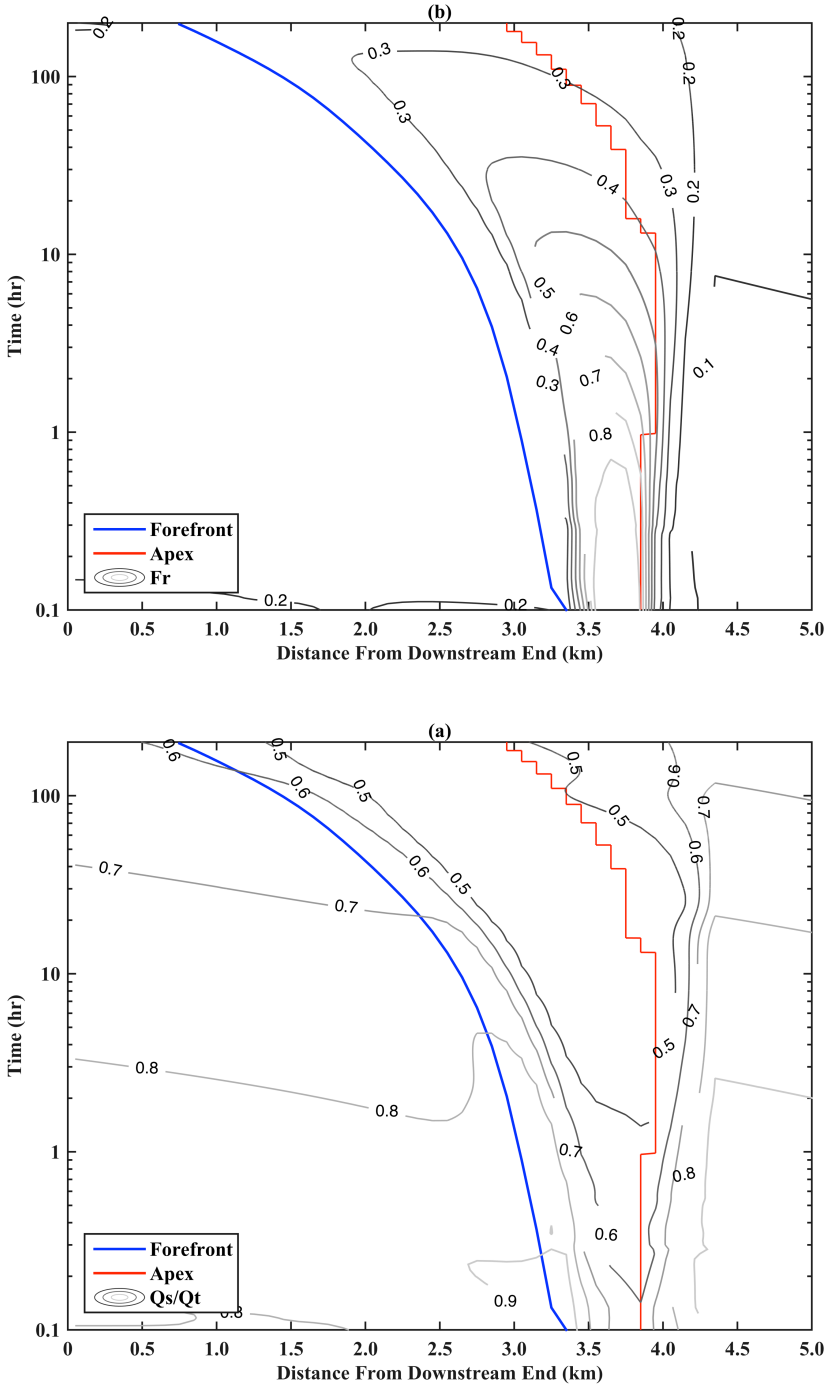

Figure 3-15: Influence of (a) the ratio of suspended load to total load and (b) the magnitude of the Froude number on the propagation behavior

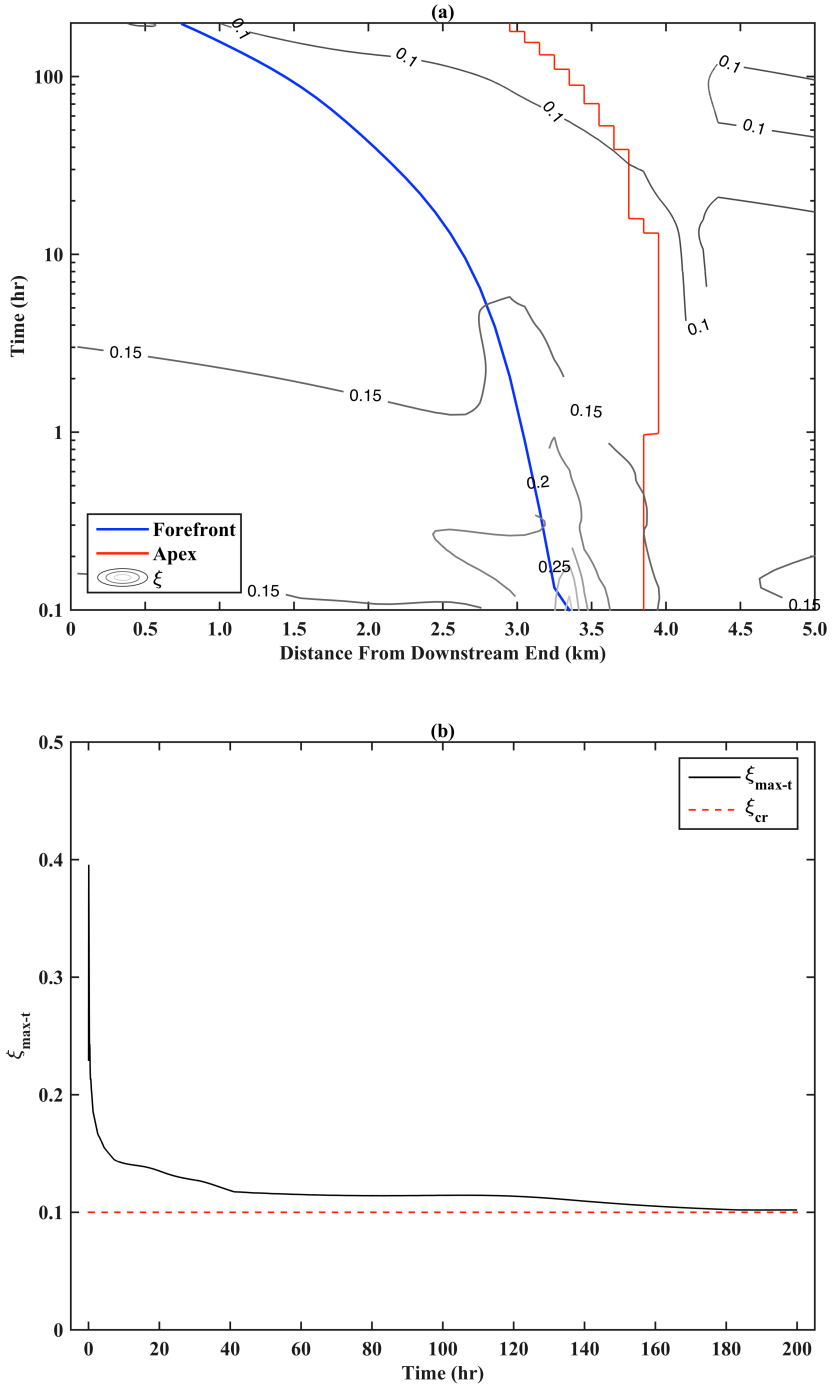

Figure 3-16: Influence of (a) the adaptive numerical scheme and (b) the maximum value of ξ per time interval on the propagation behavior

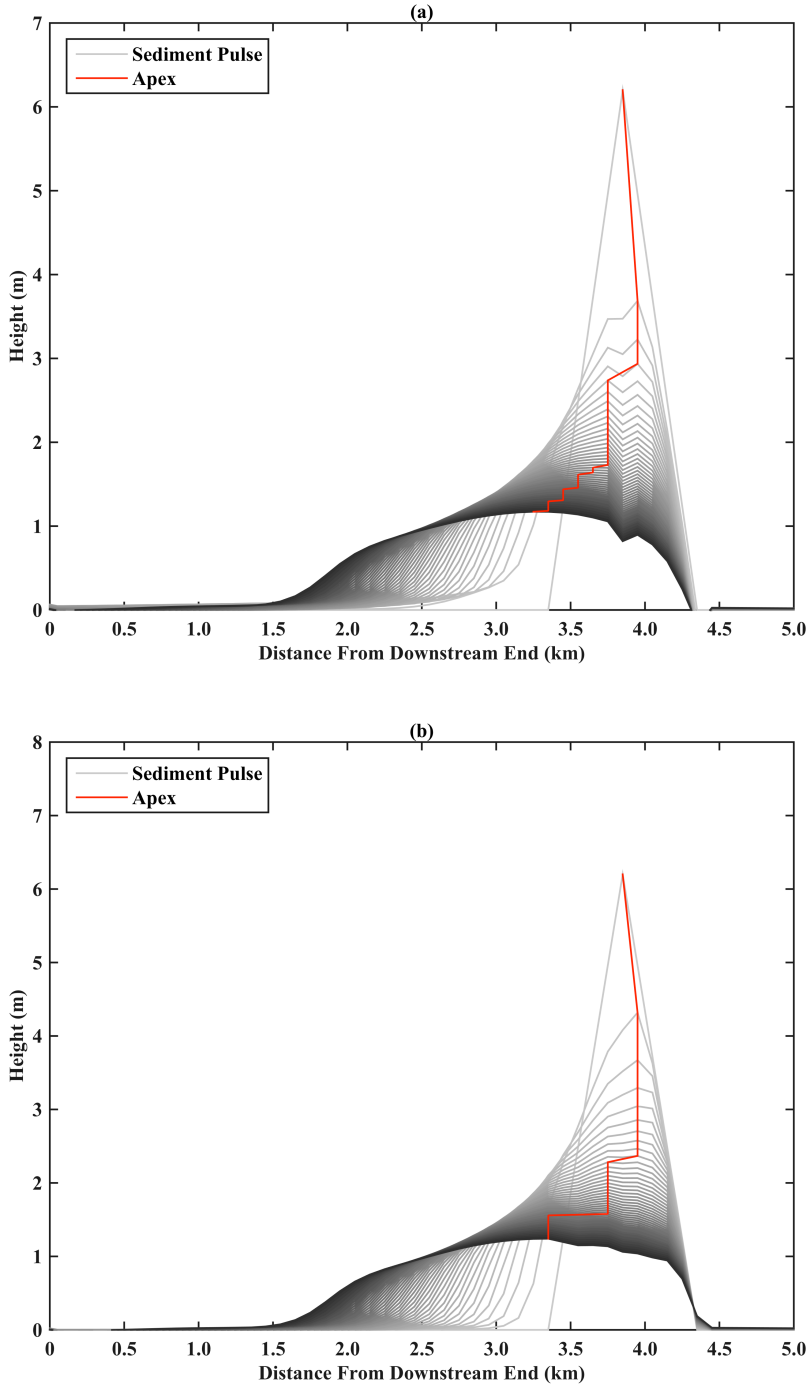

Figure 3-17: Longitudinal profiles of the temporal evolution of the sediment pulse height for (a) the finer pulse and (b) the coarser pulse (profiles are shown every 2 hours)

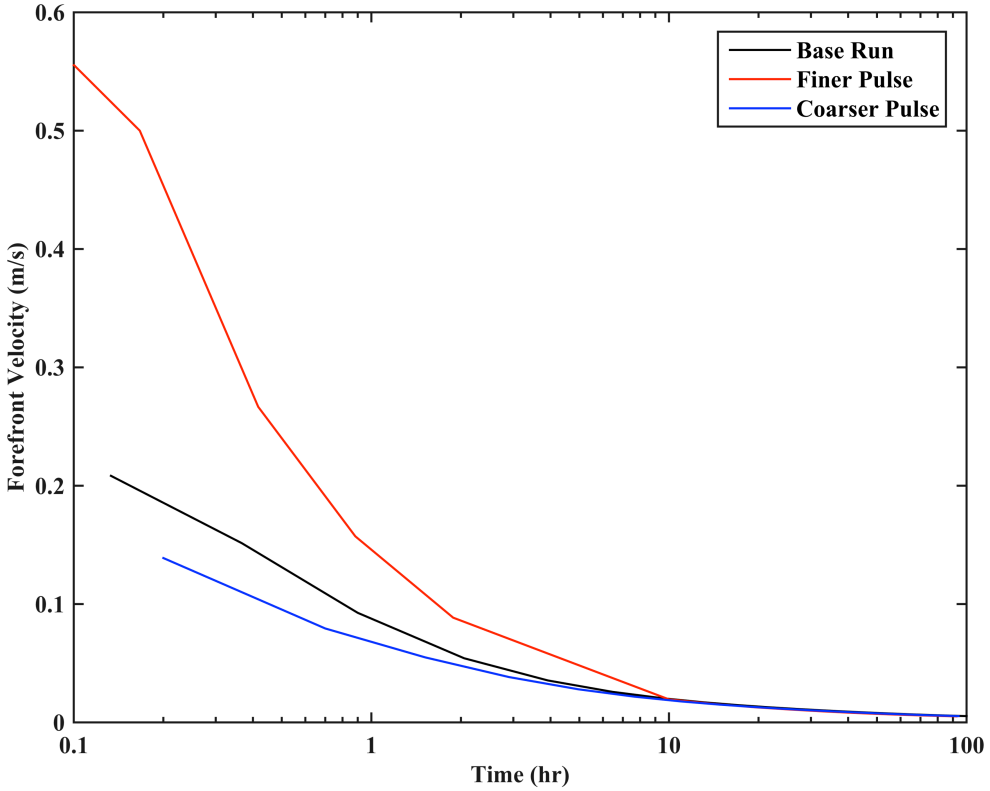

Figure 3-18: Comparison of the propagation velocity of the sediment pulse forefront

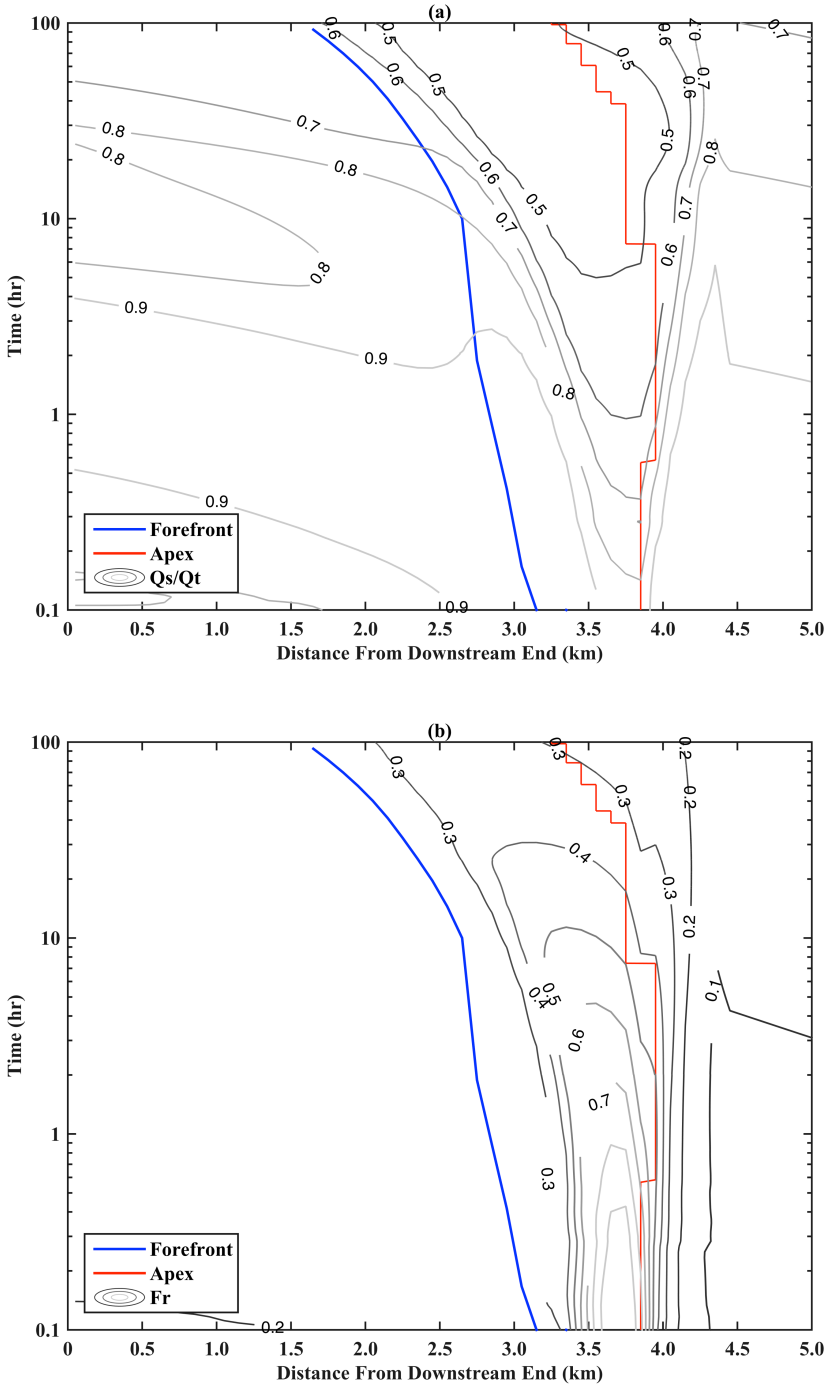

Figure 3-19: Influence of (a) the ratio of suspended load to total load and (b) the magnitude of the Froude number on the propagation behavior of the finer pulse

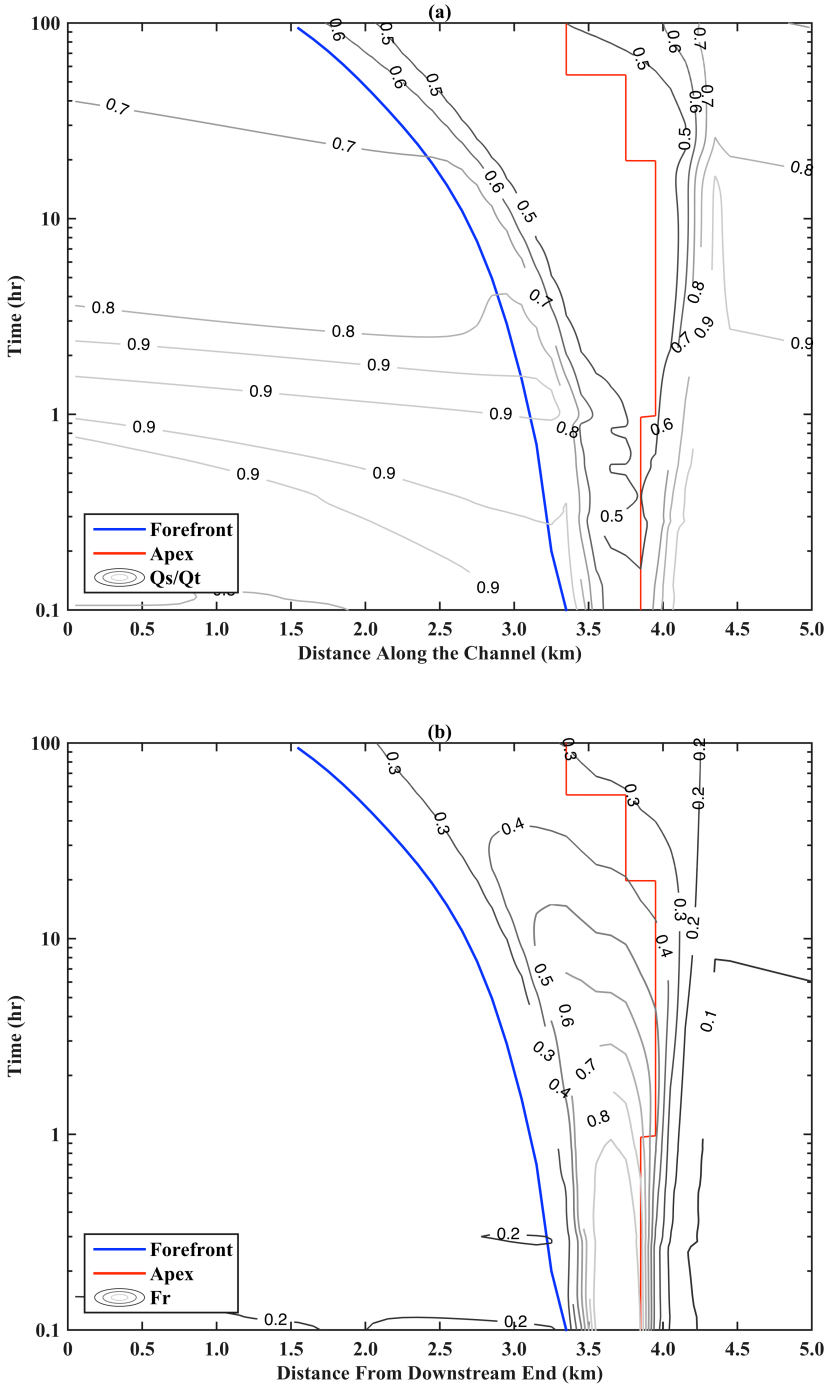

Figure 3-20: Influence of (a) the ratio of suspended load to total load and (b) the magnitude of the Froude number on the propagation behavior of the coarser pulse

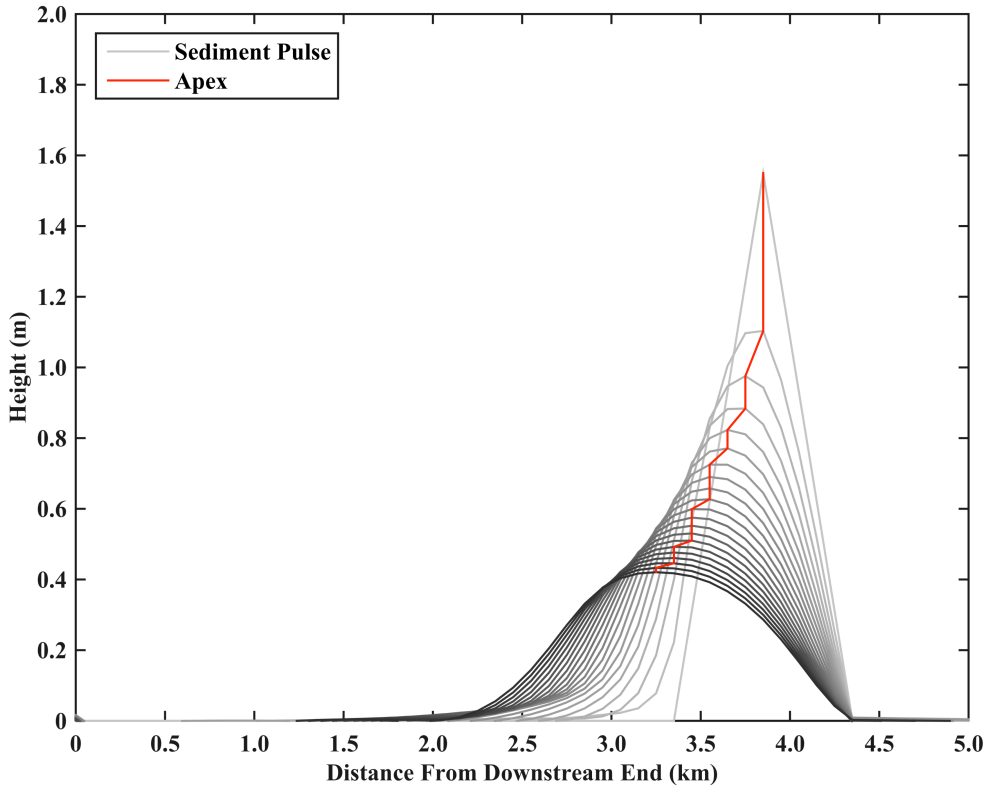

Figure 3-21: Longitudinal profiles of the temporal evolution of the sediment pulse height for a reduced volume (profiles are shown every 5 hours)

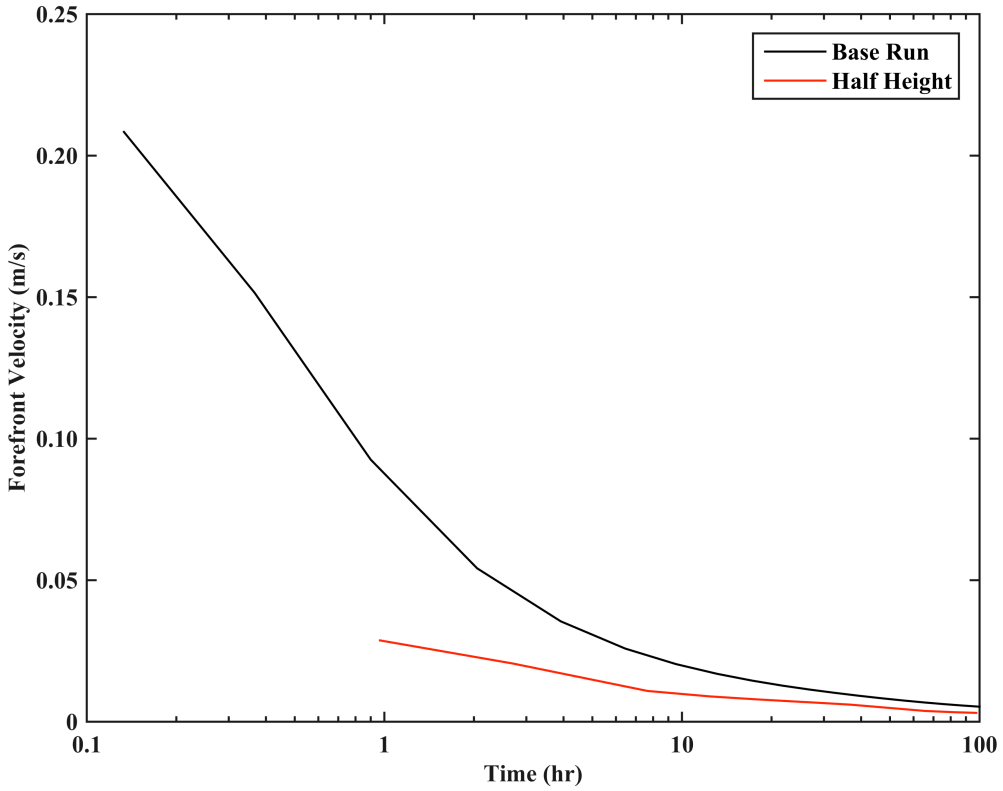

Figure 3-22: Comparison of the propagation velocity of the sediment pulse forefront for a reduced volume

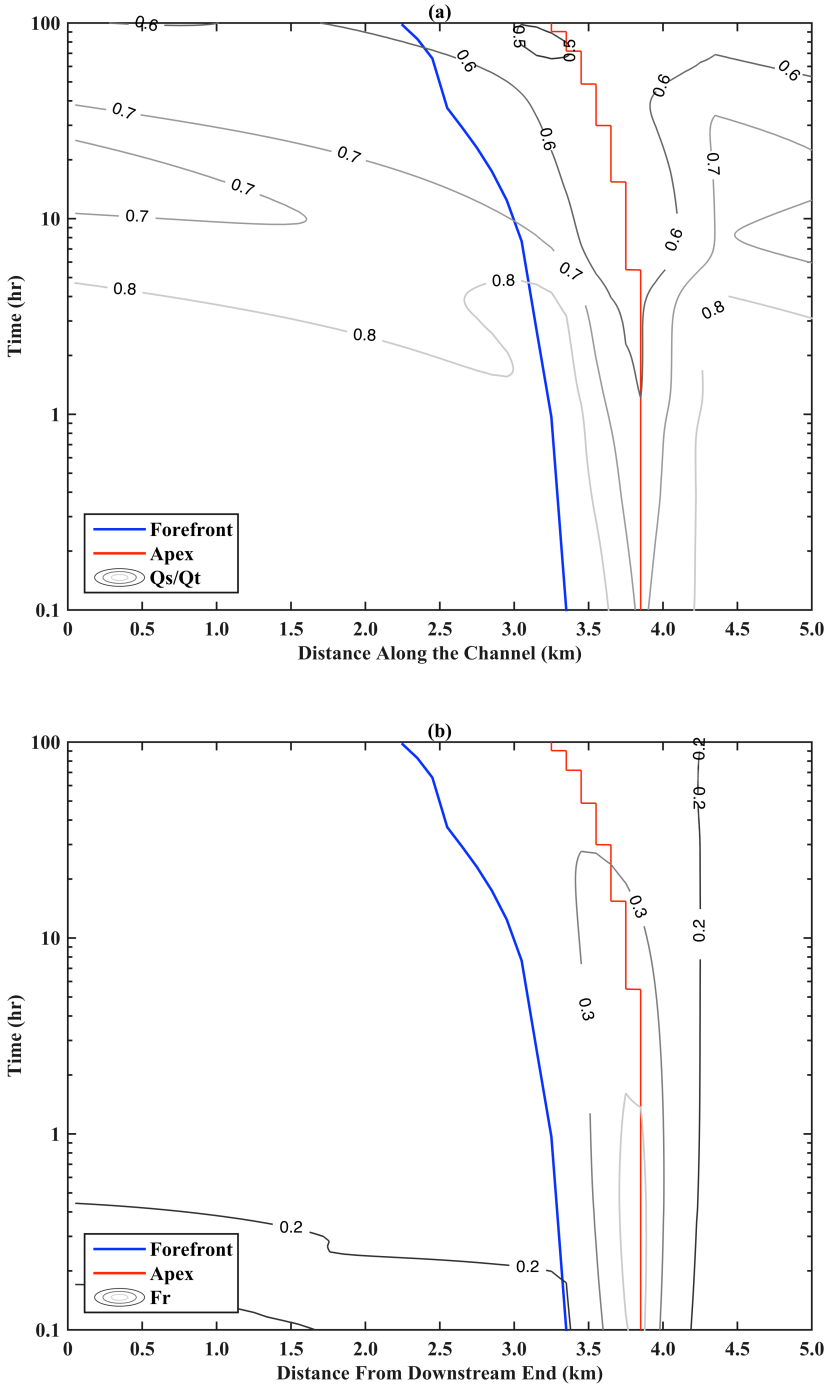

Figure 3-23: Influence of (a) the ratio of suspended load to total load and (b) the magnitude of the Froude number on the propagation behavior for a reduced volume

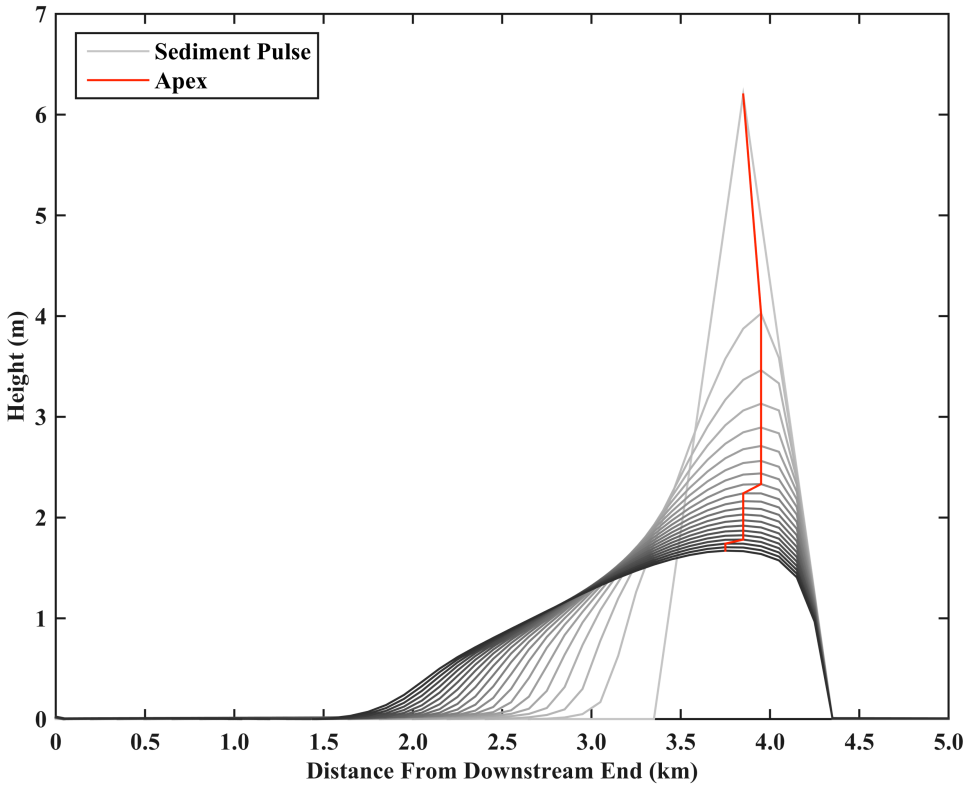

Figure 3-24: Longitudinal profiles of the temporal evolution of the sediment pulse height for a reduced ambient discharge (profiles are shown every 5 hours)

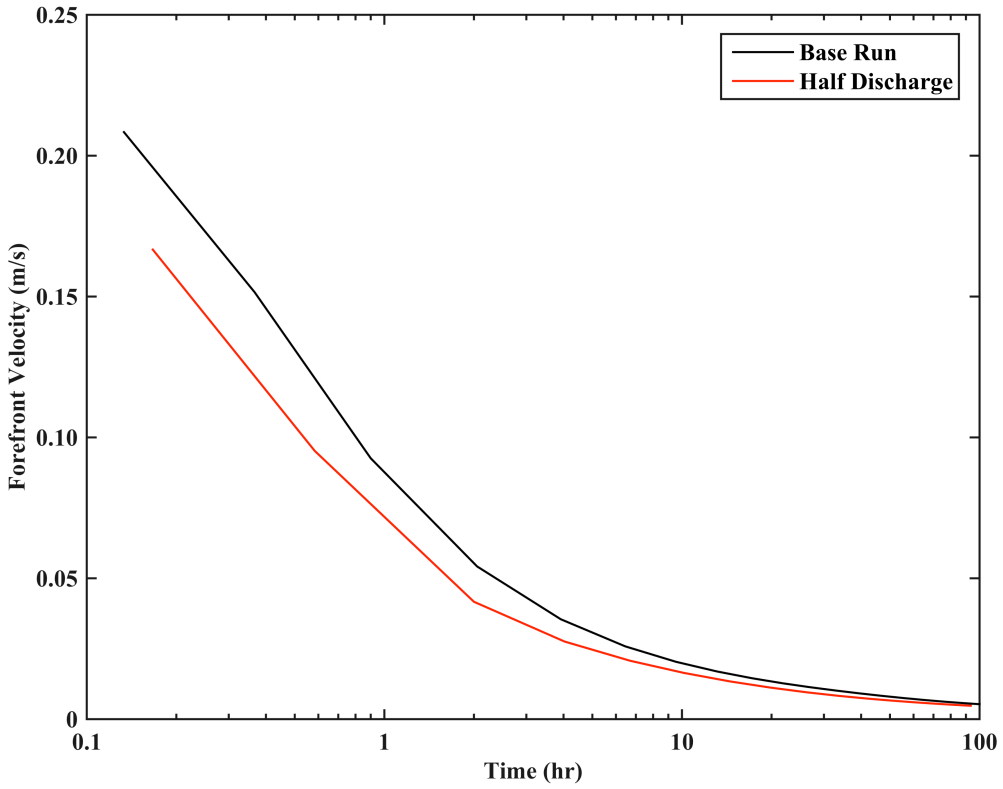

Figure 3-25: Comparison of the propagation velocity of the sediment pulse forefront for a reduced ambient discharge

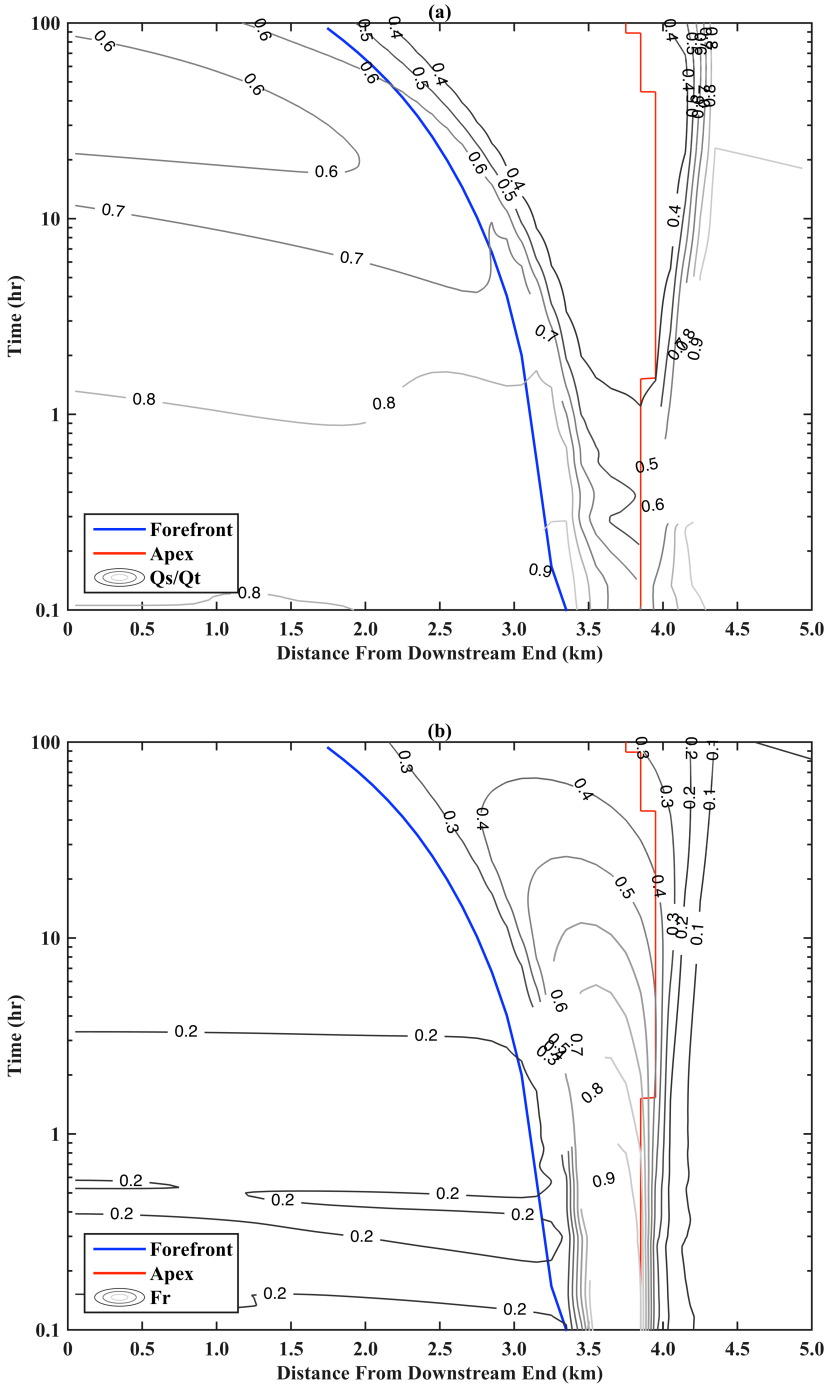

Figure 3-26: Influence of (a) the ratio of suspended load to total load and (b) the magnitude of the Froude number on the propagation behavior for a reduced ambient discharge

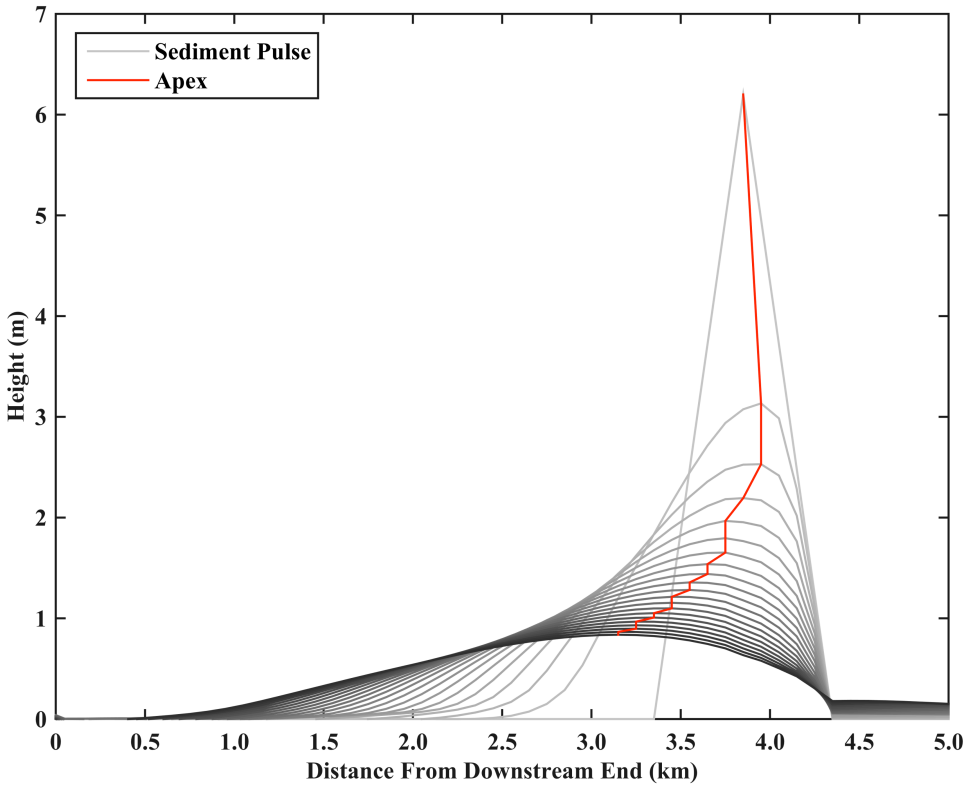

Figure 3-27: Longitudinal profiles of the temporal evolution of the sediment pulse height for an increased channel slope (profiles are shown every 5 hours)

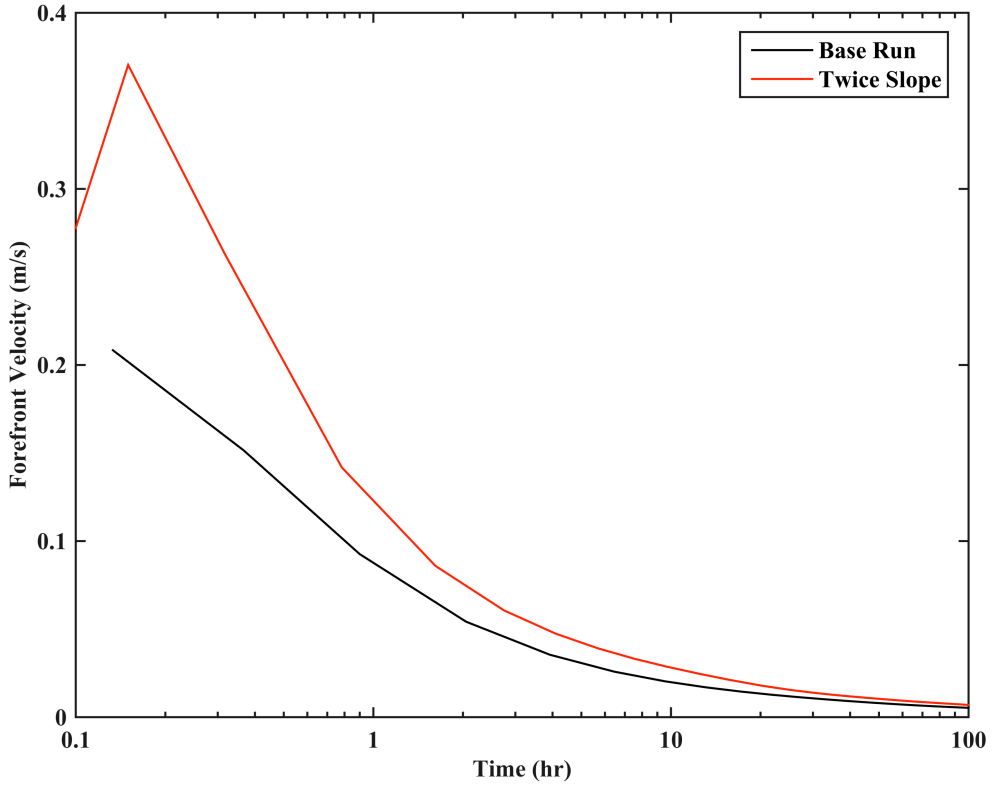

Figure 3-28: Comparison of the propagation velocity of the sediment pulse forefront for an increased channel slope

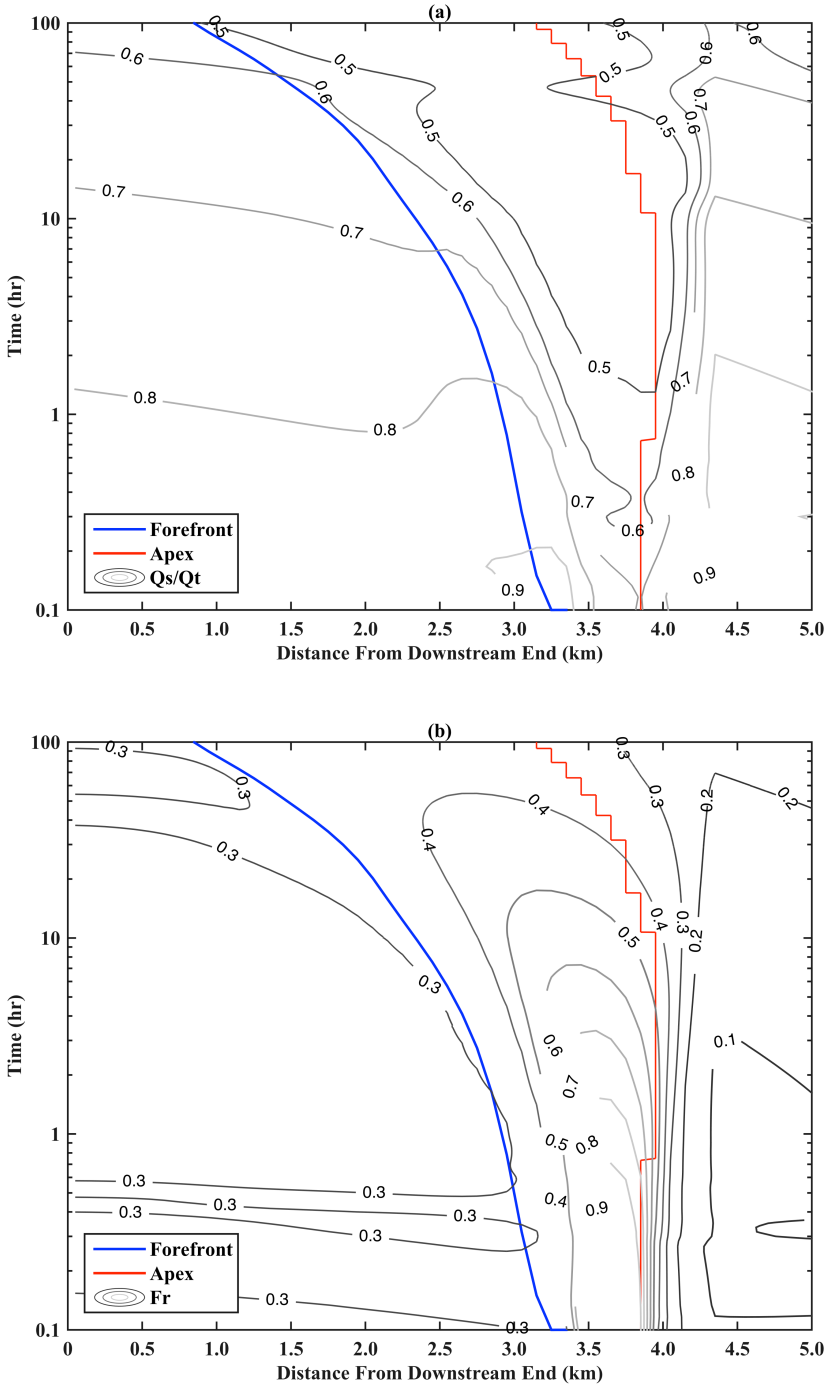

Figure 3-29: Influence of (a) the ratio of suspended load to total load and (b) the magnitude of the Froude number on the propagation behavior for an increased channel slope

CHAPTER 4. EXAMINING THE FATE OF SEDIMENT PULSES UNDER SEVERE HYDROLOGIC AND HYDRAULIC CONDITIONS

Abstract

Numerical simulations to examine the fate of a fine-grained sediment pulse under severe hydrologic and hydraulic conditions are presented in this paper. The objectives are to examine the effect of the magnitude, duration, and frequency of hydrologic events on the propagation behavior, and to quantify the impact of these disturbances on riverine environments subjected to severe hydraulic conditions. The study focused on a hypothetical breach of a tailings containment cell at the Coles Hill uranium deposit in southern Virginia, USA, and the subsequent propagation of the dam-break induced sediment pulse in the downstream river network. Results indicate that the aforementioned storm characteristics primarily impact the relationship between pre- and post-pulse conditions, the dissipation of the pulse peak discharge, and the travel time of the pulse apex, whereas the complexity of riverine environments subjected to severe hydraulic conditions is reflected by the distribution of aggradation/degradation patterns and the evolution of suspended sediment concentration profiles.

4.1. Introduction

Recent natural and anthropogenic events highlight the geomorphic and environmental impacts associated with large amounts of loose sediment suddenly deposited in river corridors. Relevant examples of such phenomena, which are defined herein as sediment pulses, include the landslide that occurred near Oso, Washington, USA in March of 2014 that deposited an estimated 8 million cubic meters of sediment into the North Fork Stillaguamish River (Iverson et al., 2015), the failure of a tailings dam in Brazil in November of 2015 that released nearly 30 million cubic meters of mine waste into the Doce River (Agurto-Detzel et al., 2016), and the removal of Condit Dam on the White Salmon River in Washington, USA in October of 2011 that freed approximately 1.6 million cubic meters of impounded material (Wilcox et al., 2014). These events were associated with a considerable increase in sediment load delivered to downstream reaches, and therefore, caused substantial channel and floodplain deposition, damage of infrastructure, impairment of aquatic ecosystems and drinking water supplies, and in some cases, the loss of several human lives.

Sediment-flow hazards such as the ones illustrated above are expected to become more common as the intensity of rainfall events has significantly increased due to the influence of various human activities (e.g. Kirschbaum et al., 2012; Wooten et al., 2016). Satellite observations and numerical simulations carried out by Allan and Soden (2008) revealed that the recorded amplification of these events is in fact larger than predicted by climate models, implying that expected precipitation extremes may be underestimated. Such climatic changes will thus have a direct impact on the magnitude, duration, and frequency of flows in riverine environments (Viers, 2011). In October of 2015, for instance, a severe rainfall event with a return period that ranged between 500-yr and 1000-yr resulted in extensive flooding from the central to the coastal areas of the state of South Carolina, USA (CISA, 2015). The storm generated peak discharge records at 17 US Geological Survey (USGS) streamflow gaging stations (Feaster et al., 2015), and triggered the failure of the retaining structure and subsequent release of the impounded sediment in 36 dam locations throughout the state (NPDP, 2016).

There is a need, therefore, to develop a better understanding of the behavior of sediment pulses under severe hydrologic and hydraulic conditions that might trigger their occurrence and accelerate their propagation in river corridors. These conditions govern the reconfiguration of the deposited material, dictating sediment transport rates, concentration of suspended solids, and aggradation/degradation patterns, as well as regulate the overall time period over which geomorphic and environmental impacts persist. The present study aims to shed light on this issue by examining the fate of a fine-grained sediment pulse under the influence of storms of various intensities. The study focuses on the numerical modeling of a hypothetical breach of a (non-existing) tailings containment cell at the undeveloped Coles Hill uranium deposit in southern Virginia, USA, and the subsequent propagation of the dam-break induced sediment pulse in the downstream river network. Specifically, the objectives of this research are: (1) to examine the effect of the magnitude, duration, and frequency of hydrologic events on the propagation of sediment pulses, and (2) to quantify the impact of these disturbances on riverine environments subjected to severe hydraulic conditions. The intent is to improve the resilience of river corridors to the occurrence of sediment pulses by developing an advanced understanding of the fundamental mechanisms that govern their behavior, and hence, provide decision makers with reliable information for planning, management, and risk evaluation purposes.

Initially, the characteristics of the study area are presented, including a general description of the Coles Hill uranium deposit. Next, details about the applied modeling methodology are provided. These contain information about the model formulation, estimation of relevant parameters, solution methodology, and calibration procedure. Lastly, results of the numerical simulations are presented and their implications discussed and contextualized.

4.2. Study Area

The Coles Hill uranium deposit is located in the southern part of the state of Virginia, USA, between the towns of Chatham and Gretna in central Pittsylvania County (Figure 4-30). The deposit, which is the largest known undeveloped uranium ore reserve in North America, consists of an estimated resource of 120 million pounds of uranium

(Santoy Resources, 2009), and is located in a primarily agricultural region with only a few sparsely populated areas in its surroundings. If the mining site were to be developed, it is anticipated that large amounts of waste by-products (i.e. tailings) would be generated during the processing operations and that, according to regulations, they would have to be stored on site, in containment cells designed to last over a thousand years without breaching (USNRC, 2002). Therefore, due to the environmental impact that its development might have in the future, a large, comprehensive, and continuing investigation is being conducted to characterize the geological, geochemical, and hydrological conditions associated with this deposit (e.g. Gannon et al., 2012; Kingston et al., 2012; Castro-Bolinaga and Diplas, 2014; Castro-Bolinaga et al., 2014; Levitan et al., 2014; Levitan et al., 2015; Tappa et al., 2014).

The main uranium ore bodies are located between the channels of two small streams, Whitethorn Creek to the north, and one of its tributaries, Mill Creek, to the south. As shown in Figure 4-30, Whitethorn Creek flows for approximately 5 km from its confluence with Mill Creek to its confluence with the Banister River, which further downstream flows into the Dan River, the Roanoke River, and ultimately into important regional water bodies such as Kerr Reservoir and Lake Gaston, close to the border between the states of Virginia and North Carolina. In particular, the study presented in this paper focuses on the reaches of Mill Creek and Whitethorn Creek due to their proximity to the deposit, while a subsequent investigation will center on a 52-km reach of the Banister River from its confluence with the Whitethorn Creek to the Banister Lake Dam (Figure 1). Castro-Bolinaga and Diplas (2014) found that the long, narrow lake that has formed upstream of this structure (i.e. the Banister Lake) hinders the capacity of the Banister River to move sediment, causing a sizable reduction of the flow velocity and boundary shear stress as water enters the reservoir. Hence, it is expected that the Banister Lake will have an important role in the fate of tailings downstream of the Coles Hill uranium deposit.

4.3. Modeling Methodology

The present modeling effort consists of two separate component models. First, a model that simulates the release of tailings from a containment cell located in the vicinity of the

deposit into the nearby stream network, and secondly, a morphodynamic model that examines the propagation of the dam-break induced sediment pulse in the downstream river network.

4.3.1. Release of Tailings Component Model[2]

The two-dimensional (2-D) computational fluid dynamics software ANSYS Fluent was used to simulate the release of the tailings sediment pulse due to the failure of a containment cell. In particular, the volume of fluid (VOF) method (Hirt and Nichols, 1981) within the multiphase-flow modeling suite was implemented. This method applies a surface-tracking technique that allows modeling immiscible fluids by accounting for their volume fraction (VF) throughout the computational domain (ANSYS, 2013). Such an approach has been effectively used to reproduce the behavior of post-liquefaction soils (e.g. Huang et al., 2012) and clear-water dam-break flows (e.g. LaRocque, 2012), which are both relevant applications concerning this study.

A worst-case failure scenario was established following the regulations authored by the US Nuclear Regulatory Commission (USNRC, 1980) and the US Code of Federal Regulation (USCFR, 2014). This scenario considers: (1) a containment cell that is located partially above the local ground surface level, (2) the tailings to be in liquefaction phase as they would be during the active stage of the mining operations, and (3) the failure to be triggered by an extreme hydrologic event. The location selected for the containment cell is shown in Figure 4-31. It should be noted that this location is hypothetical and has been defined only for modeling purposes. If the mining site were to be developed, the actual location of this facility is unknown to date. Moreover, the containment cell location depicted in Figure 4-31 is placed outside the Probable Maximum Flood (PMF) inundation zone (Castro-Bolinaga and Diplas, 2014) as required by USNRC (1980) to ensure that this facility would not be vulnerable to the occurrence of severe flooding conditions.

The evaluated failure scenario would release the tailings sediment pulse into the channel of Mill Creek (Figure 4-31). Hence, the ANSYS Fluent model focused on the cross-sectional profile of the natural terrain between the selected location and the latter watercourse. This profile, which is delineated in Figure 4-32, is simplified by considering

[2] Component model developed and implemented by E. Zavaleta

five different slopes over a 600-m long section from the closest side of the containment cell to the centerline of Mill Creek. As indicated in Figure 4-32, only the amount of tailings located above the local ground surface level is considered movable and thus available for transport. This represents a volume of approximately 0.5 million cubic meters of sediment assuming a superficial area of 40 acres. Moreover, the ANSYS Fluent model accounts for a 1.8-m tall layer of water placed on the top of the tailings. This layer consists of the required height to limit wind erosion (USNRC, 2002) and the amount of rainfall expected due to the Probable Maximum Precipitation (PMP) (Kingston, 2012).

The Bingham plastic rheological model (Wan and Wang, 1994) was used to capture the non-Newtonian behavior of the liquefied tailings. This model has been effectively applied in the past for analyzing the mechanisms that govern the flow of mine tailings following a dam failure (e.g. Jeyapalan et al., 1983a, 1983b), which provides confidence in its suitability for the present study. The relevant properties of the tailings are presented in Table 4-11. These properties were determined based on a sediment sample characterized primarily as silty-sand with 49% by weight of fines (i.e. particles in the silt and clay size range), and having a median grain size (d_{50}) of 0.074 mm. Even though this characterization has been defined only for modeling purposes, it is expected that the actual properties of the tailings would be very similar to those given in Table 4-11.

For the numerical simulations, the computational domain was divided into 88000 quadrilateral cells using spatial discretization parameters in the x- and y-direction that ranged from 0.25-0.50 m and 0.05-0.25 m, respectively. The purpose of this non-uniform mesh is to adequately capture the behavior of the rapidly propagating sediment pulse forefront as it moves downslope. The use of these types of grids improves the overall accuracy of the simulation by accounting for regions within the computational domain where gradients of relevant variables are rather large (Anderson, 1995). Lastly, the ANSYS Fluent model was validated using data from clear-water dam-break laboratory experiments conducted at the US Army Corps of Engineers (USACE) Waterways Experimental Station (USACE, 1960). This effort demonstrated that the model is able to satisfactorily predict the temporal variation and peak values of water discharge and flow depth, as well as the rate of propagation of the flood wave.

4.3.2. Sediment Pulse Propagation Component Model

The one-dimensional (1-D) morphodynamic model developed by Castro-Bolinaga et al. (2016a) is used to assess the fate of the dam-break induced tailings sediment pulse in the river network downstream of the Coles Hill uranium deposit. The model is formulated based on the St. Venant shallow water equations for the water-sediment mixture, and considers the movement of sediment as bedload and suspended load. A novel technique that applies either the decoupled or the coupled approach depending on local flow and sediment transport conditions is used to solve the system of governing equations. This solution technique has the advantage that it adopts the more suitable of these approaches within different regions of the computational domain without compromising the global accuracy and efficiency of the model (Castro-Bolinaga et al., 2016a). Such feature is particularly relevant to this study since pronounced suspended-load driven regimes are expected to occur during the initial short-term phase following the tailings sediment pulse entering Mill Creek, and the fact that these phenomena are not accurately represented by decoupled models (e.g. Cui et al., 2014). Moreover, it should be noted that an expanded version of the model of Castro-Bolinaga et al. (2016a) that considers non-uniform sediment transport conditions is applied herein. Details of this revised version are provided in Castro-Bolinaga at al. (2016b). The reader is referred to these publications for detailed information regarding the formulation of the system governing equations and its associated solution methodology, as well as the employed empirical closure relations and numerical methods.

The study river network consists of two reaches: (1) Mill Creek from the selected location of the containment cell to its confluence with Whitethorn Creek, and (2) Whitethorn Creek from its confluence with Mill Creek to its confluence with the Banister River. A plan view of the spatial distribution of these reaches is shown in Figure 4-31. Data for constructing the river terrain model were obtained from the hydraulic model developed by Castro-Bolinaga and Diplas (2014). These data primarily include channel bathymetry and slope, and Manning's n values to describe the boundary roughness. Additionally, the properties of the riverbed material were determined based on sediment samples collected at various locations along the channel of the modeled reaches. Sieve analyses were performed to define their grain size distribution, and hence, the available

fraction of each sediment class required to simulate non-uniform transport conditions. A summary of the main characteristics of the study river network is presented in Table 4-12.

The propagation of the tailings sediment pulse was examined for the 10-yr, 100-yr, and 500-yr storms. The corresponding hydrographs, with peak discharges at the inlet of each reach provided in Table 4-13, were obtained from an event-based hydrologic model developed by Kingston et al. (2012). These hydrographs were implemented as the upstream boundary condition for the unsteady flow simulations, whereas rating curves of water surface elevation versus discharge generated by the aforementioned hydraulic model were set as the downstream boundary condition. The number of cross-sections was defined based on the geomorphic characteristics of the river channels, resulting in an average distance between consecutive cross-sections of 158.3 m for Mill Creek and 150.9 m for Whitethorn Creek. Regarding the temporal discretization parameter, the explicit time-marching algorithm applied by the adaptive morphodynamic model of Castro-Bolinaga et al. (2016a) requires the maximum value of the time step (Δt) to satisfy the Courant-Friedrichs-Lewy (CFL) stability condition. A value of Δt of 0.1 s was used herein as a result of numerical tests carried out during execution of the model to guarantee that a stable solution was achieved.

4.4. Results and Discussion

The release of tailings component model focuses on defining the volumetric rate at which the sediment pulse enters the nearby stream network. This information is represented as a sediment graph, and constitutes the single most important input required by the pulse propagation component model to determine sediment transport rates, concentrations of suspended solids, and aggradation/degradation patterns in the downstream river network.

4.4.1. Release of Tailings Sediment Pulse

The downslope movement of the sediment pulse occurs very rapidly after the failure of the tailings containment cell. Results indicate that the pulse forefront accelerates sharply, traveling approximately 50 m in just 5 s, and then continues to travel at an average rate of 10 m/s until it reaches the centerline of Mill Creek. Figure 4-33 illustrates the

propagating pulse forefront at two instances after its release, highlighting the rapid reconfiguration of the impounded material and ensuing drawdown of the tailings surface level. In this figure, the depicted contours of tailings VF represent the ratio of the volume of tailings to the total volume of each computational cell. A value of VF equal to 1 implies that the computational cell is completely filled with tailings, whereas a VF of 0.5 denotes that they occupy only half the computational cell. It should be noted that the same approach is used within the VOF method to describe the temporal variation of the free surface for the remaining fluids throughout the computational domain (Figure 4-32).

The tailings sediment graph at the centerline of Mill Creek is presented in Figure 4-34. The model predicts that the material enters Mill Creek 60 s after the failure of the containment cell, with a peak volumetric discharge of 265.4 m^3/s occurring 120 s after its release. Moreover, the sediment graph reveals that the bulk of the volume is conveyed to Mill Creek within the first 5 min following the release of the pulse, and that close to 25 min are required for the considered amount of tailings to completely reach this watercourse. The hydrograph corresponding to volume of water placed on top of the tailings to account for wind erosion protection and the PMP is also shown in Figure 4-34. This hydrograph, despite having a relatively short duration, has a maximum flow rate of 166.1 m^3/s, which is larger than that corresponding to the 500-yr storm (Table 4-13). Such additional discharge is expected to affect the propagation of the tailings sediment pulse, enhancing the capacity of Mill Creek to transport sediment.

Given that the results of the 2-D ANSYS Fluent model represent variables per unit channel width, the sediment graph and hydrograph depicted in Figure 4-34 assume a breach width of the earth-retaining dam equal to 50 m (Figure 4-32). This value was selected following Brunner (2014) as a worst-case scenario based on the dimensions of the dam, and a range of breach characteristics collected from several agencies (e.g. USACE, Federal Energy Regulatory Commission, and National Weather Service). Furthermore, numerical tests carried out during the application of the model suggest that the results are highly dependent on the magnitude of the tailings plastic viscosity. It was found that this variable governs the overall downslope movement of the sediment pulse, controlling therefore the duration and peak discharge that define the shape of the sediment graph. Herein, in an effort to reduce its associated uncertainty (e.g. Jeyapalan,

1982), the plastic viscosity (Table 4-11) was experimentally determined based on a sample prepared using material characteristic of area surrounding the site at a sediment concentration of 46.8% (by volume). Due to the rather limited number of datasets available to contextualize this value, however, it is important to consider the particularities of each study before selecting the magnitude of the plastic viscosity.

4.4.2. Propagation of Tailings Sediment Pulse

For the numerical simulations, it was assumed that the failure of the containment cell coincided with the maximum discharge of the evaluated storms at Mill Creek, in addition to considering bankfull conditions as base flow during the passage of these storms. The intent is to provide conservative estimates of the pulse propagation rate, as these assumptions represent a worst-case scenario that enhance the sediment transport capacity of the study river reaches. The temporal variation of the discharge of total sediment load (Q_t) at the outlet of Mill Creek and Whitethorn Creek after the failure of the containment cell is illustrated in Figure 4-35. Therein, the sediment pulse is also shown to facilitate the assessment of the pre- and post-pulse prevailing conditions for the modeled hydrologic events.

Results indicate that Q_t increases with respect to pre-pulse values as the sediment wave propagates through the study reaches. Figure 4-35 shows that the extent of this increase is correlated with the intensity of the hydrologic event, with a less pronounced rise of Q_t as the scale of the storm becomes larger. In the case of Mill Creek, the maximum increase is recorded during the 10-yr storm, in which the ratio of Q_t post-pulse to Q_t pre-pulse (i.e. $Q_{t\text{-}increase}$) is 18.6, while a minimum a value of $Q_{t\text{-}increase}$ equal to 1.8 is computed for the 500-yr storm. Likewise, the maximum and minimum values of $Q_{t\text{-}increase}$ in the case of Whitethorn Creek are 7.4 and 1.3 for the 10-yr and 500-yr storms, respectively. This behavior is directly related to the hydraulic regime that governs the pre-pulse riverine environment. As the severity of the storm strengthens, flow velocities and boundary shear stresses within the channel increase, enhancing thus the capacity of the river to entrain and transport sediment downstream. Therefore, larger values of Q_t are present in the reach before considering the contribution of the sediment pulse.

The peak values of Q_t (i.e. $Q_{t\text{-}peak}$) computed in the study reaches after the failure of the containment cell are reported in Table 4-14. The variation of $Q_{t\text{-}peak}$ suggests that the initial sediment pulse peak discharge of 265.4 m^3/s is considerably dissipated while traveling through Mill Creek, with a maximum reduction of approximately 71% for the 10-yr storm and a minimum reduction of nearly 23% for the 500-yr storm. Such dissipation is due to the limited capacity of the relatively small Mill Creek to accommodate the surplus of sediment. As the magnitude of the storm increases, however, this capacity increases as well and the stream is able to transport a larger amount of the deposited material downstream. Moreover, a transient fining of the riverbed is triggered during the dissipation of $Q_{t\text{-}peak}$ as shown in Figure 4-36. The reduced sediment transport capacity generates a temporal accumulation of fine-grained sediment on the surface layer of the riverbed, causing the reach-averaged d_{50} to be significantly reduced from its original value of 2.4 mm. Consistent with the enhanced sediment transport capacity, the transient fining process is less pronounced for the 500-yr storm, and becomes gradually more noticeable as the storm return period increases (Figure 4-36).

Results presented in Table 4-14 indicate that $Q_{t\text{-}peak}$ increases as the tailings sediment pulse migrates downstream. This behavior is produced by the contribution of the upland watershed of Whitethorn Creek, which adds a considerable volume of water and facilitates the transport of the material. Furthermore, the pulse migration exhibits an important translational component, as evidenced in Figure 4-35 by the horizontal displacement of $Q_{t\text{-}peak}$. The travel time of the pulse apex between the location of the containment cell and the outlet of Mill Creek, as well as between the outlet of the latter stream and that of Whitethorn Creek are provided in Table 4-15. Results indicate that the time required to propagate through the study reaches is dictated by the magnitude of the hydrologic event, with larger storms enhancing the overall downstream movement of the pulse apex. The very rapid translational migration shown in Figure 4-35 and Table 4-15, in which the pulse apex is able to travel nearly 10 km in less than one hour, is due to its fine-grained composition, and short-term suspended-load driven regimes that have the capacity to transport large amounts of material.

The temporal variation of the reach-averaged volumetric suspended sediment concentration (i.e. C_{reach}) is illustrated in Figure 4-37. As expected, the magnitude of

C_{reach} increases significantly after the sediment pulse enters the study reaches. In the case of Mill Creek, Figure 4-37 denotes that the scale of this increase depends on the particular hydrologic event, with a maximum value of Creach of approximately 0.5 (by volume) for the 10-yr storm and a minimum value of Creach close to 0.35 (by volume) for the 500-yr storm. Additionally, results show that such increase is temporary, as C_{reach} returns to its pre-pulse magnitude after the sediment wave has propagated through the watercourse. On the other hand, in the case of Whitethorn Creek, the influence of the hydrologic event is only slightly noticeable in the variation of Creach. While the trend is similar to that of Mill Creek with the intensity of the storm determining its maximum value, backwater effects from the larger Banister River govern the evolution of C_{reach}. These effects consist of high water depths and low flow velocities that facilitate the settling of relatively coarse to medium grain sizes, while maintaining the very fine sediment in suspension for long periods of time. Figure 4-37 indicates that the influence of the Banister River is most significant for the 100-yr and 500-yr storm, as the variation between the pre- and post-pulse conditions is less pronounced. The aforementioned variation of C_{reach} is better understood by examining the reach-averaged fractional volumetric suspended sediment concentration (i.e. $C_{reach\text{-}k}$). Figure 4-38 and Figure 4-39 shows the evolution of $C_{reach\text{-}k}$ for the finer material (i.e. d_k = 0.125 mm, d_k = 0.188 mm, and d_k = 0.375 mm, where d_k is the representative grain size of sediment class k) in Mill Creek and Whitethorn Creek, respectively, for the modeled hydrologic events. The intent is to describe the impact of the fine-grained sediment pulse, which is primarily composed of grain sizes in these classes.

The temporal variation of $C_{reach\text{-}k}$ shows that the maximum value of C_{reach} is directly related to the capacity of the flow to transport fine material. As observed in Figure 4-38 and Figure 4-39, the maximum value of $C_{reach\text{-}k}$ is computed for the finest sediment class (i.e. d_k = 0.125 mm), which constitutes more than 40% of the initial pulse gradation. In the case of Mill Creek, this maximum value is reduced as the severity of the storm increases, with $C_{reach\text{-}k}$ varying from 0.25 to 0.15 (by volume) from the 10-yr to 500-yr storms. On the other hand, in the case of Whitethorn Creek $C_{reach\text{-}k}$ remains nearly constant, except for the scenario of the 10-yr storm in which the backwater effects of the Banister River are not as prominent. As illustrated in Figure 4-38 and Figure 4-39, the

contribution of the fine-grained sediment pulse accounts for approximately 50% of C_{reach}, independently of the hydrologic event. Additionally, these figures show that the value of $C_{reach\text{-}k}$ for the remaining two classes does not depend on the evaluated storm nor varies significantly between pre- and post-pulse conditions. This behavior is caused by the limited supply of these grain sizes, which are mostly present in the riverbed, rather than by a transport-controlled regime as for the case of the finest material.

Lastly, the profiles of maximum aggradation and degradation after the propagation of the tailings sediment pulse are shown in Figure 4-40 for Mill Creek and Figure 4-41 for Whitethorn Creek. It should be noted that these profiles do not represent any specific instance in time. Alternatively, they illustrate the maximum levels of deposition and erosion that were computed at each cross-section during the entire simulation. In the case of Mill Creek, the maximum levels of deposition are located close to the upstream and downstream ends of the study reach, which correspond to sections characterized by a relatively flat topography. Moreover, Figure 4-40 suggests that such levels are independent of the hydrologic event being routed, whereas Figure 4-41 denotes they are in fact strongly dependent in the case of Whitethorn Creek. This dependency is caused by the backwater effects of the Banister River, which become more pronounced as the magnitude of the evaluated storm increases. As shown in Figure 4-41, the high water depths and low flow velocities that characterized these effects trigger a severe aggradation of the riverbed.

4.5. Conclusions

A coupled modeling effort to predict the fate of a fine-grained sediment pulse under severe hydrologic and hydraulic conditions has been presented in this paper. The objective was to assess the effect of the magnitude, duration, and frequency of hydrologic events on their propagation behavior, and to quantify the impact of riverine environments subjected to severe hydraulic conditions. The study focused on a hypothetical breach of a tailings containment cell at the undeveloped Coles Hill uranium deposit in southern Virginia, USA, and the subsequent propagation of the dam-break induced sediment pulse in the downstream river network. The numerical simulations consisted of the application of two separate component models. First, a model to simulate the release of tailings from

a containment cell located in vicinity of the deposit into the nearby stream network, and secondly, a morphodynamic model that examined the propagation of the dam-break induced sediment pulse under the influence of the 10-yr, 100-yr, and 500-yr storms.

Results of the release of tailings component model suggest that downslope movement of the sediment pulse occurs very rapidly. The model predicted that the pulse would initially enter the nearby watercourse 60 s after the failure of the containment cell, depositing the bulk of the volume within the first 5 min. The developed sediment graph, which constitutes the single most important input for the ensuing component model, indicates that a maximum volumetric discharge of 265.4 m^3/s is achieved two minutes after the failure, and that close to 25 min are required to convey the total volume of released tailings to the nearby stream network. Furthermore, numerical tests revealed that the results of this component model are highly sensitive to the magnitude of the plastic viscosity, controlling the duration and peak discharge that define the shape of the sediment graph. Herein, this variable was experimentally determined based on a sample prepared using materials characteristic of the area surrounding the study site. Nonetheless, due to the rather limited number of datasets available in the literature to contextualize this value, it is of paramount importance to consider the particularities of each case before deciding on the magnitude of the plastic viscosity to use in the model.

The sediment pulse propagation component model indicates that the magnitude, frequency, and duration of hydrologic events primarily influence the temporal variation of the discharge of total sediment load. Specifically, such characteristics have a marked impact on the relationship between pre- and post-pulse conditions, the dissipation of the pulse peak discharge, and the travel time of the pulse apex. Results suggest that the impact of the sediment pulse is more pronounced for relatively small events (e.g. 10-yr storm), as the amount of material deposited in the stream is considerably larger than that corresponding to pre-pulse conditions. On the other hand, large events (e.g. 500-yr storm) are capable of significantly enhancing the capacity of the watercourse to entrain and move sediment downstream, resulting therefore in larger transport rates before considering the contribution of the pulse.

Regarding the peak discharge dissipation and travel time of the pulse apex, the scale of the hydrologic event is directly related to the degree of attenuation and the downstream propagation velocity. Small events trigger a greater dissipation of the pulse peak discharge and a slower movement of the pulse apex, whereas the high flow rates associated with large events are able to move the pulse more rapidly, producing hence a smaller degree of attenuation of its peak discharge. A transient fining of the riverbed and an increase in the concentration of suspended solids in the water column accompany these phenomena as the stream adjusts to accommodate the surplus of material. Furthermore, the complexity of riverine environments subjected to severe hydraulic conditions is reflected by the distribution of aggradation and degradation patterns, as well as by the streamwise variation of the suspended sediment concentrations. Results indicate that backwater effects produced by large storms generate high water depths and low flow velocities that facilitate the settling of relatively coarse to medium grain sizes, while maintaining the very fine sediment in suspension for long periods of time.

A better understanding of the characteristics that govern the propagation of fine-grained sediment pulses under severe hydrologic and hydraulic conditions allow us to improve the resilience of river corridors to these sediment-flow hazards by providing decision makers with reliable information for planning, management, and risk evaluation purposes. The study presented in this paper constitutes a relevant example of such an application, providing a preliminary assessment of the impact that a catastrophic failure of a tailings containment cell at the Coles Hill uranium deposit would have in downstream rivers and reservoirs.

References

Agurto-Detzel, H., Bianchi, M., Assumpcao, M., Schimmel, M., Collaco, B., Ciardelli, C., Barbosa, J.R., Calhau, J., 2016. The tailings dam failure of 5 November 2015 in SE Brazil and its preceding seismic sequence. *Geophys. Res. Lett.* 43.

Allan, R.P., Soden, B.J., 2008. Atmospheric Warming and the Amplification of Extreme Events. *Science* 321, 1481-1484.

Anderson, J.D., 1995. *Computational Fluid Dynamics: The Basics with Applications*. McGraw-Hill.

ANSYS, 2013. *ANSYS Fluent User Guide*. ANSYS, Inc., Canonsburg, Pennsylvania, USA.

Brunner, G., 2014. Using HEC-RAS for Dam-Break Studies. US Army Corps of Engineers, Hydrologic Engineering Center, Davis, CA, USA.

Carolinas Integrated Science and Assessment (CISA), 2015. *The South Carolina Flood of 2015*. Available on-line at: http://www.cisa.sc.edu (Aug. 1, 2016).

Castro-Bolinaga, C.F., Diplas, P., 2014. Hydraulic Modeling of Extreme Hydrologic Events: Case Study in Southern Virginia. *J. Hydraul. Eng.* 05014007.

Castro-Bolinaga, C.F., Zavaleta, E., Diplas, P., 2014. A coupled modeling effort to study the fate of contaminated sediments downstream of the Coles Hill deposit, Virginia, USA, in: *Proc. Sediment Dynamics from the Summit to the Sea, IAHS Publication 367*, New Orleans, Louisiana, USA, December 11-14, 2014.

Castro-Bolinaga, C.F., Diplas, P., Bodnar, R.J., 2016a. An Adaptive Morphodynamic Model for Water Flow, Sediment Transport, and Riverbed Evolution in Alluvial Rivers, *Adv. Water Resour.* (under review).

Castro-Bolinaga, C.F., Diplas, P., Bodnar, R.J., 2016b. Numerical Analysis of the Propagation of Fine-grained Sediment Pulses in Alluvial Rivers. *Environmental Fluid Mechanics* (to be submitted).

Cui, Y., Wooster, J.K., Braudrick, C.A., Orr, B. K., 2014. Lessons Learned from Sediment Transport Model Predictions and Long-Term Postremoval Monitoring: Marmot Dam Removal Project on the Sandy River in Oregon. *J. Hydraul. Eng.* 04014044.

Feaster, T.D., Shelton, J.M., Robbins, J.C., 2015. *Preliminary Peak Stage and Streamflow Data at Selected USGS Streamgaging Stations for the South Carolina Flood of October 2015*. US Geological Survey Open-File Report 2015-1201, Reston, Virginia, USA.

Gannon, J.P., Burbey, T.J., Bodnar, R.J., Aylor, J., 2012. Geophysical and geochemical characterization of the groundwater system and the role of the Chatham Fault in groundwater movement at the Coles Hill uranium deposit, Virginia, USA. *Hydrogeology Journal* 20, 45-60.

Gesch, D., Oimoen, M., Greenlee, S., Nelson, C., Steuck, M., Tyler, D., 2002. The national elevation dataset. *Photogramm. Eng. Remote Sens.* 68(1), 5-11.

Gesch, D. B. (2007). The national elevation dataset. *Digital elevation model technologies and applications: The DEM users manual*. American Society for Photogrammetry and Remote Sensing, Bethesda, MD, USA.

Hirt, C.W., Nichols, B.D., 1981. Volume of Fluid (VOF) Method for the Dynamics of Free Boundaries. *J. Comput. Phys.* 39, 201-225.

Huang, Y., Mao, W., Zheng, H., Li, G., 2012. Computational fluid dynamics modeling of post-liquefaction soil flow using the volume of fluid method. *Bull. Eng. Geol. Environ.* 71, 359-366.

Iverson, R.M., George, D.L., Allstadt, K., Reid, M.E., Collins, B.D., Vallance, J.W., Schilling, S.P., Godt, J.W., Cannon, C.M., Magirl, C.S., Baum, R.L., Coe, J.A., Schulz, W.H., Bower, J.B., 2015. Landslide mobility and hazards: Implications of the 2014 Oso disaster. *Earth Planet. Sci. Lett.* 412, 197-208.

Jeyapalan, J.K., 1982. Dam-break studies for mine tailings impoundments, in: *Proc. Uranium Mill Tailings Management Fifth Symposium*, Fort Collins, Colorado, USA, December 9-10, 1982.

Jeyapalan, J.K., Duncan, J.M., Seed, H.B., 1983a. Analyses of Flow Failures of Mine Tailings Dams. *J. Geotech. Eng.* 109(2), 150-171.

Jeyapalan, J.K., Duncan, J.M., Seed, H.B., 1983b. Investigation of Flow Failures of Tailings Dams. *J. Geotech. Eng.* 109(2), 172-189.

Kingston, W.J., 2012. Hydrologic Modeling of a Probable Maximum Precipitation Event Using HEC-HMS and GIS Models - A Case Study of Two Watersheds in Southern Virginia. Masters Thesis, Virginia Tech, Blacksburg, Virginia, USA.

Kingston, W.J., Castro-Bolinaga, C.F., Zavaleta, E., Diplas, P., 2012. Probable maximum flood inundation modeling: a case study in southern Virginia, in: Murillo, R. (Ed.), *Proc. River Flow 2012*, San Jose, Costa Rica, September 5-7, 2002.

Kirschbaum, D., Adler, R., Adler, D., Peters-Lidard, C., Huffman, G., 2012. Global Distribution of Extreme Precipitations and High-Impact Landslides in 2010 Relative to Previous Years. *J. Hydrometeorol.* 13, 1536-1551.

LaRocque, L.A., 2012. Experimental and Numerical Modeling of Dam-Break and Levee-Breach Flows. Doctoral Dissertation, University of South Carolina, Columbia, South Carolina, USA.

Levitan, D. M., Schreiber, M. E., Seal, R. R., II, Bodnar, R. J., Aylor, J. G., 2014. Developing protocols for geochemical baseline studies: An example from the Coles Hill uranium deposit, Virginia, USA. *Appl. Geochem.* 43, 88-100.

Levitan, D.M., Zipper, C.E., Donovan, P., Schreiber, M.E., Seal, R.R., II, Engle, M.A., Chermak, J.A., Bodnar, R.J., Johnson, D.K., Aylor, J.G., Jr., 2015. Statistical analysis of soil geochemical data to identify pathfinder elements associated with mineral deposits: an example from the Coles Hill uranium deposit, Virginia, USA. Journal of Geochemical Exploration 154, 238-251.

National Performance of Dams Program (NPDP), 2016. October 2015 South Carolina Dam Failures. Available on-line at: http://npdp.stanford.edu/2015_SC_Flood_Failures (Aug. 1, 2016).

Santoy Resources LTD, 2009. *Technical Report on the Coles Hill Uranium Property Pittsylvania County, Virginia, United States of America, NI 43-101*. Santoy Resources, British Columbia, Canada.

Tappa, M. J., Ayuso, R.A., Bodnar, R.J., Aylor, J.G., Beard, J., Henika, W.S., Vazquez, J.A., Wooden, J.L., 2014. Age of host rocks at the Coles Hill uranium deposit, Pittsylvania County, Virginia, based on zircon U-Pb geochronology. *Econ. Geol.* 109(2), 513-530.

US Army Corp Engineers (USACE), 1960. *Floods Resulting from Suddenly Breached Dams, Report 1, Conditions of Minimum Resistance, Hydraulic Model Investigation, Miscellaneous Paper No. 2-374*. US Army Corps of Engineers, Vicksburg, Mississippi, USA.

US Code of Federal Regulation (USCFR), 2014. *Criteria Relating to the Operation of Uranium Mills and the Disposition of Tailings or Wastes Produced by the Extraction or Concentration of Source Material from Ores Processed Primarily for Their Source Material Content, Title 10, Part 40, Appendix A*. US Code of Federal Regulations, Washington, DC, USA.

US Geological Survey National Hydrography Dataset (USGS NHD), 2007. Available on-line at: http://nhd.usgs.gov/ (Jun. 23, 2014).

US Nuclear Regulatory Commission (USNRC), 1980. *Final Generic Environmental Impact Statement on Uranium Milling, Project M-25, Summary and Text, Volume I, NUREG-0706*. US Nuclear Regulatory Commission, Washington, DC, USA.

US Nuclear Regulatory Commission (USNRC), 2002. *Design of Erosion Protection for Long-Term Stabilization: Final Report, NUREG-1623*. US Nuclear Regulatory Commission, Washington, DC, USA.

Viers, J.H., 2011. Hydropower Relicensing and Climate Change. *J. Am. Water Resour. Assoc.* 47(4), 655-661.

Wan, Z., Wang, Z., 1994. *Hyperconcentrated Flow*. Monograph Series, Int. Assoc. of Hydraul. Res., Balkema.

Wilcox, A.C., O'Connor, J.E., Major, J.J., 2014. Rapid reservoir erosion, hyperconcentrated flow, and downstream deposition triggered by breaching of 38 m tall Condit Dam, White Salmon River, Washington. *J. Geophys. Res. Earth Surf.* 119.

Wooten, R.M., Witt, A.C., Miniat, C.F., Hales, T.C., Aldred, J.L., 2016. Frequency and Magnitude of Selected Historical Landslide Events in the Southern Appalachian Highlands of North Carolina and Virginia: Relationship to Rainfall, Geological and Ecohydrological Controls, and Effects, in: Greenberg, C.H., Collins, B.S. (Eds.), *Natural Disturbances and Historic Range of Variation, Type, Frequency, Severity, and Post-disturbances Structure in Central Hardwood Forests USA*, Springer.

Table 4-11: Relevant properties of the tailings defined for modeling purposes

Property	Units	Value
Dry (bulk) density	kg/m^3	1300
Fully saturated density	kg/m^3	1800
Plastic viscosity	Pa·s	0.35

Table 4-12: Summary of main characteristics of the study river reaches

Reach	Length	Channel Slope[1]	Width[1,2]	Depth[1,2]	d_{50}
	km	m/km	m	m	mm
Mill Creek	5.2	3.6	7.8	1.7	2.4
Whitethorn Creek	4.8	2.4	17.7	2.8	2.4

[1] Reach-averaged values; [2] Bankfull conditions

Table 4-13: Peak discharge at the inlet of the modeled river reaches

Reach	10-yr	100-yr	500-yr
	m^3/s	m^3/s	m^3/s
Mill Creek	22.0	65.6	109.8
Whitethorn Creek	52.4	155.8	261.9

Table 4-14: Peak discharge of total sediment load in the study reaches after the failure of the containment cell

Reach	**10-yr**	**100-yr**	**500-yr**
	m^3/s	m^3/s	m^3/s
Mill Creek	76.4	137.5	205.2
Whitethorn Creek	107.4	191.8	301.9

Table 4-15: Travel time of the sediment pulse apex

Storm	Mill Creek	Whitethorn Creek
	$t_{trvavel}$	$t_{trvavel}$
	min	min
10-yr	19	25
100-yr	13	19
500-yr	10	16

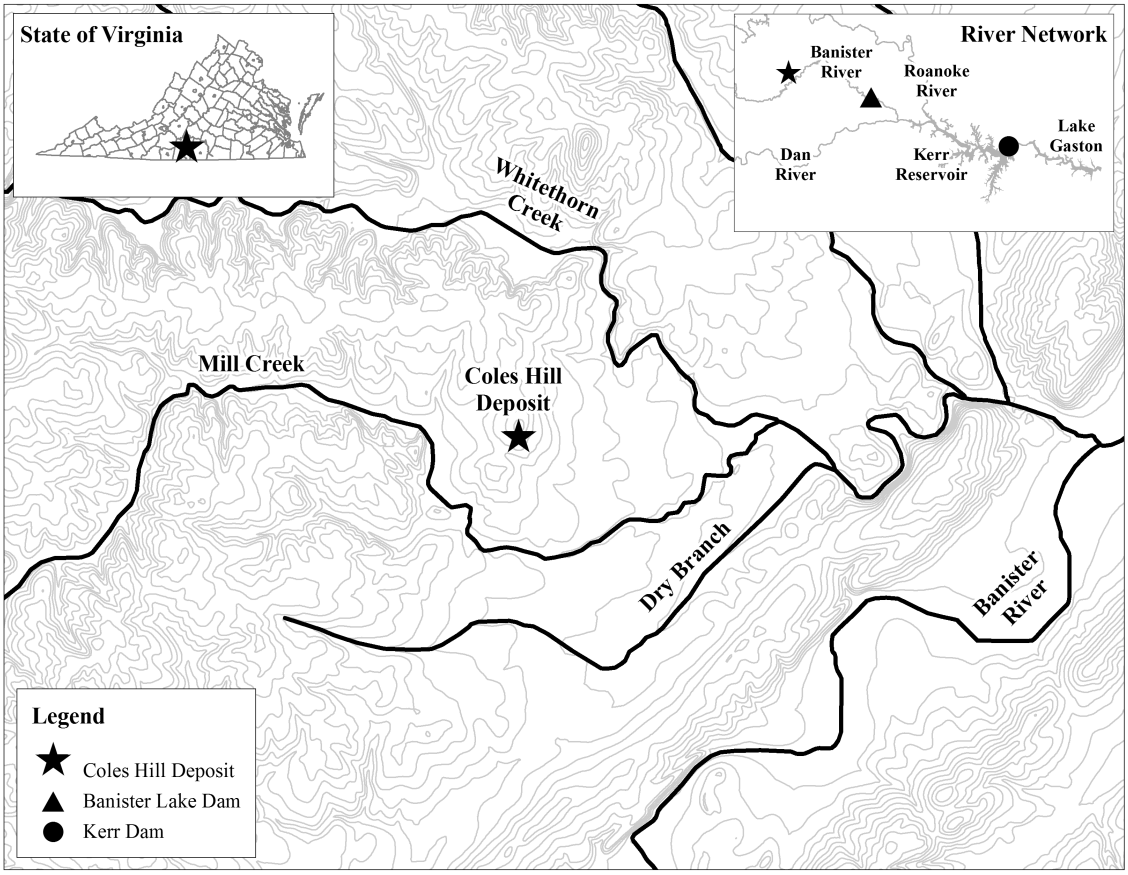

Figure 4-30: Location of the Coles Hill uranium deposit (contour lines are shown every 5 m) (data from USGS NHD, 2007; Gesch, 2007; Gesch et al., 2002)

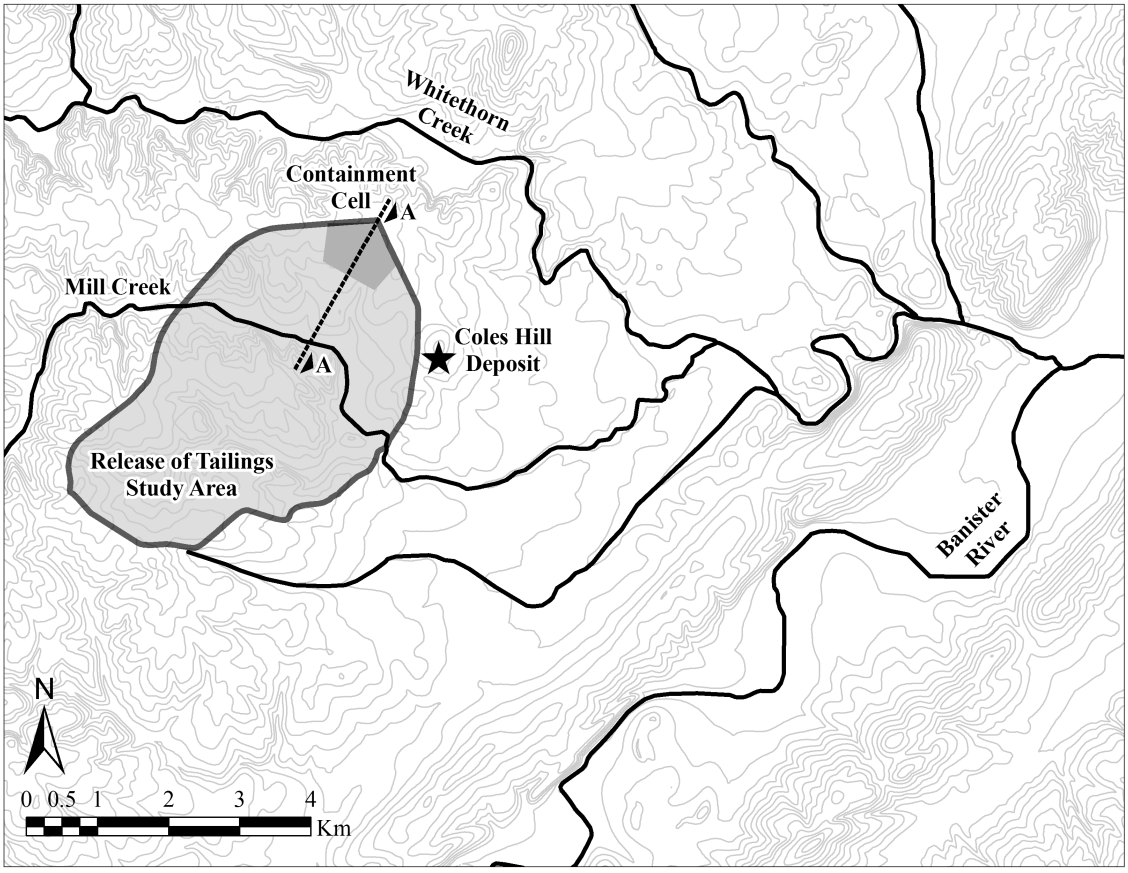

Figure 4-31: Hypothetical location of the tailings containment cell defined for modeling purposes (data from USGS NHD, 2007; Gesch, 2007; Gesch et al., 2002)

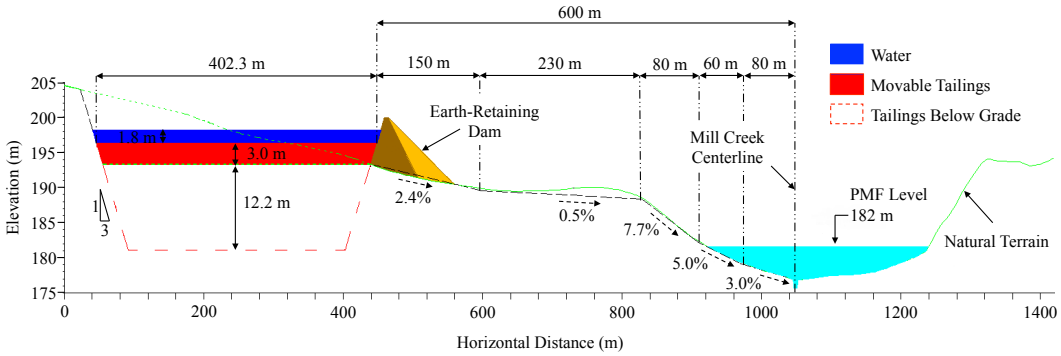

Figure 4-32: Cross-sectional profile A-A considered by the ANSYS Fluent model (the ratio of vertical to horizontal scale is equal to 40)

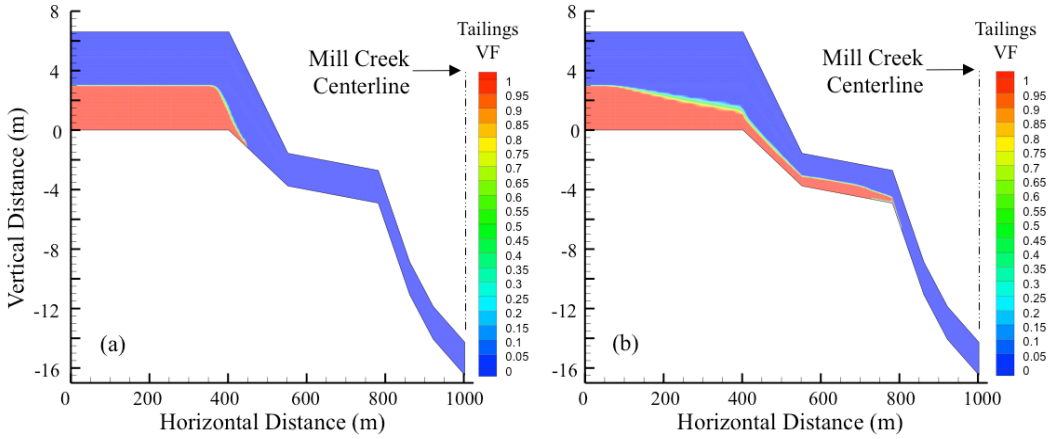

Figure 4-33: Downslope movement of the sediment pulse (a) 5 s and (b) 50 s after the failure of the tailings containment cell

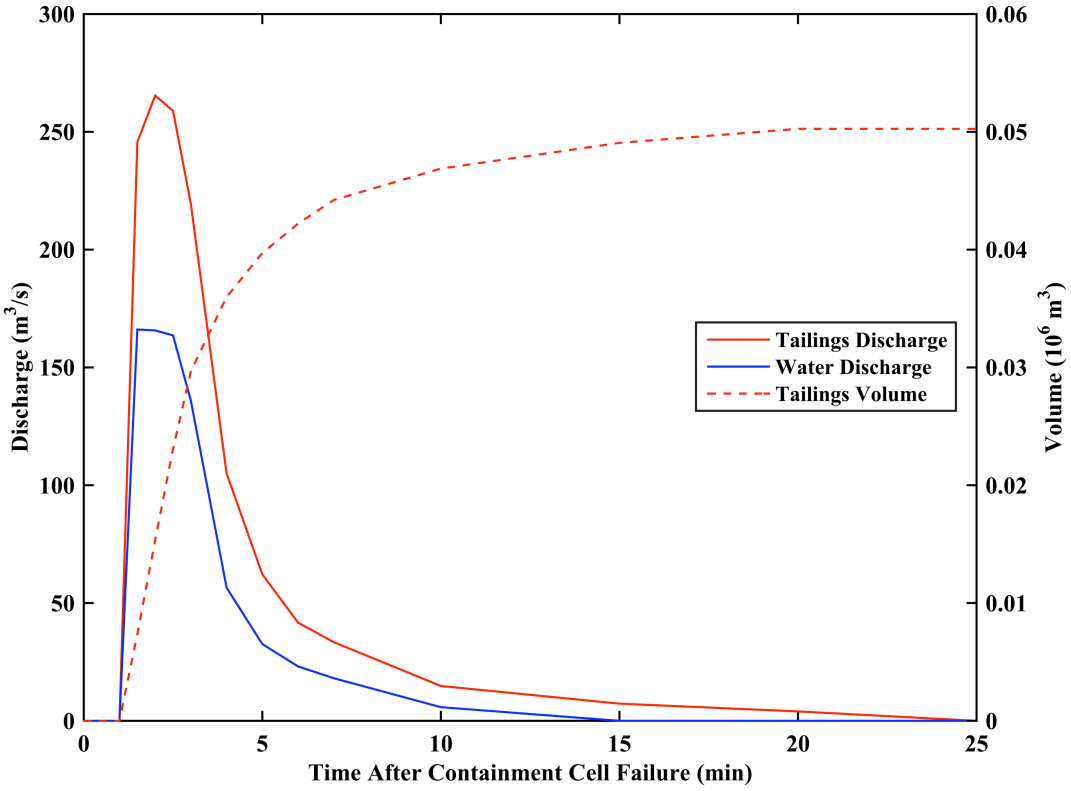

Figure 4-34: Volumetric discharge and volume of tailings, as well as of water on top of the tailings, at the centerline of Mill Creek

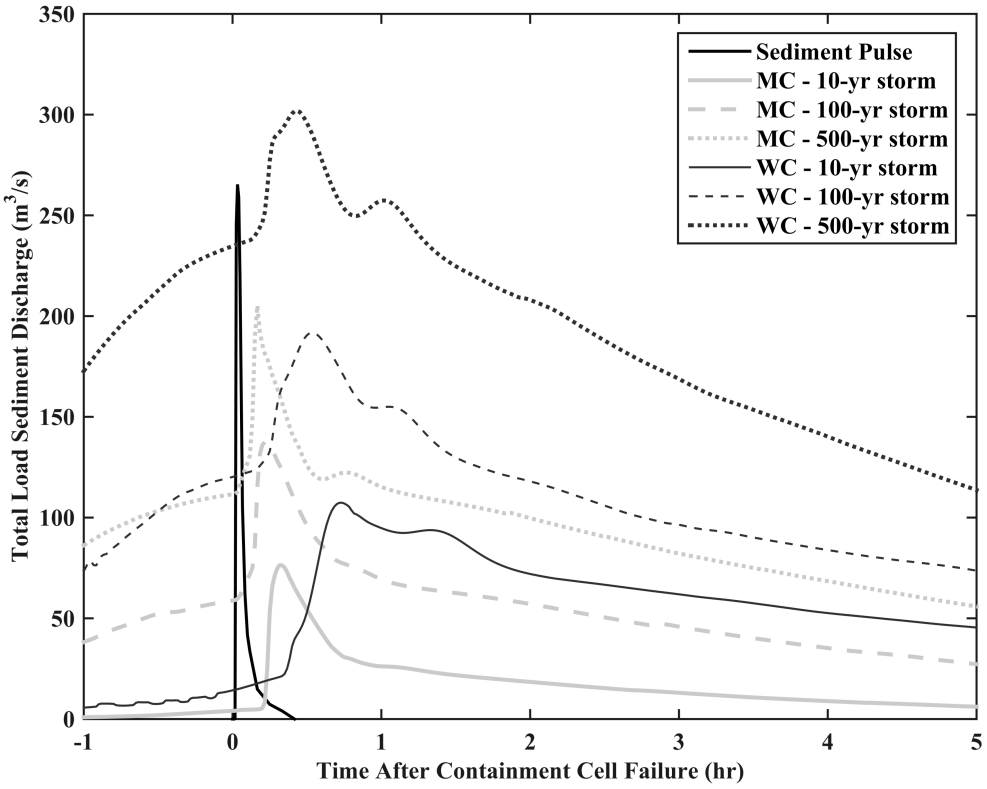

Figure 4-35: Temporal variation of the volumetric discharge of total sediment load at the outlet of Mill Creek (MC) and Whitethorn Creek (WC) after the failure of the containment cell

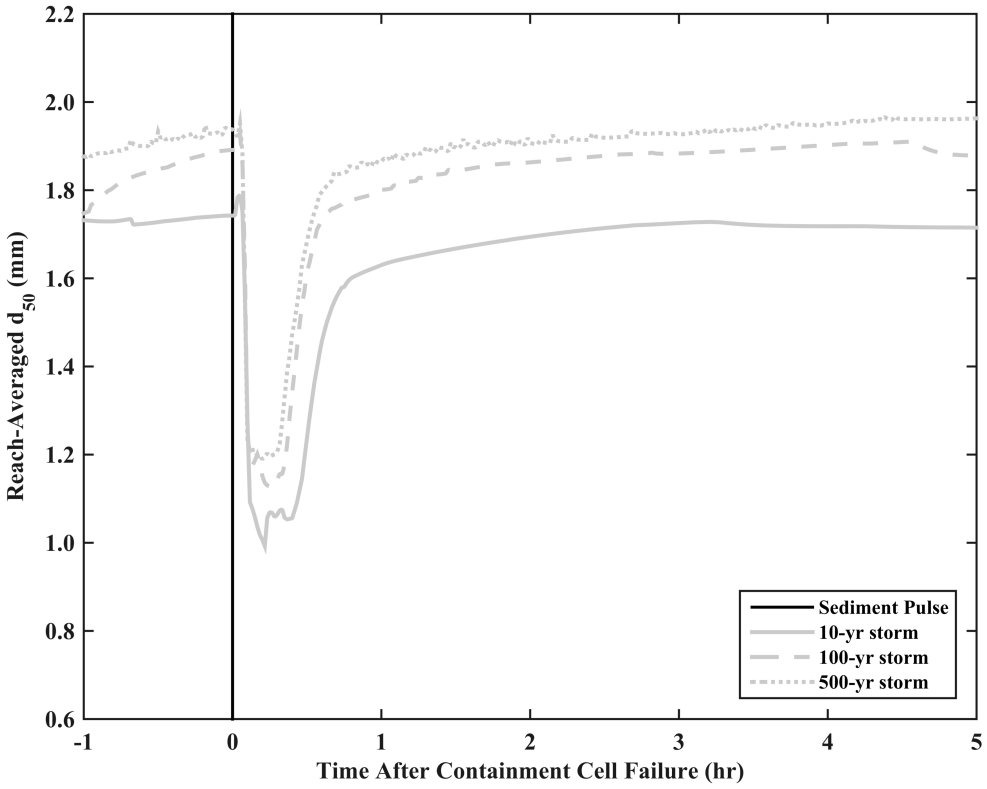

Figure 4-36: Transient fining of the riverbed during the propagation of the tailings sediment pulse

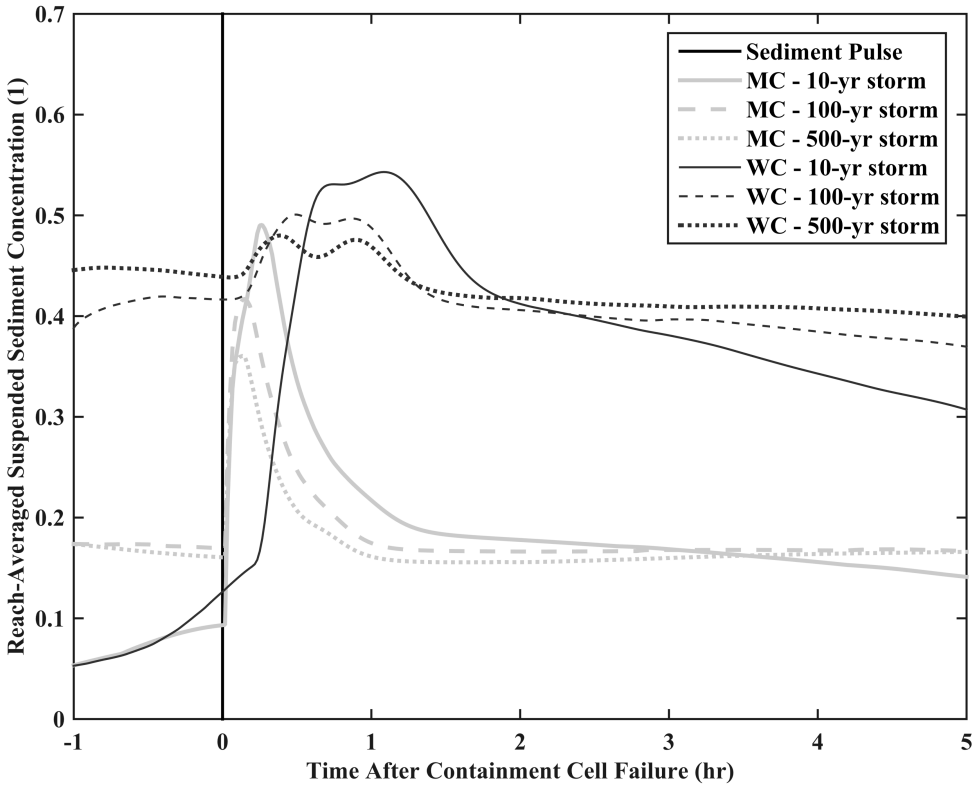

Figure 4-37: Temporal variation of the reach-averaged volumetric suspended sediment concentration

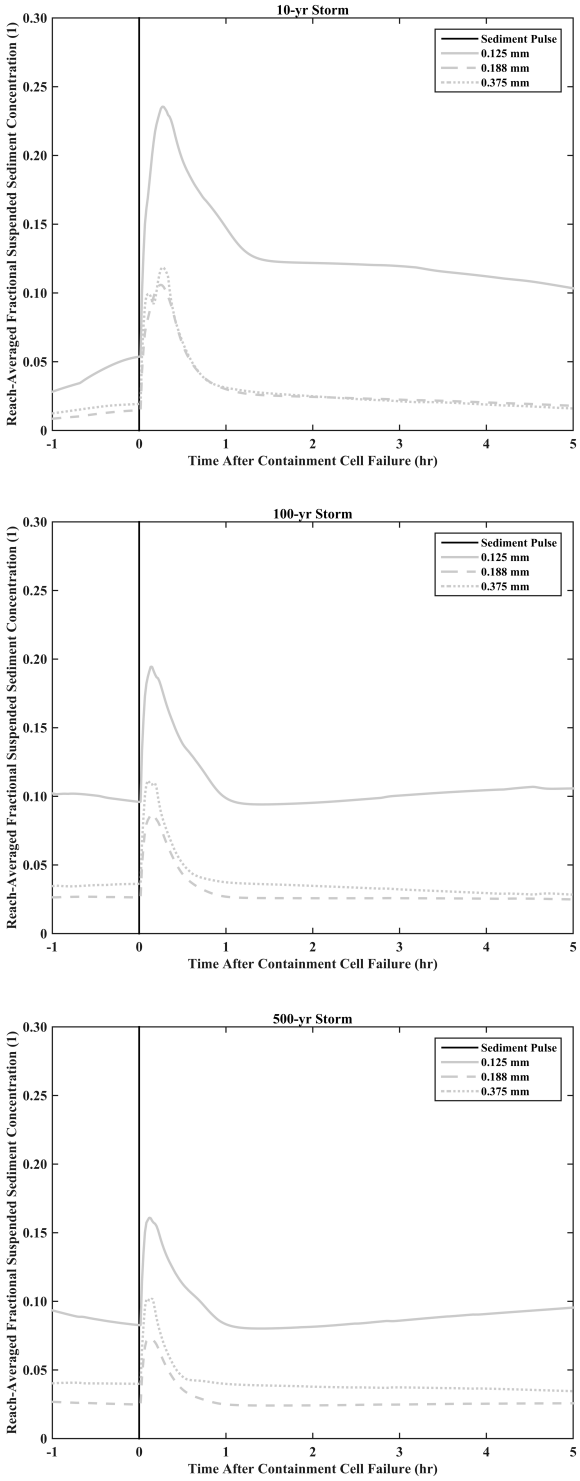

Figure 4-38: Temporal variation of the reach-averaged fractional volumetric suspended sediment concentration of fine material in Mill Creek

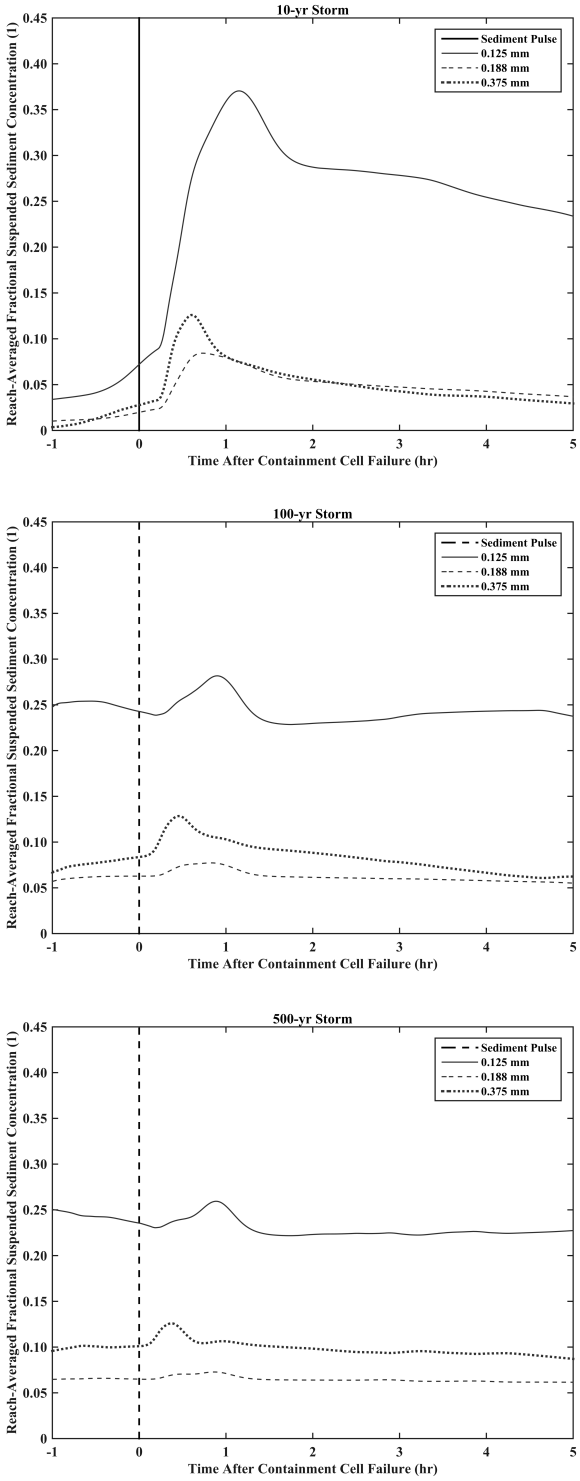

Figure 4-39: Temporal variation of the reach-averaged fractional volumetric suspended sediment concentration of fine material in Whitethorn Creek

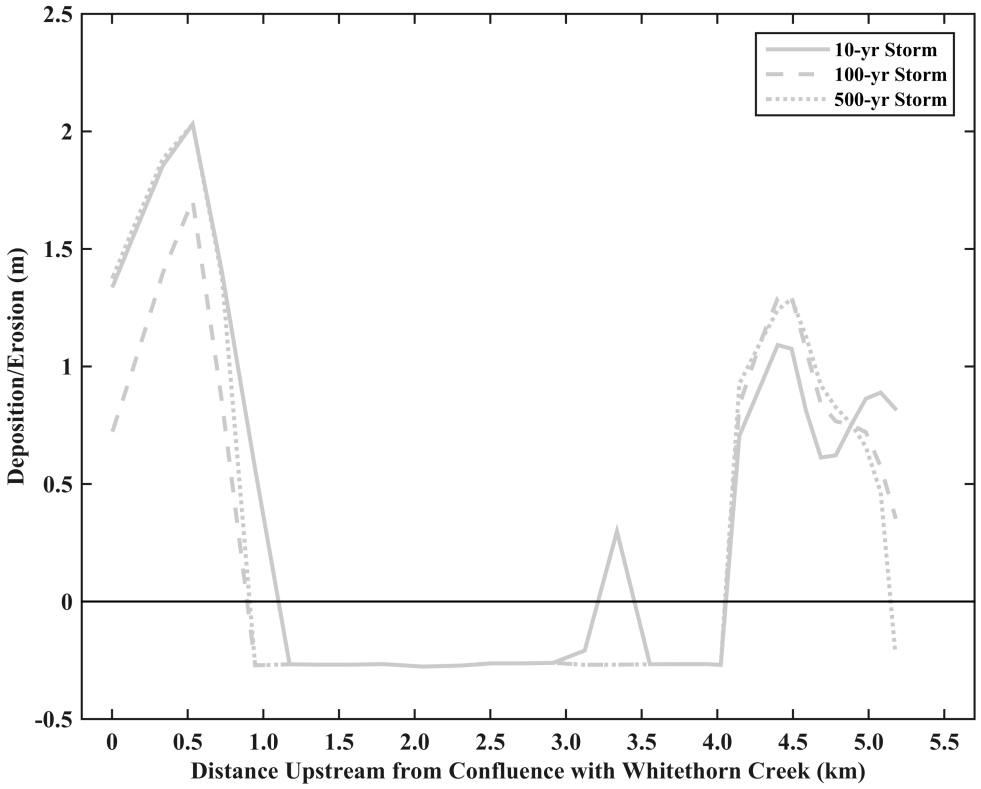

Figure 4-40: Maximum levels of aggradation and degradation patterns after the propagation of the tailings sediment pulse through Mill Creek

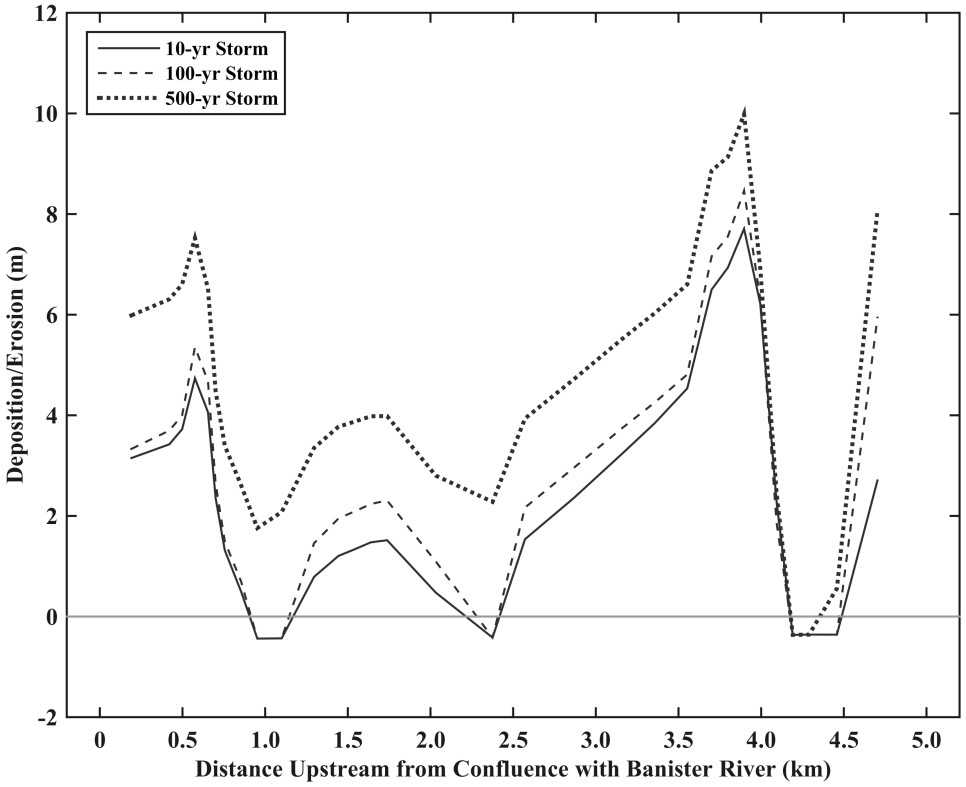

Figure 4-41: Maximum levels of aggradation and degradation patterns after the propagation of the tailings sediment pulse through Whitethorn Creek

CHAPTER 5. CONCLUSIONS

5.1. Findings

5.1.1. Numerical Modeling of Morphodynamic Processes in Alluvial Rivers

A 1-D adaptive morphodynamic numerical model was developed to examine the suitability of the decoupled and coupled modeling approach for capturing the dynamic interactions among water flow, the transport of sediment, and the evolution of the riverbed. The model applies a novel solution methodology for the system of governing equations that adopts the more adequate of these approaches within different regions of the computational domain depending on local flow and sediment transport conditions. The key findings are summarized as follows:

- A dimensional analysis of the St. Venant shallow water equations for conservation of mass and momentum of the water-sediment mixture revealed that a criterion to select between the decoupled and coupled approach must consider the dynamic relationship between the Froude number and the concentration of total sediment load.
- The densimetric Froude number proved to be an appropriate parameter to account for the aforementioned dynamic relationship, and allowed for the derivation of a dimensionless number ξ to express it quantitatively.
- Two distinct modeling approach regions were defined based on an experimentally derived threshold of ξ (i.e. ξ_{cr}), namely, a decoupled approach region characterized by $\xi < \xi_{cr}$, and a coupled approach region in which $\xi \geq \xi_{cr}$. A large database of flume experiments indicated that the former region is in good agreement with morphodynamic processes dominated by bedload transport, whereas the latter region is characterized by suspended-load driven flows with large amounts of solids in the water column.
- The coupled modeling approach should be used in applications where fine sediment is largely present to improve the fidelity of the numerical simulations, particularly during the initial short-term period in which river corridors undergo rapid hydrodynamic and morphodynamic adaptations.

- A number of validation cases demonstrated the suitability of the proposed solution methodology to adjust to the variety of temporal scales exhibited by fluvial processes in alluvial rivers. This provides confidence in the use of derived dimensionless number ξ as a criterion to define a range of applicability for the decoupled and the coupled modeling approach.

5.1.2. The Behavior of Fine-Grained Sediment Pulses in Alluvial Rivers

A numerical analysis to characterize the propagation of fine-grained sediment pulses in alluvial rivers was carried out to investigate the influence of the pulse grain size distribution and volume, as well as the influence of the ambient discharge and channel slope, on the dominant propagation mechanisms. The key findings are summarized as follows:

- The propagation of the fine-grained sediment pulses in alluvial rivers occurs in two distinct phases; an initial dispersion-dominated phase and an ensuing translational-dominated phase.
- The initial phase is governed by suspended-load driven regimes that actively entrain material from the top part of the pulse, carrying finer sediment further downstream while depositing coarser particles close to the original forefront location. As a result, a rapid downstream movement of the pulse forefront and a nearly vertical variation of the pulse apex elevation characterize this phase.
- The second phase is no longer controlled by suspended load, but rather by a combination of this mode of transport in the vicinity of the pulse forefront and bedload transport across the pulse core region. Therefore, the propagation velocity of the pulse forefront considerably decreases, while the pulse apex exhibits a pronounced translational movement in the streamwise direction.
- The Froude number proved to be the parameter that governs the transition between the aforementioned phases, with a marked reduction in its magnitude triggering the onset of the translational-dominated behavior. Numerical tests indicated that such transition occurs around a value of the Froude number between 0.4 and 0.5 independently of the evaluated variable.

- The influence of tested parameters, namely, pulse grain size distribution and volume, ambient discharge and channel slope, was observed to be relevant to the intensity and duration of each phase.

5.1.3. The Effect of Severe Hydrologic and Hydraulic Conditions on the Propagation of Fine-Grained Sediment Pulses in Alluvial Rivers

The propagation of a fine-grained sediment pulse was examined under the influence of storms of various intensities to assess the effect of the magnitude, duration, and frequency of hydrologic events, as well as of the ensuing severe hydraulic conditions in riverine environments. The key findings are summarized as follows:

- The magnitude, duration, and frequency of hydrologic events have a marked impact on the relationship between pre- and post-pulse conditions, the degree of dissipation of the pulse peak discharge, and the travel time of the pulse apex.
- In terms of pre- and post-pulse conditions, the impact of the sediment pulse is inversely proportional to the scale of the hydrologic event. For relatively small storms, the amount of material deposited in the stream represents a significant increase in total load transport rates as compared to pre-pulse conditions. Instead, large events are capable of entraining and carrying substantial amounts of sediment downstream, resulting in high total load transport rates even before considering the contribution of the pulse.
- Likewise, the degree of dissipation of the pulse peak discharge and the travel time of the pulse apex are inversely related to the scale of the hydrologic event, with small storms producing a greater attenuation and a longer time than large storms. Such behavior is due to the increasing capacity of the flow to move sediment as the severity of the storm strengthens.
- The riverbed and flow field dynamically adjust their grain size distribution and concentration of suspended solids to accommodate the surplus of material, with a more pronounced fining process and higher concentrations recorded for small storms.

- Severe hydraulic conditions in riverine environments primarily affect aggradation and degradation patterns, as well as the streamwise variation of suspended sediment concentrations. This is particularly relevant for river networks, in which backwater effects from relatively large watercourses facilitate the settling of material in the coarse to medium grain size range, while maintaining the very fine sediment in suspension for long periods of time.

5.2. Broader Impact and Limitations

The numerical effort presented in this dissertation advances the current state-of-the-art in two core research areas. First, the numerical modeling of morphodynamic processes, and secondly, the propagation of fine-grained sediment pulses in alluvial rivers. The application of the proposed adaptive modeling framework addresses an important limitation of commonly used decoupled models: their inaccuracy when reproducing the particularities of fluvial processes at the initial short-term phase. As demonstrated throughout this study, such phase, which is characterized by rapid hydrodynamic and morphodynamic adaptations, is more adequately captured by a coupled modeling approach. The adaptive framework allows us to accurately simulate such phenomena by adopting the more suitable modeling approach during different time periods and within different sections of the computational domain without compromising the global accuracy and efficiency of the numerical model. Such capability is due to the derived form of the dimensionless number ξ, which accounts for the dynamic relationship between the Froude number and the volumetric concentration of total sediment load, providing a suitable quantitative measure of the ratio between the morphodynamic and hydrodynamic time scales.

The present work also demonstrated that the evolution of fine-grained sediment pulses in alluvial rivers is governed by hydrodynamic and morphodynamic processes that differ from those embedded in current pulse propagation numerical models. These models are primarily intended for gravel-bed streams and omit the influence of relevant features of alluvial rivers. In particular, the effect of suspended-load driven regimes is not adequately represented in their model formulation and solution technique, in addition to not considering the occurrence of relatively low values of the Froude number given their

original scope. The former feature directly impacts the initial short-term propagation behavior, whereas the latter feature enhances the degree of translation exhibited by the sediment pulses as they migrate downstream over a longer time period. It is highlighted in this study that accurately reproducing this overall behavior is highly dependent on the implemented modeling approach, which is addressed herein by applying the proposed adaptive modeling framework. While previous studies have preliminary identified how fine-grained sediment pulses evolve, a detailed description of the fundamental propagation mechanisms and their implications towards numerical modeling was missing from the present state of knowledge. Such enhance understanding ultimately contributes towards improving numerical models and prediction methods that are used nowadays for assessing the fate of fine-grained sediment pulses in river corridors.

Lastly, the identified limitations of the proposed adaptive modeling framework are listed below. Its use should be restricted to applications that do not satisfy any of the following:

- Sediment pulses composed of very fine-grained cohesive material in the silt and clay size range (i.e. $d_{50} < 0.125$ mm).
- Sediment pulses composed of coarse-grained material in the gravel size range (i.e. $d_{50} > 2$mm), unless appropriate empirical closure relations (e.g. bedload transport equation) are implemented.
- Cases where important stratification effects are expected to occur.
- Cases in which the volumetric concentration of suspended sediment is greater than 0.6, which is the assumed limit between hyperconcentrated and debris flow.
- Flow regimes characterized by important secondary flows or marked three-dimensional features.

5.3. Recommendations for Future Research

It is envisioned that additional work in the following areas will strengthen the findings and expand the contribution of this research:

- A formal perturbation analysis of the St. Venant shallow water equations for the conservation of mass and momentum of the water sediment mixture would

provide a more rigorous framework to verify the suitability of the proposed dimensionless number ξ.

- A detailed numerical analysis focusing only on the initial short-term phase of the propagation process would help to more accurately identify the degree of deviation between the decoupled and the coupled modeling approach. Such effort should be accompanied by laboratory experiments and field data in order to corroborate the findings of the numerical model.
- The development of a rheological component sub-model and its implementation in the adaptive morphodynamic model would account for the impact of hyperconcentrated flows on the overall propagation behavior. This is particularly relevant for small storms, which have a reduced sediment transport capacity and therefore are prone to trigger high concentrations of suspended solids in the water column.